AD

USAAML TECHNICAL REPORT 65-17

THEORETICAL AND EXPERIMENTAL STUDIES OF AIRFOIL CHARACTERISTICS IN NONUNIFORM SHEARED FLOW

By

W. G. Brady

May 1965

U. S. ARMY AVIATION MATERIEL LABORATORIES

FORT EUSTIS, VIRGINIA

CONTRACT DA 44-177-AMC-70(T)

CORNELL AERONAUTICAL LABORATORY, INC.

DDC Availability Notice

Qualified requesters may obtain copies of this report from DDC.

This report has been furnished to the Department of Commerce for sale to the public.

Disclaimer

The findings in this report are not to be construed as an official Department of the Army position, unless so designated by other authorized documents.

When Government drawings, specifications, or other data are used for any purpose other than in connection with a definitely related Government procurement operation, the United States Government thereby incurs no responsibility nor any obligation whatsoever; and the fact that the Government may have formulated, furnished, or in any way supplied the said drawings, specifications, or other data is not to be regarded by implication or otherwise as in any manner licensing the holder or any other person or corporation, or conveying any rights or permission, to manufacture, use or sell any patented invention that may in any way be related thereto.

Disposition Instructions

Destroy this report when it is no longer needed. Do not return it to the originator.

HEADQUARTERS
U S ARMY TRANSPORTATION RESEARCH COMMAND
FORT EUSTIS, VIRGINIA 23604

This report has been reviewed by the U. S. Army Transportation Research Command, and the results and conclusions are considered to be technically sound. The report is published for the exchange of information and the stimulation of ideas.

NOTE

On 1 March 1965, *after this report had been prepared,* the name of this command was changed from U.S. Army Transportation Research Command to:

U.S. ARMY AVIATION MATERIEL LABORATORIES

Task 1P125901A142
Contract DA 44-177-AMC-?0(T)
USAAML Technical Report 65-17
May 1965

THEORETICAL AND EXPERIMENTAL STUDIES OF AIRFOIL CHARACTERISTICS IN NONUNIFORM SHEARED FLOW

CAL Report AF-1841-S-1

by W. G. Brady

Prepared by

Cornell Aeronautical Laboratory, Inc.
Buffalo, New York

for

U. S. ARMY AVIATION MATERIEL LABORATORIES
FORT EUSTIS, VIRGINIA

SUMMARY

The results of a continuing theoretical and experimental investigation of airfoil characteristics in nonuniform sheared flows are presented. The theoretical investigation was concerned with attempts to determine the cause of anomalous maximum lift behavior of airfoils in two-dimensional nonuniform sheared flows. The various theoretical approaches attempted are outlined, and details are presented of a numerical method, programmed on an IBM 7044 computer, to compute pressure distributions about airfoils in two-dimensional inviscid nonuniform sheared flows with certain specified velocity profiles and with wind-tunnel walls. Numerical results are not yet available from this program.

A wing spanning the wind-tunnel test section and partially immersed in an axisymmetric nonuniform sheared flow jet representative of a propeller slipstream was investigated in the experimental program. It was determined that separation characteristics of airfoil sections inside and outside the jet were quite different. Complete separation inside the jet was delayed to higher angles of attack, and considerably higher lift, than for the airfoil sections outside the slipstream. Up to angles of attack at which separation occurred on those wing sections outside the jet, section aerodynamic lift and moment inside the slipstream, particularly near the jet centerline, appeared to follow closely the corresponding two-dimensional nonuniform sheared flow airfoil characteristics. Outside the jet, section aerodynamic lift and moment did not agree as well with the corresponding two-dimensional uniform flow airfoil characteristics. Also, considerably higher maximum lift was obtained outside the jet than for the corresponding two-dimensional airfoil in a uniform flow. Although section aerodynamic characteristics varied spanwise along the wing with differing vertical positions relative to the jet, there appeared to be no vertical position of the wing at which significantly more lift was generated on sections inside the slipstream at any angle of attack below complete separation.

FOREWORD

The work described in this report was accomplished by the Cornell Aeronautical Laboratory, Inc. (CAL), Buffalo, New York, for the U. S. Army Transportation Research Command (USATRECOM), Fort Eustis, Virginia, over a 14-month period started in June 1963. The work was performed under Contract DA 44-177-AMC-70(T), "Nonuniform Shear Flow Investigation." This work is a continuation of a research program carried out at CAL over a period of several years up to 1961 under Contract DA 44-177-TC-439.

Mr. W. G. Brady of CAL was project engineer and author of this report. Mr. J. Balcerak of CAL conducted the experimental program; J. Grace of CAL made substantial contributions to the analytical studies; and both contributed to this report. The significant contributions of Messrs. J. Nemeth, C. Ryan, and Dr. I. C. Statler of CAL to the investigation and the many helpful discussions between the author and Mr. R. Vidal of CAL are appreciated.

Mr. J. McHugh and, subsequently, Mr. P. Cancro administered the project for USATRECOM.

TABLE OF CONTENTS

LIST OF ILLUSTRATIONS

LIST OF SYMBOLS

c	Airfoil chord
C_d	Drag coefficient based on local free-stream dynamic pressure, q
C_l	Lift coefficient based on local free-stream dynamic pressure, q
$\hat{C}_l$	Lift coefficient based on average dynamic pressure, $\hat{q}$
C_{m_f}	Moment coefficient referenced to airfoil midchord, based on local free-stream dynamic pressure
D	Upstream and downstream distance from airfoil where disturbance due to airfoil is negligible
$g(x)$	Height of free boundary above y = 0 dividing regions of differing vorticity; see Figure 4
h	Height of airfoil midchord reference above center of shear screen
h_{AU}, h_{AL}	Airfoil profile coordinates, upper surface and lower surface, respectively
$I(x,y)$	Acceleration potential; $I(x,y) \equiv \frac{p(x,y)}{\rho}$
K	Shear parameter; $K \equiv \frac{c}{U}\frac{dU}{dy}$
k	Parameter proportional to free-stream shear (or velocity gradient); see Equation (2)
$\bar{k}$	Parameter proportional to shear gradient in parabolic sheared flow
L	$2L$ = Wind-tunnel test section height
p	Static pressure
q	Free-stream dynamic pressure at the location of the model midchord (without the model present)
q_o	Free-stream dynamic pressure outside of the nonuniform axially symmetric jet

$\bar{q}$	Average free-stream dynamic pressure over the jet cross-section at model wing reference station
$\hat{q}$	$= \frac{1}{2}(q_0 + \bar{q})$
R_c	Reynolds number based on wing chord and local free-stream velocity
r	Radius of the nonuniform axially symmetric jet at the shear screen, prior to mixing with free stream
U	Uniform free-stream velocity in x direction
$U(y)$	Nonuniform free-stream velocity in x direction
U_0	Minimum velocity in free-stream parabolic sheared flow; see Equation (2)
U_1, U_2, U_3	Free-stream velocities, defined in Figure 5
u, v	Velocity components in x and y directions, respectively; subscript "0" refers to free-stream values
$\vec{u}$	Velocity vector
(x, y, z)	Cartesian coordinate system; in wind-tunnel tests, x is parallel to wind-tunnel test section walls, positive downstream, y is parallel to wing midchord, z is perpendicular to x-y plane, positive up. Origin is in plane of wing midchord, on slipstream centerline.
α	Angle of attack; subscript "G" refers to wing geometric angle of attack, subscript "s" refers to section, or local, angle of attack.
γ_1, γ_2	Vortex-sheet strength distribution on wind-tunnel walls; see Figure 5
γ_{A1}, γ_{A2}	Vortex-sheet strength distribution on airfoil surfaces; see Figure 5
$\vec{\omega}$	Vorticity
ρ	Density
τ	Airfoil thickness-to-chord ratio
ψ	Stream function
ψ_0	Stream function of free stream
ψ_1	Disturbance stream function

INTRODUCTION

The research reported here had its genesis in a program of theoretical and experimental research on low-speed aerodynamics as applied to STOL and VTOL aircraft which was conducted at the Cornell Aeronautical Laboratory over a period of time ending in late 1961. A classical problem that was examined was that of the interaction of a propeller slipstream with a wing. One of the first assumptions usually made in dealing with this problem analytically is that the slipstream consists of a uniform jet. This assumption obviously neglects an important feature of propeller slipstreams, in that the slipstream velocity is in reality a function of radius, i. e., the flow is a sheared flow.

Considerable effort during the research at CAL was devoted to a study of the influence of sheared flows on airfoil characteristics. References 1, 2, 3, and 4 report on the results of this study. The approach used was to treat theoretically the most elementary flow of the problem (airfoil in two-dimensional, linearly sheared flow) and to attempt to extend these results to more complex configurations by experimental means.

Reference 1 presents an extension to cambered airfoils of the theory of Tsien (Reference 5) for a symmetric Joukowski airfoil in a two-dimensional inviscid, incompressible flow with a linearly varying free-stream velocity gradient. In Reference 2 an experimental investigation is reported in which the theoretical results of Reference 5 were checked and which examined experimentally the effects on a two-dimensional airfoil of a two-dimensional nonuniform sheared flow with free-stream velocity profile similar to that in a propeller slipstream. During the course of these experiments it was discovered that nonuniform shear could have a marked effect on airfoil stall characteristics. These stall characteristics were examined in more detail in the research reported in Reference 3. Finally, Reference 4 presented the results of a preliminary experimental investigation of the effects of shear on a two-dimensional airfoil in a simulated three-dimensional slipstream.

The work reported here is a continuation of the experimental study of the two-dimensional wing in a three-dimensional sheared flow and also treats the theory of two-dimensional nonuniform sheared flows in an attempt to determine the mechanism responsible for the marked changes in airfoil stall characteristics which were demonstrated experimentally in Reference 3. It was felt desirable to complete the three-dimensional experimental program before resuming experimental work with two-dimensional nonuniform sheared flows. The experimental wing data obtained are presented and compared, where possible, with relevant two-dimensional data and

with theory. Details of a method which was developed for computing the aerodynamic characteristics of an airfoil in two-dimensional inviscid, non-uniform sheared flows are presented, although implementation of a digital computer program for numerical calculations is as yet incomplete.

CONCLUSIONS

On the basis of the work done and the results obtained, the following conclusions can be drawn regarding the theoretical studies conducted and regarding the experimental aerodynamic characteristics of airfoils in a three-dimensional nonuniform sheared flow representative of a propeller slipstream.

Theory

1. It is confirmed that available two-dimensional uniform or nonuniform shear airfoil theory is inadequate for the prediction of airfoil aerodynamic characteristics at angles of attack near stall in a flow with large shear and shear gradients typical of propeller slipstreams.

2. A method of numerical analysis was derived and programmed for a computer which should enable predictions to be made of aerodynamic lift and moment on an airfoil in a two-dimensional nonuniform sheared flow. The analytical method is not limited to small disturbances or small shear and shear gradient.

Experiment

3. Up to nearly the angle of attack at which the portion of the wing outside the axially symmetric nonuniform jet stalled, section aerodynamic lift and moment characteristics at and near the jet centerline were similar to those obtained in a two-dimensional flow with similar free-stream velocity distributions and Reynolds numbers; above this angle of attack, three-dimensional effects appear to become significant.

4. In contrast, three-dimensional effects appear to be significant outside the jet at angles of attack below the stall. Airfoil section characteristics were not comparable to uniform flow two-dimensional airfoil section characteristics for the same airfoil prior to complete separation on the wing outside the jet, and substantially higher maximum lift was obtained.

5. Outside the jet, flow separation from the wing upper surface was abrupt, with a marked drop in lift coefficient. Inside the jet, complete separation of the wing upper surface flow was delayed to higher angles of attack resulting in considerably higher lift than for the wing outside the jet. Inside the jet, the flow over the wing upper surface was marked by a gradual forward movement of the separation point from the airfoil trailing edge as angle of attack increased beyond the angle at which the flow outside the jet was fully separated.

6. There appeared to be no vertical location of the wing in the jet at which significantly more lift was generated on that portion of the wing inside the slipstream, in spite of differences in the spanwise lift distribution at the various vertical locations of the wing.

RECOMMENDATIONS

On the basis of the results presented herein and in Reference 3, the following recommendations are made:

1. Development of the analytical technique for predicting airfoil aerodynamic characteristics in two-dimensional, inviscid, nonuniform sheared flow should be continued.

2. Airfoil pressure distributions should be obtained experimentally for the two-dimensional nonuniform sheared flow corresponding to that for the data of Reference 3, in an attempt to determine the influence of such flow on airfoil pressure gradients and, hence, on separation.

TECHNICAL DISCUSSION

THEORETICAL PROGRAM

Summary of Previous Sheared Flow Research at CAL

Primary emphasis in the study reported here has been on the aerodynamic characteristics of airfoils near maximum lift in two-dimensional nonuniform shear flows; hence, this review will concentrate principally on this aspect.

The investigation of Reference 3 was concerned with experiments on a symmetric Joukowsky airfoil in a two-dimensional nonuniform sheared flow. The free-stream velocity profile of this flow was similar to that in a propeller slipstream. This investigation concentrated on those regions in the flow where the shear, or velocity gradient, was relatively small and where the shear gradient, or second derivative of the velocity, was large. Typical lift data obtained in the investigation of Reference 3 are shown in Figures 1 and 2. The data in Figure 1 are reduced to coefficient form using the average velocity in the slipstream. These data then provide a direct comparison of the magnitude of the airfoil lift at the various positions in the nonuniform stream. The data in Figure 2 are reduced to coefficient form using the local free-stream velocity. By "local free-stream velocity" is meant the velocity at the position of the wing midchord in the undisturbed flow (model not present). It should be noted that the local free-stream velocity is a convenient reference for sheared flows only when comparing data obtained with similar velocity profile distributions.

It can be seen in Figures 1 and 2 that the airfoil section lift coefficient varies markedly with location of the wing in the slipstream. As an illustration, consider the data in Figure 1 obtained with the airfoil located at $h/r = + 1/8$ and $h/r = - 1/8$. The corresponding difference in airfoil position is small and about equal to 75 percent of the airfoil maximum thickness. The data show, however, that by moving the airfoil from above to below the slipstream centerplane through this distance, the airfoil lift was almost doubled at the highest angles of attack. Moreover, impending stall was indicated at $h/r = + 1/8$ but was not evident at the highest angles of attack at $h/r = - 1/8$. Consequently, one might anticipate even higher lifts at higher angles of attack for $h/r = - 1/8$.

The data in Figure 1 show that further increases in lift can be realized by shifting the airfoil further below the slipstream centerplane. The data obtained at $h/r = - 3/16$ show a 20 percent increase in lift over that obtained at $h/r = - 1/8$ at the highest angles of attack. Data were not obtained at positions below $h/r = - 3/16$, but the trend suggests that the optimum position was not necessarily reached.

During the two-dimensional research, boundary-layer observations were made using oil-film techniques to determine the extent of separation on the airfoil upper surface. These data showed that when separation occurred, it was acceptably two-dimensional and that no unusual three-dimensional separation processes were present. Moreover, these data showed that separation was delayed to higher angles of attack when the airfoil was positioned below the slipstream centerplane than when the airfoil was positioned above the centerplane.

Preliminary section-force data were next obtained with the same airfoil in an axially symmetric nonuniform jet (Reference 4). The data obtained in the vicinity of the jet centerline appeared to suggest that the destalling phenomenon observed in two-dimensional flow was also present in the axially symmetric flow.

The pertinent available inviscid sheared-flow airfoil theories are presented in Reference 5 (exact solution for linear sheared flow), Reference 1 (theory of Reference 5 extended to cambered airfoils), and Reference 6 (approximate solution for nonuniform shear flow with slightly parabolic velocity profile). It was demonstrated in Reference 2 that the results of the exact theory of Reference 5 (for two-dimensional uniform shear) is in as good agreement with experimental data for an airfoil in a two-dimensional uniformly sheared flow as are the predictions of exact potential flow airfoil theory with the corresponding uniform flow experimental airfoil data. The theory of Reference 5 was also applied to the airfoil in nonuniform sheared flows, by applying corrections to the theory to account for the free boundaries in the sheared flow; these corrections are similar to wind-tunnel wall corrections. It was found that agreement of the uniform sheared flow theory thus corrected with the corresponding experimental results was, at best, only fair. Section lift coefficients were in fair agreement when the local shear was nearly uniform; otherwise, agreement was poor. It should be noted that the free-boundary correction to aerodynamic coefficients was a significant portion of the final computed value.

Inherent in the nonuniform sheared flow theories of References 6 and 7 is a small shear gradient assumption. Hence, these theories are not directly applicable to the highly sheared nonuniform flows considered experimentally in References 2 and 3; in fact, predictions based on a direct application of the theory of Reference 6, disregarding the small shear gradient assumption, are in gross disagreement with the pertinent experimental results. It was concluded that in order to deal successfully with nonuniform shear-flow aerodynamics with shears and shear gradients comparable to those of the tests, either a modification of the theory of Reference 6, or an entirely new theory, was required.

At the termination of the sheared-flow aerodynamics research reported in References 1 to 4, therefore, there remained the unexplained variations of

lift, and delay of stall under certain circumstances, in two-dimensional nonuniform sheared flows. The need for a nonuniform sheared-flow airfoil theory applicable to large shear and shear gradients was also evident. Such a theory would not only benefit investigations of the lift variations and stall behavior, but would also be useful in treating a number of other problems involving rotational flows.

Fundamental Theoretical Considerations

In the previous experimental program at CAL it was shown that the lift behavior of an airfoil section in a certain nonuniform sheared flow could change considerably when the airfoil is located at different positions in the flow. It was also clear that available theory was inadequate for treating the problem. A theoretical study was undertaken with the ultimate objective of providing an analytical technique for predicting aerodynamic characteristics of airfoils in arbitrary two-dimensional, inviscid, nonuniform sheared flows. The assumptions and conditions underlying the investigation are as follows:

(1) The flow and airfoil section are two-dimensional.
(2) The flow is inviscid and incompressible.
(3) The mathematical model must be such as to allow for large shear and shear gradients in the free stream.
(4) The flow model must be consistent with large disturbances in the flow field.

The reason for specifying Condition 4 above is related to the experimental findings that a sheared flow may either promote or retard flow separation at large angles of attack. Therefore, if one is to consider large angles of attack, the corresponding large disturbances generated must be tolerated. This implies that the linearizing techniques used in thin airfoil theory would not be valid for those cases in which a high angle of attack is considered.

The main characteristics of a sheared flow which distinguishes it from a nonsheared flow is the fact that it is rotational. The powerful techniques of potential theory, including conformal mapping, that can be used for two-dimensional irrotational flow problems, are generally not applicable to rotational flows. To illustrate the types of mathematical difficulties involved, the following brief summary of the equations governing a rotational, incompressible, inviscid steady-flow problem is given.

From the continuity equation

$$div\ \vec{u} = 0$$

where

$$\vec{u} = (u, v),$$

we may define a stream function ψ as

$$u = -\frac{\partial \psi}{\partial y}$$

$$v = \frac{\partial \psi}{\partial x},$$

thereby satisfying the continuity equation identically. Taking the curl of the two-dimensional, steady equations of motion, and defining the vorticity, $\vec{\omega}$, as $\vec{\omega} = \text{curl } \vec{u}$, we find the two-dimensional steady vorticity equation

$$(\vec{u} \cdot div)\vec{\omega} = 0.$$

By employing the stream function and definition of vorticity, this equation can be written as

$$\frac{\partial(\psi, \nabla^2\psi)}{\partial(x, y)} = 0,$$

which implies

$$\nabla^2\psi = f(\psi), \tag{1}$$

i.e., $\nabla^2\psi$ is a constant along a streamline (where the stream function is a constant). It can be shown that, in two-dimensional flow, this constant is the vorticity; that is, the vorticity is a constant along a streamline in an inviscid two-dimensional rotational flow. From Equation (1), one can see that the form of $f(\psi)$ depends on the solution ψ. Therefore, for the general sheared flow, one is faced with solving

$$\nabla^2\psi = f(\psi)$$

subject to specified boundary conditions. This, in general, is a nonlinear partial differential equation.

In the following, a number of papers concerned with airfoils or other shapes in sheared flows are reviewed. In each of these the authors have attempted to reduce the general equation above to a form more amenable to solution by means of various approximations. Each of these approaches represents a limiting case because of the approximations. Such limiting cases are

often of great utility. For example, they provide analytical checks for a more general, but more approximate, solution. In many instances these limiting cases represent the only solutions that can be obtained with reasonable effort. It is sometimes found that predictions based on such solutions are reasonably accurate even in cases beyond the theoretically valid range of applicability.

Tsien's Theory -- Two-Dimensional Uniform Shear

The problem considered by Tsien (Reference 5) is one of a symmetric Joukowski airfoil placed in a linearly sheared inviscid stream. Far ahead of the body in the free stream the velocity distribution is given by

$$\left.\begin{aligned} u &= U_0\left(1+\frac{ky}{c}\right) \\ v &= 0 \end{aligned}\right\}. \tag{2}$$

For this velocity profile one finds that the vorticity is a constant. The governing equation can therefore be written as

$$\nabla^2\psi = \frac{kU_0}{c} \quad . \tag{3}$$

The function ψ is split into two parts, one representing the undisturbed stream function ψ_0 and the other the disturbance stream function ψ_1. ψ_0 can be shown to be

$$\psi_0 = U_0\left(y+\frac{ky^2}{2c}\right);$$

ψ_1 must, therefore, satisfy

$$\nabla^2\psi_1 = 0. \tag{4}$$

Because the vorticity is constant throughout the flow, disturbances introduced into the flow cannot distort this vorticity distribution. The problem remaining is to solve Equation (4) subject to certain boundary conditions. Since ψ_1 satisfies Laplace's equation, a conformal transformation of the boundary conditions from the airfoil plane to the circle plane may be used in obtaining the solution for ψ_1 .

The results of Tsien's analysis show that:

(1) The drag on the body remains zero, as in the nonsheared case.
(2) The lift coefficient is increased linearly with k , the nondimensional velocity gradient, for small k .

Tsien's theory is an exact inviscid theory for the case of a uniform sheared flow of unlimited extent about an arbitrary two-dimensional body. For a nonuniform sheared flow it represents a limiting case for vanishing shear gradient. It is apparent from the formulation that extension of this theory to nonuniform sheared flows is not feasible.

Lighthill's Theory -- Three-Dimensional Source in Two-Dimensional Nonuniform Shear

Lighthill's approach (Reference 8) was to seek a solution to the flow problem of a weak three-dimensional source in a general two-dimensional nonuniform sheared flow. From this "fundamental" solution, it was hoped that the problem of a body in a general shear flow could be formulated and solved.

As noted above, the undisturbed flow field is two-dimensional,

$$\left.\begin{aligned} u_o &= U(y) \\ v_o &= 0 \\ w_o &= 0 \end{aligned}\right\}$$

Since $U(y)$ is to be a general function, the size of the shear or its distribution is not limited. Although the shear is unlimited, small disturbance assumption is made, thereby allowing a linearization of the equations of motion. Combining the continuity and momentum equations for a three-dimensional source in a two-dimensional sheared flow, we find the governing equation to be

$$U(y)\,\nabla^2 v - \frac{d^2U}{dy^2} = m\,U(o)\,\delta(x)\,\delta'(y)\,\delta(z) \qquad (5)$$

where $\delta(\ )$ is the Dirac delta function $\delta'(\ )$ is its derivative and m is the source strength. Once this equation is solved for the perturbation velocity v, we can then solve independently for u and w.

In arriving at a solution via Fourier transform techniques, Lighthill separates the problem into consideration of two regions, one near the disturbance and the other far away from it. Then, employing two asymptotic expansions, each valid in one of the regions, he obtains the solution to Equation (5). A matching of the solutions in the intermediate region then gives a solution for the problem valid for all regions surrounding the body.

Two principal results from Lighthill's analysis are:

(1) For the solution expanded in ascending powers of the radial distance from the source, the first term of the series yields the primary flow (source itself), and the second term is the small disturbance approximation to the shear secondary flow and depends only on $U(o)$ and $dU(o)/dy$, the velocity and shear at the origin.

(2) For large radial distances far from the source, a source in a shear layer produces in any region of uniform flow outside the shear layer a disturbance equivalent to a source of different strength in a different position.

Lighthill's theory represents a limiting case in that it is applicable to an arbitrary nonuniform sheared flow but is limited to small disturbances. If the theory could be developed to the point where it is applicable to an airfoil, presumably the theory would be limited to thin airfoils at small angles of attack.

In order that the Lighthill theory could be applied to a two-dimensional airfoil, fundamental solutions must be obtained for both a two-dimensional source and a vortex in the two-dimensional nonuniform sheared flow. For the two-dimensional source, the governing partial differential equation, corresponding to Equation (5), is

$$\nabla^2 v - \frac{1}{U(y)} \frac{d^2U(y)}{dy^2} v = \frac{1}{U(y)} U(o)\,\delta(x)\,\delta'(y) . \qquad (6)$$

Once the fundamental solution for the source (Equation (6)) and the corresponding solution for the vortex were obtained, a lifting airfoil could be represented by a distribution of such sources and vortices. Some effort was devoted to finding a solution to Equation (6); this was abandoned, ultimately, when the decision was made to concentrate on the theoretical approach finally adopted.

Jones' Theory -- Two-Dimensional Nonuniform Shear

The theory of E. E. Jones (Reference 6) is derived from prior work by Nagamatsu (Reference 7). However, Jones avoids a questionable assumption made by Nagamatsu.

The free-stream velocity distribution assumed by Jones was as follows:

Again, a stream function ψ is defined where $\psi = \psi_0 + \psi_1$. ψ_0 can be expressed as

$$\psi_0 = -U_0\left(y + \frac{ky^3}{6h^2}\right).$$

ψ_1 may be shown to satisfy

$$\nabla^2\psi_1 = \psi_1\frac{\partial f}{\partial \psi_0} + \frac{1}{2}\psi_1^2\frac{\partial^2 f}{\partial \psi_0^2} + \cdots$$

where

$$\frac{\partial f}{\partial \psi_0} = \frac{\bar{k}}{h^2 + \bar{k}\frac{y^2}{2}}\,, \qquad \frac{\partial^2 f}{\partial \psi_0^2} = \frac{(\bar{k})^2 h^2}{U_0\left(h^2 + \bar{k}\frac{y^2}{2}\right)^3}\,.$$

Now, assume that $(\bar{k}y^4/2h^2) \ll 1$ (i. e., assume a small shear and shear gradient in the free stream); then we find

$$\nabla^2\psi \approx \frac{\bar{k}}{h^2}\psi_1\,.$$

This equation is then solved using as the boundary conditions those of a thin airfoil. The procedure adopted by Jones was to transfer the equations and the boundary conditions from the airfoil plane to the circle plane. The equations in the transformed plane can be reduced to a pair of Mathieu equations, if the airfoil is limited to small angles of attack and small camber.

The principal results of Jones' analysis are:

(1) For small $\bar{k}$ the lift and moment increase with an increase in $\bar{k}$ and α , the angle of attack.
(2) The predicted drag is negative (in the thrust direction) and becomes increasingly negative with angle of attack.

The Jones theory is a limiting case for small shear and shear gradient and, in its final solution, for small disturbances. The same basic approach can be used to obtain an extension which appears to be applicable to arbitrary bodies in two-dimensional nonuniform sheared flows with arbitrary shear and shear gradient. Such an extension was formulated during the present research and is presented here. Although no effort was made to carry the theory beyond the formulation stage (and, in fact, the analytical problems associated with such an effort may well be formidable), it is believed that this approach represents the ultimate hope for an analytical solution, within the requirements for large disturbances, valid for large shear and shear gradient.

In this approach one assumes a free-stream velocity distribution

$$U(y) = U + u_o = U\left[1 + \sum_{n=1}^{\infty}\left(\frac{u_{on}}{U}\right)\sin\left(\frac{n\pi y}{a}\right)\right] \tag{7}$$

where a is a reference length. Then

$$\psi_o = U\left[y - \sum_{n=1}^{\infty}\left(\frac{u_{on}}{U}\right)\left(\frac{a}{n\pi}\right)\cos\left(\frac{n\pi y}{a}\right)\right] . \tag{8}$$

After Jones,

$$\psi = \psi_o + \psi_1 ,$$

$$\nabla^2\psi_1 = \nabla^2\psi_o + \nabla^2\psi_1 = f(\psi) = f(\psi_o + \psi_1)$$

or

$$\nabla^2\psi_o = f(\psi_o + \psi_1) - \nabla^2\psi_o .$$

But

$$\nabla^2\psi_o = f(\psi_o) = -U\sum_{n=1}^{\infty}\left(\frac{u_{on}}{U}\right)\left(\frac{n\pi}{a}\right)\cos\left(\frac{n\pi y}{a}\right) \tag{9}$$

so that

$$\nabla^2\psi_1 = f(\psi_o + \psi_1) - f(\psi_o). \tag{10}$$

Expanding the right-hand side of Equation (10) in a Taylor series,

$$f(\psi_o + \psi_1) - f(\psi_o) = \psi_1\left(\frac{\partial f}{\partial \psi_o}\right) + \frac{1}{2!}(\psi_1)^2\frac{\partial^2 f}{\partial \psi_o^2} + \frac{1}{3!}(\psi_1)^3\frac{\partial^3 f}{\partial \psi_o^3} + \cdots . \tag{11}$$

If ψ_1 is expressed as

$$\psi_1 = \psi_{10} + \psi_{11}\left(\frac{u_{01}}{U}\right) + \psi_{12}\left(\frac{u_{01}}{U}\right)^2 + \psi_{13}\left(\frac{u_{01}}{U}\right)^3 + \cdots$$

(that is, consider only the first term of the series on the right-hand side of Equation (7)), if the operations indicated in Equation (11) are carried out

and expressed in terms of a power series in (u_{o_1}/U), and if the terms of the same power of (u_{o_1}/U) are collected together, there results

$$\left.\begin{aligned} \nabla^2\psi_{10} &= 0 \\ \nabla^2\psi_{11} &= F_0(\psi_{10}) \\ \nabla^2\psi_{12} &= F_1(\psi_{11}) \\ \nabla^2\psi_{1j} &= F_{1-j}(\psi_{1(j-1)}) \end{aligned}\right\} \quad . \tag{12}$$

Note that the equation for ψ_{1j} involves only the $\psi_{1(j-1)}$ in the nonhomogeneous term. Hence, Equations (12) constitute a series of successive approximations for ψ_1, for a velocity distribution represented by a sine wave. Once the appropriate boundary conditions for an airfoil in the flow are derived, solutions to as high a degree of accuracy as desired could presumably be obtained, subject, of course, to analytical difficulties inherent in obtaining solutions to the Helmholz partial differential equations of Equations (12).

A similar development to the above is possible in terms of the acceleration potential, $I = p/\rho$. However, the partial differential equations which result, although also linear and nonhomogeneous, are somewhat more complicated than those in Equations (12).

Of the various theoretical approaches considered thus far to the problem of a thick airfoil at large angles of attack in a nonuniform sheared flow with large shear and shear gradients, only one appears to merit serious consideration: the extension of the Jones theory exemplified by Equations (12). However, it is possible that serious analytical problems must be dealt with in attempting solutions via this approach.

Developments in other research for USATRECOM at CAL have suggested an approach which, although also presenting analytical problems, appears to offer more immediate useful analytical results than any of those considered thus far. This approach is presented in detail in the following section. It is also a limiting case in that it deals with free-stream nonuniform sheared flow velocity profiles in which the shear gradient is infinite at certain points in the two-dimensional flow.

Two-Dimensional Inviscid, Incompressible Nonuniform Sheared Flow Theory -- Approach Adopted

1. General:

During the course of the present research, a digital computer program for computing an axially symmetric free-streamline flow (finite impinging jet) was reported in Reference 9. The success of this program indicated a method of approach which should permit the calculation of the aerodynamic

characteristics, including pressure distributions, of any two-dimensional airfoil at arbitrary angle of attack (in nonseparated flow) in two-dimensional nonuniform sheared flows with arbitrary shear. The only restriction appears to be that the free-stream velocity profile is such that it can be approximated by piecewise linear segments. Examples of such profiles are shown in Figure 3.

It is clear from Figure 3 why the proposed method of analysis represents a limiting case for infinite shear gradient. The shear gradient is infinite in Figure 3 at those points where the piecewise linear velocity segments are joined (point (a) in Figure 3(B) and point (c) in Figure 3(C)).

It should be recalled that the fundamental difficulty in treating two-dimensional inviscid nonuniform sheared flows analytically is related to the fact that the fundamental governing equation

$$\nabla^2\psi = f(\psi) \qquad (1)$$

is nonlinear. This equation states that the vorticity in the flow is a constant along streamlines; inasmuch as the shape of the streamline is one of the unknowns in the problem, the functional form of the right-hand side of Equation (1) above is not known a priori. If the free-stream velocity profile can be approximated by piecewise linear segments, as in Figure 3, then the streamlines passing through those points at which the velocity gradient changes (points (a), (b) and (c) in Figure 3, for example) separate regions of constant vorticity throughout the flow. Thus, the relationship to the free-streamline flow problem (free-boundary problem) is clear; as part of the solution of the problem, the shape of those streamlines separating regions of constant vorticity must be determined. In effect, we have replaced a problem with a nonlinear governing equation and known boundary conditions by a problem with a linear governing equation ($\nabla^2\psi$ = constant) within regions with free (and, hence, unknown) boundaries.

The solution of the free-boundary problem reported in Reference 9 was obtained numerically by means of an iterative technique. The particular iterative method used in that solution required a large number of iterations before satisfactory convergence was obtained. However, also reported in Reference 9 is the theoretical justification for an improved iteration method. Although this method has not yet been proven by actual calculations, it should provide much more rapid convergence than that method actually employed in the calculations of Reference 9.

It was concluded that the development of a digital computer program based on the refined iterative technique reported in Reference 9 to compute the pressure distribution on a thick airfoil at any angle of attack in a nonuniform shear flow (within the limitations of a piecewise linear velocity profile) was feasible. Formulation of the requisite theory and programming of the computer program have been completed; checkout of the program was well

underway at the time of the completion of the present contract. Details of the theory and its implementation on the CAL IBM 7044 digital computer are presented in the following sections of this report.

Such a program would serve the requirements of the present research most effectively, as compared to other approaches considered during the present work and as previously discussed. The inherent advantages are:

(1) There are no theoretical limitations as to the size of the shear.

(2) There are no limitations as to small disturbances; for non-separated flow, any angle of attack and any airfoil thickness and profile can be treated.

(3) Wind-tunnel wall effects can be included.

(4) Development of the computer program is, in principle, relatively straightforward; there are no apparent unresolved theoretical problems requiring lengthy investigations.

The obvious disadvantages are:

(1) The nonuniform sheared flows that can be treated are restricted by the piecewise-linear velocity profile requirement.

(2) Implementation of a relatively complex computer program nearly always gives rise to difficulties, both foreseen and unforeseen.

(3) Although an iterative technique similar to that proposed here was successful in the work reported in Reference 9 , the proposed technique is untried, particularly for a rotational flow, as is dealt with here.

The computer program has been written for a two-dimensional nonuniform sheared flow in a wind tunnel with a velocity profile like that of Figure 3(B). This velocity profile has the advantage of being the simplest nonuniform sheared flow velocity profile to which the theory can be applied, which is a worthwhile consideration for the initial calculations. Although this velocity profile does not correspond in all respects to that for which the data of Figures 1 and 2 were obtained, it does match quite closely the flow in the center, including the region of abrupt change in shear. It is when the airfoil is in proximity to this abrupt change in shear that the marked changes in lift behavior occur. Modification of the computer program for the more complex profile of Figure 3(C) would be a straightforward process, once the workability of the program has been established.

It is difficult to assess with any exactness the implications of the restriction to piecewise-linear velocity distributions. In effect, we are replacing a

free-stream vorticity distribution like that of the solid line in Sketch (A), below, with one like that of the dashed line.

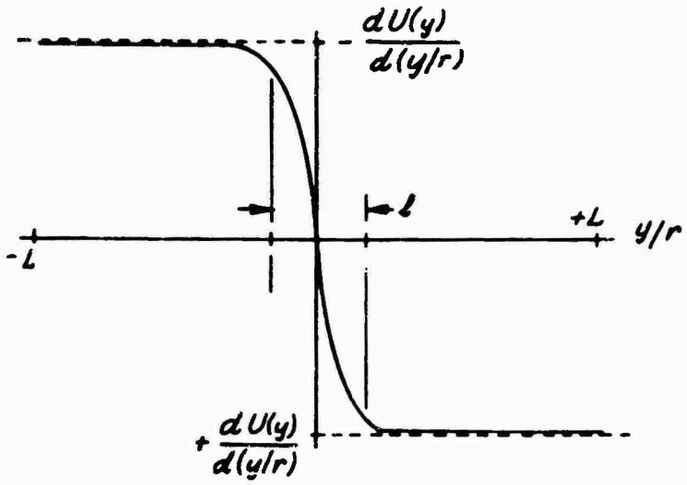

Sketch (A)

Perhaps the best way to consider this aspect is that the theory represents a limiting case of infinite shear gradient and that this is the only restriction on the theory. For the airfoil located close to the discontinuity in slope of the velocity distribution, it might be that the ratio of the distance ℓ in Sketch (A) to airfoil thickness, as well as the ratio of ℓ to the displacement of the airfoil chord away from the discontinuity, must be small, for the approximation to be a reasonable one.

2. Fundamental Equations:

The flow model on which the analysis is based is illustrated in Figure 4. The effect of the wind-tunnel walls could have been accounted for by a reflection technique, as is usually done for wind-tunnel wall corrections. Instead, the wind-tunnel walls are represented by vortex sheets of variable strengths $\gamma_i(x)$, where $i = 1$ refers to the lower wall and $i = 2$ refers to the upper wall. Likewise, the airfoil surfaces are represented by vortex sheets of variable strengths $\gamma_{a1}(x)$ and $\gamma_{a2}(x)$. It is believed that this representation for the wind-tunnel walls will result in a considerable saving in computer time.

Point (a), Figure 4, in the velocity profile marks the boundary, represented by the function $g(x)$, between different constant values of the vorticity; in Figure 4, the vorticity above this boundary is

$$\omega_+ = -\frac{U_2 - U_3}{L} = -\omega$$

and below this boundary is

$$\omega_- = \frac{U_1 - U_3}{L} = \omega.$$

The functions γ_1, γ_2, γ_{A1}, γ_{A2} and $g(x)$ are the unknowns which are to be determined.

The velocity components u and v can be written

$$u(x,y) = u_w + u_\omega + u_A$$

$$v(x,y) = v_w + u_\omega + v_A \tag{13}$$

where (u_w, v_w) are contributed by the wind-tunnel wall singularity distribution, (u_ω, v_ω) arise from the vorticity ω in the shear flow, and (u_A, v_A) are the result of the airfoil singularity distribution. These follow directly from application of the Biot-Savart induction law, and are as follows:

$$u_w(x,y) = -\frac{1}{2\pi}\left\{\int_{-\infty}^{\infty}\frac{\gamma_2(\xi)(y-L)\,d\xi}{(x-\xi)^2+(y-L)^2} + \int_{-\infty}^{\infty}\frac{\gamma_1(\xi)(y+L)\,d\xi}{(x-\xi)^2+(y+L)^2}\right\} \tag{14}$$

$$v_w(x,y) = \frac{1}{2\pi}\left\{\int_{-\infty}^{\infty}\frac{(x-\xi)\,\gamma_2(\xi)\,d\xi}{(x-\xi)^2+(y-L)^2} + \int_{-\infty}^{\infty}\frac{(x-\xi)\,\gamma_1(\xi)\,d\xi}{(x-\xi)^2+(y+L)^2}\right\} \tag{15}$$

$$u_\omega(x,y) = \frac{\omega}{2\pi}\int_{-\infty}^{\infty}\left\{\int_{-L}^{g(\xi)}\frac{(y-\eta)\,d\eta}{(x-\xi)^2+(y-\eta)^2} - \int_{g(\xi)}^{L}\frac{(y-\eta)\,d\eta}{(x-\xi)^2+(y-\eta)^2}\right\}d\xi \tag{16}$$

$$v_\omega(x,y) = -\frac{\omega}{2\pi}\int_{-\infty}^{\infty}\left\{\int_{-L}^{g(\xi)}\frac{(x-\xi)\,d\eta}{(x-\xi)^2+(y-\eta)^2} - \int_{g(\xi)}^{L}\frac{(x-\xi)\,d\eta}{(x-\xi)^2+(y-\eta)^2}\right\}d\xi \tag{17}$$

$$u_A(x,y) = -\frac{1}{2\pi}\left\{\int_{x_L}^{x_T}\frac{\sqrt{1+\left[h'_{AU}(\xi)\right]^2}\left[y-h_{AU}(\xi)\right]\gamma_{A2}\,d\xi}{(x-\xi)^2+\left[y-h_{AU}(\xi)\right]^2} + \int_{x_L}^{x_T}\frac{\sqrt{1+\left[h'_{AL}(\xi)\right]^2}\left[y-h_{AL}(\xi)\right]\gamma_{A1}\,d\xi}{(x-\xi)^2+\left[y-h_{AL}(\xi)\right]^2}\right\} \tag{18}$$

$$v_A(x,y) = \frac{1}{2\pi}\left\{\int_{x_L}^{x_T}\frac{\sqrt{1+\left[h'_{AU}(\xi)\right]^2}(x-\xi)\,\gamma_{A2}\,d\xi}{(x-\xi)^2+\left[y-h_{AU}(\xi)\right]^2} + \int_{x_L}^{x_T}\frac{\sqrt{1+\left[h'_{AL}(\xi)\right]^2}(x-\xi)\,\gamma_{A1}\,d\xi}{(x-\xi)^2+\left[y-h_{AL}(\xi)\right]^2}\right\} \tag{19}$$

where $h'(x) \equiv \frac{dh}{dx}$.

3. Boundary Conditions:

The boundary conditions which must be satisfied are:

(1) Velocity components normal to the wind-tunnel walls are zero, or

$$v(x,\pm L) = 0. \tag{20}$$

(2) Velocity components normal to the airfoil surface are zero, i.e.,

$$\frac{dh_A}{dx} = \frac{v(x,h_A(x))}{u(x,h_A(x))}. \tag{21}$$

(3) The boundary $g(x)$ is a streamline, that is,

$$\frac{dg}{dx} = \frac{v(x, g(x))}{u(x, g(x))} \quad . \tag{22}$$

Also, the Kutta-Joukowski condition must be satisfied at the airfoil trailing edge; i. e., the velocity at the trailing edge is finite.

Equations (20), (21) and (22), with Equations (13), result in five nonlinear, integral (in the case of Equation (22) integro-differential) equations for the five unknown functions γ_1 , γ_2 , γ_{A1}, γ_{A2}, and g . It is possible to obtain a solution only by recourse to a high-speed, high-storage-capacity digital computer.

The nonlinearity in the problem arises through $g(x)$; if g were known, then solutions for the γ's could be obtained by a direct inversion procedure on the computer. This inversion procedure is relatively well known and was used in the solution of the normally impinging jet, Reference 9, and previously in work reported in Reference 10. It is based on an adaptation of Fredholm's solution to the linear Fredholm integral equation (Reference 11). Hence, it is the nonlinearity inherent in g which makes the use of an iteration technique necessary.

Consider the flow tangency boundary condition on the free boundary $g(x)$, Equation (22):

$$u(x, g(x)) \frac{dg}{dx} - v(x, g(x)) = 0 \, . \tag{23}$$

For an assumed free-boundary curve g_a other than that for the exact solution, there would result

$$u(x, g_a) \frac{dg_a}{dx} - v(x, g_a) = E(x, g_a) \, . \tag{24}$$

For purposes of numerical calculation on a digital computer, the integrals constituting u and v are evaluated as follows. In the far field, for $x > D$, $x < -D$, it is assumed that the flow disturbance introduced by the airfoil is negligible; hence, free-stream flow conditions apply and are known. The coordinate axis between $-D \leq x \leq D$ is divided into a number of increments. Each of the integrals involved has one of the unknown quantities (for example, γ_1 and γ_2 in Equation (14)) in the integrand. It is assumed that in each of the above increments, this unknown quantity is constant, although, of course, the unknown varies from increment to increment. It so happens that all integrals involved in the present analysis are integrable in closed form, if the unknown quantity involved is assumed to be a constant. For example, on this basis, the first integral in Equation (14) can be written

$$\int_{-\infty}^{\infty} \frac{\gamma_2(\xi)(y-L)\,d\xi}{(x-\xi)^2+(y-L)^2} = \gamma_2(-D)\int_{-\infty}^{-D} \frac{(y-L)\,d\xi}{(x-\xi)^2+(y-L)^2}$$

$$+\sum_{i=1}^{M} \gamma_{2i}\int_{-D+(i-1)\Delta x}^{-D+i\Delta x} \frac{(y-L)\,d\xi}{(x-\xi)^2+(y-L)^2}$$

$$+\gamma_2(D)\int_{+D}^{\infty} \frac{(y-L)\,d\xi}{(x-\xi)^2+(y-L)^2}\,.$$

On this basis, Equation (24) can be stated (at $x = x_n$)

$$\sum_{i=0}^{M} \Delta u_i\left((g_a)_i, (g_a)_n, x_n\right)\frac{d(g_a)_n}{dx}$$

$$-\sum_{i=0}^{M} \Delta v_i\left((g_a)_i, (g_a)_n, x_n\right) = E_n\left(x_n, (g_a)_n\right) \quad ; \quad n = 0, 1, \cdots, M. \tag{25}$$

Now, let

$$(g_a)_i = g_i + (\Delta g)_i \tag{26}$$

where g_i is the exact value of g at $x = x_i$ and $(\Delta g)_i$ is the incremental error in $(g_a)_i$ at $x = x_i$. If Equation (26) is substituted in Equation (25) and the terms Δu_i, Δv_i are expanded to first order in Δg_i, there results

$$\sum_{i=0}^{M} \overline{\Delta u_i}\,(\Delta g)_i\,\frac{d(g_a)_n}{dx} - \sum_{i=0}^{M} \overline{\Delta v_i}\,(\Delta g)_i \approx E_n \quad ; \quad n = 0, 1, \cdots M \tag{27}$$

where Equation (23) has been applied; $\overline{\Delta u_i}$, $\overline{\Delta v_i}$ are the coefficients of the first-order terms in $(\Delta g)_i$ of the expansions of Δu_i, Δv_i. Equation (27) for $n = 0$ to $n = M$ results in $M+1$ linear, simultaneous algebraic equations in the $M+1$ unknowns $(\Delta g)_i$, $i = 0$ to M. However, the g_i are also unknown; hence, the substitution

$$(g)_i \approx (g)_{a_i} \tag{28}$$

is made in the coefficients $\overline{\Delta u_i}$, $\overline{\Delta v_i}$, and in E_n in Equation (27).

This is the basis of the proposed iteration scheme. The initial assumed shape of the free-streamline boundary $[(q_a)_i]_0$ is used in Equation (24) to compute the $E_n(x_n, q_{an})$. The $M+1$ equations resulting from Equation (27) (with Equations (28) included) are solved for the $[(\Delta g)_i]_0$, $i = 0$ to M. The process is repeated with

$$[(q_a)_i]_1 = [(q_a)_i]_0 - [(\Delta g)_i]_0, \qquad i = 0 \text{ to } M. \tag{29}$$

The iteration proceeds until, at the j^{th} iteration, say, all the $[(\Delta g)_i]$ are as small as desired.

4. Implementation of Digital Computer Program:

The general computational procedure adopted is as follows:

(1) An initial shape of the free boundary $q(x)$ is assumed.

(2) The boundary conditions that the flow is tangential at the wind-tunnel walls and the airfoil surface together with the assumed $q(x)$ are used to determine the strength distribution of the vortex sheets representing the walls and airfoil surfaces.

(3) The coefficients of Equations (27) are computed, and the resulting equations are solved for the Δq_i. A second approximation to q is derived from Equation (29).

(4) The iteration proceeds for the adjusted boundary (by going back to Step 1).

The boundary conditions at the wind-tunnel walls and at the airfoil surface, Step 2, are satisfied at discrete points, or values of x, along these surfaces. The vortex-sheet strengths, γ_1, γ_2, γ_{A1}, and γ_{A2}, and also $q(x)$, are assumed to be constant within the increment Δx centered on each of these points (but, of course, varying from point to point). The various integrals in the expressions for u and v (Equations (15)) can then be expressed as sums,* as previously noted. Substituting the resulting expressions for u and v into the wind-tunnel wall and airfoil-surface boundary conditions, Equations (20) and (21), and evaluating at each of the specified values of x, there results a series of linear, simultaneous equations in the unknown γ_i's and γ_{Ai}'s. For $|x|$ large enough, the values of $\gamma_i(x)$ approach constant limiting values, and this fact is utilized to limit the number of simultaneous equations which must be solved.

*The multiple integrals in the expressions for u_ω, v_ω (Equations (16) and (17)) are readily reduced to single integrals with respect to ξ.

The flow field is divided up into a number of regions. For regions progressively closer to the airfoil, smaller and smaller integration increments can be taken so as to improve numerical accuracy.

The Kutta-Joukowski trailing-edge condition is applied by requiring that the flow angularity at the trailing edge be equal to the airfoil angle of attack. This is a satisfactory condition for the Joukowski airfoil with its cusped trailing edge.

The integrals in the expressions for u_A , v_A , Equations (18) and (19), are all taken with respect to the x -axis. Inasmuch as at $x = x_L$, h'_{AU} and h'_{AL} are infinite, it is necessary in the airfoil nose region to transform the integrals properly and integrate in this region with respect to the y -axis.

At the present time, the computer program has been completed and is being checked. When work is resumed on this program, it is planned to complete the program checkout and then compute pressure distributions for an airfoil profile (corresponding to that of the experimental two-dimensional nonuniform shear tests of References 2 and 3) in a wind-tunnel flow corresponding to Figure 3(B). At the same time, it is planned to obtain experimental airfoil pressure distributions for the same airfoil profile in the same free-stream velocity profile. Such pressure distributions obtained for the specified velocity profile would enable the validity of the inviscid theory to be determined. Once this has been established, it is believed that the theory described here will provide a powerful tool for further research on nonuniform sheared flows.

EXPERIMENTAL PROGRAM -- AXISYMMETRIC NONUNIFORM SHEARED FLOW

Previous Experiments

The initial research at CAL on the effects of axisymmetric nonuniform sheared flow on airfoil characteristics is reported in Reference 4. The intent was to obtain aerodynamic data for a two-dimensional wing in a nonuniform sheared flow simulating the effect of a propeller slipstream, but under controlled conditions and without the slipstream rotation inherent in a propeller slipstream.

The experiments were made in the subsonic leg of the CAL One-Foot High-Speed Wind Tunnel. This leg of the wind tunnel has a test section with a cross section of 17 inches by 24 inches and is operated as a closed-throat nonreturn-type tunnel. The test section stagnation pressure is one atmosphere, and the speed range in the clear test section is from 0 to 100 fps.

The shear in the test flow was generated by a screen placed across the wind-tunnel test section upstream of the model. The theory of the design of this screen was presented in Reference 4. The design called for a velocity distribution linear with radius in the slipstream and with a value of the shear parameter, $\kappa = 2$. These parameters are close to those used in the two-dimensional nonuniform sheared flow research reported in Reference 2.

The shear screen shown in Figure 5 was constructed of high-solidity uniform screen to produce the uniform external stream. The nonuniform portion, producing the 6-inch-diameter axisymmetric shear flow, consisted of 1/8-inch-diameter rods bent into concentric circles and suitably spaced to give the desired solidity. The entire screen assembly was bonded to a metal honeycomb and mounted in a metal frame. The honeycomb served to stiffen the assembly structurally and to prevent flow instabilities. The screen, producing flow external to the simulated slipstream, was uniform, though the screen theory called for a solidity distribution that varied by about 3 percent over the external flow. It was decided to simplify the fabrication by using a uniform screen, as the resulting nonuniformities would not be significant.

Previous experiments with a two-dimensional screen (References 2 and 3) showed that excessive mixing occurred between the simulated slipstream and the external flow if the slipstream was not physically separated by plates from the external flow. For this reason, the axisymmetric slipstream was constrained in a constant-area duct to a point two slipstream diameters ahead of the airfoil leading edge. The screen-duct arrangement is shown in Figure 6. The centerline of the screen was positioned 2 inches to one side of the test-section centerline in order to permit aerodynamic section data to be obtained outside the slipstream but well away from the test-section side wall.

The airfoil used in this research was an uncambered two-dimensional Joukowski airfoil with a thickness-chord ratio of 17 percent and a chord of 6 inches. A two-dimensional airfoil was selected for the experiments because of the analytic and experimental simplicity. The three-dimensional effects, therefore, were due only to the spanwise variation in shear and from the wing vorticity shed in the vicinity of the slipstream. The analytic complications due to the presence of a wing tip and the associated nonuniform spanwise loading were not present, thereby simplifying the interpretation of the results.

The model was instrumented with a three-component internal strain-gage balance to measure the loads on one section of the airfoil. This instrumented section was 0.75 inch wide. The remainder of the airfoil was similarly segmented so that the instrumented section could be positioned at any spanwise station. The model was assembled with gaps on either side of the instrumented section to prevent balance interference. The portion of the wing adjacent to and including the metric section was then wrapped with 0.005-inch-thick sheet rubber to prevent flow through the gaps, and the balance was calibrated with the sheet rubber in place. The balance was designed to measure a maximum lift of about 3 pounds.

The wind-tunnel-wall boundary layer was partially removed by wall suction in the vicinity of the wing-wall juncture to prevent, as much as possible, undesirable interaction of the wing boundary layer and the wall boundary layer. The required distribution and strength of the wall suction was determined experimentally by means of an oil-film flow visualization technique.

Limited checks of the sheared flow velocity distributions were made, and aerodynamic data were obtained for two vertical positions of the model wing with the metric section near the centerline of the slipstream. These tests were repeated during the course of the work reported here and will be discussed in due course.

Experimental Program of Present Research

The experimental portion of the present program was essentially a continuation of the work reported in Reference 4; it was intended that the experimental apparatus available from the previous test would be used. Wind-tunnel tests were of two primary types: detailed measurements of the undisturbed nonuniform sheared flow in the wind tunnel at the model midchord station, and wing model force tests.

1. Flow Calibration:

A detailed survey of the flow properties in and near the axially symmetric nonuniform jet (or slipstream) generated by the shear screen was made. Data obtained included measurements of velocity and flow angularity. A conventional 3/16-inch-diameter pitch-yaw Pitot-static probe was used for these tests. Inasmuch as the flow was rotational (sheared flow), there is an inherent error both in velocity measurements (because of streamline displacement at the probe due to shear) and in flow angularity measurements. It was found that streamline displacement effects on velocity due to shear were negligible on the basis of the theory of Reference 12. However, significant flow angularity errors were indicated for the values of K in the test flow, and the theory of Reference 12 was used to correct the measured flow angularity data. It is estimated that flow angularity data, including theoretical corrections for shear, are accurate to within ± 0.20 degree. This estimate is based on repeatability of data obtained at varying free-stream dynamic pressures and on preliminary calibrations using two probes of different diameters.

During initial flow calibration tests, it appeared that changes in the probe-support-structure configuration caused significant discrepancies in velocity measurements at certain positions in the jet. An investigation of probe-support configuration was undertaken. The configuration chosen for final tests was a cranked-arm support mounted to the wind-tunnel test section sting mount, which minimized the velocity measurement discrepancies.

Isovelocity contours for the flow in the jet are shown in Figure 7. Velocity distributions in the y direction at the four spanwise stations at which wing data were obtained are shown in Figure 8. Plots of the shear parameter, K, versus y/r at the same spanwise stations are presented in Figure 9. The shear distributions were derived from the velocity profiles. The spanwise variations of the measured flow angularity at the four vertical positions of the wing-model midchord at which data were obtained are shown in Figure 10.

It is apparent from the isovelocity plot of Figure 7 that the sheared flow in the jet was not perfectly symmetric (although the tendency of isoparametric plots to emphasize distortion should be recognized when viewing Figure 7). Those irregularities that are evident are probably due to imperfect mixing in the flow downstream of the shear screen.

A large distortion in the jet, consisting of a 1/2-inch flat plate broadside to the stream, projecting from the test-section wall, was deliberately introduced about 2 inches ahead of the wing-model leading edge at $y/r \approx 0$, $z/r \approx -0.8$. No effect was discerned at $z/r = 0$, either on airfoil aerodynamic data at $h/r \approx 0$ or on velocity distribution. It was concluded that the flow asymmetry did not justify an expensive and time-consuming attempt to improve it.

It is apparent from Figure 9(a) that for $z/r = 0.03$ the design K of 2 was obtained for $0.1 < y/r < 0.7$, and nearly obtained at $y/r = -0.2$. Measured flow angularity, Figure 10, varied from -2.5 degrees to +3 degrees. This flow angularity arises from the viscous mixing in the sheared flow and is directly related to the shear parameter K. Measurements fore and aft of the 50 percent chordline, corresponding to the wing leading- and trailing-edge locations, were made at several locations in the jet. No appreciable changes were noted in the velocity or flow angularity distributions.

2. Model Balance System Calibration:

The balance system used in the wind-tunnel tests was a standard three-component strain-gage balance which measured normal force, pitching moment, and axial force by means of a four-arm bridge circuit whose signals were channeled into a manual readout. This is the same balance system used in the experiments of Reference 4.

The balance system was calibrated with the model wing installed in the wind tunnel. The normal force and pitching moment calibrations were determined from successive incremental loadings applied at five stations spaced at 1-inch intervals along the chord of the metric section, beginning at the leading edge. The applied loadings, in pounds, were then linearized with respect to the output of the readout, in meter units, using a least-square technique. The metric section of the model wing was kept horizontal during the calibration, and very little coupling with the axial component was noted. The axial force calibration was determined from successive fore and aft incremental loadings. These data were again linearized. From all these

data, a calibration matrix was formed which was postmultiplied by the output, in meter units, of the three components to obtain the normal force, pitching moment, and axial force. These data were corrected for the tares resulting from the gravitational force at angle of attack, and then were finally resolved into lift and drag forces.

The operation and sensitivity of the readout were checked prior to calibration and before each test by placing a dummy load resistance across each bridge circuit. The tares were also checked before and after each series of tests at one spanwise station, since it was noted that the axial force calibration changed gradually over an extended period of time. This anomaly was attributed to the aging of the rubber skin over the metric section since it was determined from a calibration without the skin that the rubber skin carried about 40 percent of the axial force. This calibration technique is essentially the same as that used in the research reported in References 2, 3, and 4.

The sensitivity of the readout, including scatter, was approximately 0.0025 $\pm$ 0.00005 pound per meter unit for the normal force and 0.001 $\pm$ 0.000075 pound per meter unit for the axial force.

3. Wind-Tunnel Tests:

The wind-tunnel tests were conducted in the subsonic leg of the CAL One-Foot, High-Speed Wind Tunnel, as were those of Reference 4. The force tests in the wind tunnel were conducted with the wing model suspended from the side walls of the tunnel, in contrast to the sting mount used for the tests reported in Reference 4. The wall mount was designed and used primarily because of the limitation of the angle-of-attack range which was present in the sting mount, particularly with the wing positioned in the lower half of the slipstream (h/r 0). It was noted that at angles of attack above approximately 20 degrees, the center of rotation of the wing model in the sting mount was shifted progressively more forward of the 50 percent chord, causing a displacement of the 50 percent chordline in the jet. This displacement could be measured, and it was reduced somewhat by the flexure of the arms of the sting mount when the model was loaded. However, the choice of a side-wall mount was clearly indicated by the desire to obtain a wider range of angles of attack at all h/r's, by the simplification of the test procedure when wing support flexibility was eliminated, by the desirability of fixing the reference point on the model (wing midchord point) at all angles of attack, and by the possibility that the previously used wing-yoke assembly might have introduced significant distortion in the flow, particularly for the three-dimensional flow.

The side-wall support assembly consisted of two plates, identified as A in Figure 11, fixed to the tunnel walls; a vertical slide assembly, B, which held the wing model; an air jacket, C, which implemented suction at the tunnel walls; and a clinometer assembly, D. Plexiglas windows were installed for visual observation of the model. The wing model was attached to the wall mount with a pair of airfoil section-shaft assemblies. The wing-model was fixed in any vertical position by clamping the slide to the fixed section of the mount.

Since the wind-tunnel side-wall suction was used to minimize interference between the tunnel-wall boundary layer and the wing-model boundary layer, a series of holes was drilled on the slide assembly which comprised the tunnel wall to implement the suction. Angular displacements of the model were measured with the clinometer. The wing-model stiffness was sufficient to preclude relative angular displacement between the model and the clinometer under the airload.

Tests were conducted at each of four vertical and horizontal (spanwise) positions of the instrumented metric section in the jet listed below.

$h/r = 0.76,\ 0.46,\ -0.10,\ -0.64$
$z/r = 0.03,\ 0.54,\ 1.03,\ 1.54$

Since the vertical positions could be easily set, tests were conducted at all values of h/r for one spanwise location, or z/r. The data for each z/r were completely reduced before tests were conducted at another z/r, since the model had to be disassembled to change the spanwise location of the metric section. Although it was not necessary to recover the metric section and the gaps of the model with rubber at disassembly, the balance system was recalibrated after each change, and differences were noted in the calibrations. These were attributed to the softening of the rubber skin resulting from aging and handling. Some tests were repeated, and the data were found to be consistent with the calibration.

Balance data in the wind-tunnel tests were taken from approximately -5 degrees to 35 degrees, at two values of the dynamic pressure corresponding to free-stream velocities of approximately 60 and 90 fps, designated as "low q" and "high q", respectively, in the figures. Data were generally taken at 1 to 1.5-degree intervals below stall and at smaller increments as stall was approached. The approach to stall was generally characterized by unsteadiness in the force and moment readout. In all cases, data were obtained at angles of attack well beyond stall. Data were then taken at coarser increments with decreasing angle of attack, and the balance zeros were checked at zero airspeed between runs at high and low q. The data obtained at each angle of attack consisted of the lift, moment about the midchord point, and drag on the metric section of the model. The table on the following page summarizes the wind-tunnel test conditions.

Flow visualization tests using tufts distributed over the wing upper surface were also performed with the wing located at all vertical positions for which aerodynamic section data were obtained.

Experimental Results

1. General:

The section lift, moment, and drag data obtained are shown in Figures 12 through 23 in coefficient form. Coefficients in these figures are referenced to the local free-stream velocity. Angles of attack shown are referenced to the local free-stream flow angularity as obtained from the flow calibrations.

SUMMARY OF WIND-TUNNEL TEST CONDITION

z/r	h/r	V^* LOCAL FREE-STREAM VELOCITY ft./sec.		R_N^*		K
		HIGH q	LOW q	HIGH q	LOW q	
0.03	0.76	183	120	5.6×10^5	3.7×10^5	1.50
	0.46	138	91	4.2×10^5	2.8×10^5	2.00
	-0.10	93	61	2.9×10^5	1.9×10^5	-1.45
	-0.64	146	96	4.5×10^5	3.0×10^5	-1.55
0.54	0.76	199	131	6.1×10^5	4.0×10^5	0
	0.46	165	109	5.1×10^5	3.4×10^5	1.50
	-0.10	155	102	4.8×10^5	3.2×10^5	0.50
	-0.64	196	129	6.0×10^5	3.9×10^5	-1.10
1.03	0.76	120	79	3.7×10^5	2.4×10^5	-2.70
	0.46	169	111	5.2×10^5	3.4×10^5	-1.50
	-0.10	192	126	5.9×10^5	3.9×10^5	0
	-0.64	162	107	5.0×10^5	3.3×10^5	2.80
1.54	0.76	96	63	2.9×10^5	1.9×10^5	-0.10
	0.46	96.5	63.5	3.0×10^5	2.0×10^5	0.40
	-0.10	90.3	59.4	2.7×10^5	1.8×10^5	-0.20
	-0.64	86.7	57	2.7×10^5	1.8×10^5	0.10

*Based on local free-stream velocity.

Data were obtained at each value of h/r and z/r, except z/r = 1.54, for two values of dynamic pressure. Lift and moment data for the two values of dynamic pressure are generally in close agreement (Figures 16 through 23). The drag data, however, were inconsistent.

Although good agreement was obtained between high q and low q drag data in some cases (Figures 13 and 14), agreement was poor for the z/r = 0.03 data of Figure 12. Furthermore, negative drag was recorded in certain cases, notably z/r = 0 and z/r = 1.54 (Figures 12 and 15). The data for z/r = 0.03, h/r = +0.46 and h/r = -0.10 (Figures 12(b) and 12(c)) correspond to preliminary data presented in Reference 4, which data is also plotted in Figures 12(b) and 12(c). Agreement between the data of Reference 4 and the present data varies from poor to good. The only difference in the two experiments was the configuration of the wing-support mechanism. In the experiments of Reference 4, a sting-yoke support, exposed to the wind-tunnel air, was used, whereas in the present experiments, a side-wall mount was used. Preliminary check data were obtained during the present program using the sting-yoke mount. This preliminary drag data checked the drag data of Reference 4 at h/r = +1/2 and h/r = -1/16 relatively well.

No positive explanation for the negative drag behavior is evident. The two-dimensional nonuniform shear airfoil theory of Jones, Reference 6, predicts negative drag, proportional to the gradient of shear; however, this result is discounted because of the peculiar variation of drag with angle of attack, also predicted by the Jones theory. The inconsistency of the appearance of negative drag, and its repeatability for those configurations for which it was obtained, leads one to suspect some peculiarity of the balance system; for example, an effect of aerodynamic loading on the rubber skin. If this were the case, however, it would seem that the negative drag should have been obtained intermittently throughout the tests, including h/r = 0.54 and 1.03. Another possibility is that the readout was malfunctioning at times during the tests. If such were the case, these malfunctions were not evident during pre-test and post-test balance-system checks and calibrations. At one point during the tests, channels were switched in the readout, with no effect on repeat data. In view of the inconsistencies noted above, it would be well to consider the drag data as preliminary in nature.

The aerodynamic section data of Figures 12 through 26 are not corrected for wind-tunnel wall effects; there is no known accurate method of applying wind-tunnel wall corrections to the flow treated in these tests. However, approximate wall corrections based on two-dimensional flow conditions indicate that, at least up to the angle of attack for which the portions of the wing outside of the slipstream are first stalled, wall corrections would probably be small. Once separation occurs, the effects of wake blockage probably result in progressively larger wall effects. Although wake blockage effects are small at angles of attack where there was no stalled flow on the wing, the data for wing geometric angles of attack above approximately 14 degrees (where those portions of the wing outside the jet were stalled) are undoubtedly affected by this wake blockage.

Wake blockage can have three separate effects: (1) velocities over the wing where the flow is not separated are larger than they would be in a flow unrestrained by the wind-tunnel walls, because of mass-flow continuity requirements; (2) the pressure distribution could be altered somewhat; and (3) the increased mass flow surrounding the slipstream might tend to constrain the distortion of the slipstream as it reacts to the flow disturbance of the wing at angle of attack. Wake blockage corrections applied in routine wind-tunnel tests usually account only for the velocity increase, effect (1) above. Reference 13 states that an approximate estimate of the velocity increase due to wake blockage for three-dimensional wind-tunnel models can be obtained on the basis of model frontal area. It is estimated, based on this approximation, that at a wing angle of attack of 30 degrees, the dynamic pressure in the flow outside the slipstream is increased about 6 percent by wake blockage. A corresponding estimate of the effects of wake blockage on wing-pressure distribution inside the jet is not possible at present.

It is believed that the aerodynamic behavior of the wing inside the slipstream observed during these tests is qualitatively correct, and the data up to $\alpha \approx 15$ degrees are relatively unaffected by the wind-tunnel walls. The data above $\alpha \approx 15$ degrees are probably increasingly subject to differences as compared to the same airfoil and slipstream in a flow unconstrained by wind-tunnel walls. This should be kept in mind during the discussion that follows.

The Reynolds number range of these tests in terms of airfoil chord (see the table) was 1.8×10^5 to 6.1×10^5. In low turbulence flow, for these Reynolds numbers, transition from laminar flow to turbulence in the upper-surface (suction surface) boundary layer would occur near midchord at $\alpha = 0$ degrees, moving forward with increasing angle of attack; in any case, transition would occur not too far aft of the minimum pressure point on the airfoil upper surface. The apparent effect of the high turbulence level in the flow downstream of the shear screens in reducing the two-dimensional drag of the airfoil used in these tests in uniform sheared flow was noted in Reference 2. It would seem almost a certainty that this high turbulence level would tend to force transition in the airfoil boundary layer, much like an artificial roughening on the airfoil leading edge. However, to establish that this is the case would require a detailed experimental investigation of the airfoil boundary layers.

The wall suction used at the junction of the wing and the wind-tunnel wall did not appear to have materially affected the flow over the wing inside the slipstream, even after the outer wing stalled. There was essentially no difference in airfoil characteristics obtained at $z/r = 0.03$ with and without wall suction.

2. Wing Section Aerodynamic Characteristics and Comparison with Previous Experiment and Theory:

In the discussions of Sections 2, 3, and 4, the wing geometric angle of attack, α_G, is the angle of attack of the wing as a whole, with reference to the angle of zero flow angularity for the test section without the shear screen installed.

The local section angle of attack, α_s, is referenced for the local flow angle as measured in the free stream (with no wing model installed) of the axially symmetric jet; that is, α_g is corrected using the measured flow angularity data of Figure 10 for the corresponding value of z/r and y/r at which the model metric section was located.

When discussing or comparing various section aerodynamic data, it is clear that α_s is the correct angle of attack to be used as a reference. (For a three-dimensional wing in a uniform free stream, it so happens that α_g and α_s are the same angle.) However, when considering three-dimensional effects, as are obviously obtained for a two-dimensional wing in an axially symmetric nonuniform jet, it seems proper that geometric angle of attack, or α_g, be used as a reference angle, admitting that there may be a certain degree of arbitrariness associated with α_g. The spanwise variation of flow angularity would appear to be an obvious factor of some importance as regards, for example, spanwise (three-dimensional) variation of lift or drag.

At z/r = 0.03 and 0.54 for all h/r, the behavior of C_l (Figures 16 and 17) is characterized by nearly linear increase up to α_s between 12 degrees and 15 degrees. In this range of α_s, there then occurs a reduction of $\partial C_l / \partial \alpha$ which varies in magnitude. Above this angle of attack, C_l continues to increase to section angles of attack near 30 degrees, whereupon there is a break in the C_l vs. α_s curve indicative of complete flow separation. The range of α_s between 12 degrees and 15 degrees corresponds to angles of attack at which the wing outside the jet, as exemplified by the section at z/r = 1.54, becomes fully stalled.

At z/r = 0.03 and 0.54, the variation of $C_{m_{\frac{c}{4}}}$ with C_l is relatively smooth up to nearly the C_l for complete separation (Figures 20 and 21). There is a tendency for the center of pressure to move aft very gradually as angle of attack increases beyond the 12-degree to 15-degree range, as exemplified by the variation of $\partial C_{m_{\frac{c}{4}}} / \partial C_l$ with C_l.

At z/r = 1.03, the variation of C_l with α_s is somewhat different. Well outside the jet in the viscous mixing region at h/r = 0.76 and -0.64 (Figures 18(a) and 18(d)), there are definite breaks in the C_l vs. α_s curves at α_s = 16 degrees and α_s = 11 degrees, respectively. Corresponding to these breaks, there are breaks in the $C_{m_{\frac{c}{4}}}$ vs. C_l curves (Figures 22(a) and 22(d)) indicative of an abrupt aft movement of the center of pressure and, apparently, at least partial separation on the wing section. The C_l and $C_{m_{\frac{c}{4}}}$ data at h/r = 0.46 show a similar tendency (Figures 18(b) and 22(b)), although not so marked. The C_l and $C_{m_{\frac{c}{4}}}$ data for h/r = -0.10 (Figures 18(c) and 22(c)) just on the edge of the jet are comparable to the corresponding data at z/r = 0.03 and 0.54 inside the jet. Nearly the same variation of $C_{m_{\frac{c}{4}}}$ vs. C_l was obtained for all sections except those at z/r = 1.54 up to α_s = 12 degrees to 15 degrees.

In the uniform flow completely outside the jet at $z/r = 1.54$, the behavior of C_L with α_s (Figure 19) and of C_{m_f} with C_L (Figure 23) indicates that complete separation occurs at α_s between 12.5 degrees and 15 degrees.

Comparison of these results with theory or previous experiment is limited by available pertinent data. The present data for $z/r = 0.03$ are comparable with two-dimensional experimental data from Reference 3 (Figure 1) because of the similar free-stream velocity profiles and Reynolds numbers. Neither of the nonuniform flow theories of References 6 and 7 is applicable because of their small shear and shear gradient approximation; however, the data at $z/r = 0.03$ are compared with the uniform two-dimensional shear theory of Tsien, Reference 5 (applicable to uniform shear), modified by the free-boundary (or jet-boundary) corrections derived in Reference 2.

The two-dimensional experimental values of C_L vs. α_s and C_{m_f} vs. C_L from Reference 3 are generally in good agreement with the data for corresponding h/r at $z/r = 0.03$, even including the lift increment at zero angle of attack (Figures 16 and 20) with the possible exception of $h/r = 0.76$. This is true up to the angle of attack at which the wing outside the jet stalls. The only other comparison with two-dimensional experimental sheared flow data is for $h/r = 0.46$, $z/r = 0.54$ (shown in Figure 17(b)), where the data are from Figure 22 of Reference 2, for a nonuniform sheared-flow profile reasonably similar to that at $z/r = 0.54$. Again, agreement is good up to $\alpha_s = 11$ degrees.

For $z/r = 1.54$, the free-stream velocity profile is nearly uniform. The two-dimensional uniform flow C_L vs. α_s data from Reference 2 for the same airfoil in the same wind tunnel are in poor agreement with the present data at $z/r = 1.54$ (see Figure 19) at all values of h/r; the agreement of the C_{m_f} vs. C_L data (Figure 23) is fair, with the possible exception of the data for $h/r = -0.10$. The Reference 2 uniform-flow data were obtained at a free-stream Reynolds number of 4.5×10^5 in a clear (no shear screen installed) wind-tunnel test section. The free-stream turbulence in the flow of the Reference 2 data was undoubtedly considerably lower than that at $z/r = 1.54$ during the present tests. At $z/r = 1.54$, the data correspond to a Reynolds number of about 2×10^5. Data concerning the effects on maximum lift at stall and lift-curve slope associated with Reynolds number in the range 2×10^5 to 5×10^5 are limited. However, tests on the same model in a uniform flow with screen-generated turbulence are noted in Reference 3, where it is stated that an 8 percent increase in maximum lift was obtained as compared to the Reference 2 uniform flow data. This is somewhat smaller than the 35 percent to 60 percent increase shown in Figure 19.

Data obtained by Brenckmann, Reference 14, appear to corroborate the increase in lift at stall shown in Figure 19. His experiments were performed with a wing of 18 percent thickness-to-chord ratio partially immersed in a slipstream generated by a propeller; hence, there was only the normal free-stream wind-tunnel turbulence outside the slipstream. Although Brenckmann's data with propeller slipstream (for $z/r = 2.5$, $y/r \approx 0$) do not show the abrupt

loss of lift at $(C_L)_{max}$, they do show higher lift and higher lift-curve slope than the corresponding data without slipstream.

On the basis of the comparison of two-dimensional data from Reference 3, and the present three-dimensional data, it must be concluded that the wing aerodynamic behavior near the center of the jet with its highly nonuniform sheared flow is essentially two-dimensional up to nearly the angle of attack at which stall first occurs on the wing outside the jet. On the wing outside the jet over the same angle-of-attack range, three-dimensional effects are apparently of some importance. It appears that once that portion of the wing outside the jet stalls, the flow inside the jet over the wing is also highly three-dimensional, although only the two-dimensional experimental data in Figure 13(c) for h/r = -1/8 from Reference 3 are available at sufficiently high angles of attack to corroborate this conjecture.

At z/r = 0.03, the two-dimensional Tsien theory (Reference 5) with free-boundary corrections derived in Reference 2 agrees fairly well with the C_L vs. α data (Figure 16) for all h/r except h/r = -0.10. However, the $C_{m_{\frac{1}{4}}}$ vs. C_L variation predicted by the theory (Figure 20) is grossly in error at all h/r. For positive values of the shear parameter K, the center of pressure is predicted too far aft, and for negative K, too far forward on the wing section. No attempt at a comparison of experimental data with the theories of References 6 or 7 was made, as it was apparent that the values of K associated with the experimental data were not in accord with the assumptions upon which these theories were based.

3. Wing Lift Characteristics:

The lift variation vs. geometric angle of attack, α_G, at varying z/r for each of the four values of h/r tested is shown in Figure 24. In these plots $\hat{C}_L$ is a lift coefficient referenced to an average dynamic pressure where

$$\hat{q} = \frac{1}{2}(q_o + \bar{q}),$$

q_o is the uniform flow dynamic pressure exterior to the jet, and $\bar{q}$ is the average dynamic pressure in the jet. As $\hat{C}_L$ is based on a constant dynamic pressure, the $\hat{C}_L$ variation is then representative of the lift variation. The data for z/r = 1.54, obtained at low q, were adjusted to be comparable to the high q data on the basis of the average velocity in the free stream at z/r = 1.54 for the two mass flows.

Noteworthy in Figure 24 is the variation of section lift on the wing in the higher velocity portions of the jet. In Figure 24(a), (h/r = +0.76), the lift at z/r = 0.03 and 0.54 is only about 30 percent higher than at z/r = 1.54, although the dynamic pressures were at least four times those at z/r = 1.54. In contrast, the wing section at z/r = 0.03, h/r = -0.10 develops somewhat more lift than the z/r = 1.54 sections at very nearly the same dynamic pressure. This is in the region of the free-stream velocity profile at z/r = 0.03 where destalling effect was previously noted in the corresponding

two-dimensional nonuniform sheared flow.

Also notable in Figure 24 is that the spanwise distribution of α_ϵ for zero lift varies remarkably little. As far as the generation of total wing lift is concerned, over the entire angle-of-attack range, there appears to be no great advantage of one h/r over another. At h/r = +0.46 and -0.10, slightly higher lift is developed by the wing on the edge of the jet (z/r = 1.03).

The lift variations with wing vertical height at constant z/r's are shown in Figure 25. It is noted, particularly at z/r = 0.03 and 0.54, how little variation in lift at a given wing angle of attack there is with wing vertical location in the jet, at least up to the outer wing stall angle. Figure 25(c), for z/r = 1.03, shows more variation, but only for h/r = 0.76, which is the wing section location farthest from the jet centerline. The change in initial stall characteristics between α_ϵ = 12 degrees and α_ϵ = 16 degrees is clearly evident in Figure 25(c); h/r = 0.76, 0.46, and -0.64 are all in the outer mixing region of the jet at z/r = 1.03 (see Figure 8(c)) and, hence, closer to the portions of the wing in the outer uniform flow, which are fully stalled at these angles of attack. These sections show increasing tendency to stall, with less lift beyond α_G = 16 degrees, the further they are from h/r = 0.

As a further test of the two-dimensionality of the aerodynamic behavior of the wing at z/r = 0.03, the pertinent two-dimensional nonuniform sheared flow C_ℓ vs. α_s data from Reference 3 (some of which is shown in Figure 2) were adjusted to the dynamic pressure and α_G of the present data. The results are plotted in Figure 25(a). Up to α_G = 10 degrees, there is remarkably little variation between the data derived from the two-dimensional data of Reference 3 and the present three-dimensional data. Above α_G = 10 degrees, apparently, the three-dimensional effects become significant. It is unfortunate that data were not obtained at z/r = 0.03, h/r = +1/8 during the present three-dimensional tests. Such data would have allowed an even more positive confirmation (or rejection) of the apparent two-dimensionality of the flow over the wing near the center of the slipstream.

The data of Figures 24 and 25 are cross-plotted in Figure 26 in terms of $\hat{C}_\ell$ vs. z/r at constant wing geometric angle of attack for the various wing heights. These spanwise lift distributions are suggestive of those of low aspect ratio wings at wing geometric angles of attack beyond the initial stall. This idea is made more plausible if one considers that once the outer wing stalls, there is a marked reduction in lift on the wing at the edge of the slipstream. The corresponding change in wing circulation would result in a strong concentration of trailing vorticity from the wing at the edge of the slipstream.

4. Flow Visualization Tests:

A spanwise and chordwise distribution of tufts was attached to the upper wing surface and observed at various angles of attack in the flow at all vertical positions of the wing for which section aerodynamic coefficients were obtained.

Photos taken during the tests for h/r = -0.10 are presented in Figure 27 and are typical of the other h/r.

In Figure 27, the flow is clearly attached for angles of attack up to 12 degrees. At 12.5 degrees, the flow has separated outside the slipstream. From 17.5 degrees up to 24 degrees, the separation point of the flow inside the slipstream appears to be moving from the trailing edge forward; at 28 degrees, the flow is nearly completely separated. Although not too clearly evident in Figure 27, the chordwise separation point appeared to be further forward at a given angle of attack in the center of the slipstream than it was at either edge of the slipstream. At angles of attack above 12.5 degrees, the tufts gave evidence of considerable spanwise flow in the separated regions along the wing both inside and outside the slipstream. The spanwise flow outside the slipstream in the separation wake could be influenced by the sidewall suction; however, in many instances in the vicinity of $\alpha_c \approx 15$ degrees, the tufts on the outer wing near the wing leading edge were directed toward the wall whereas near the trailing edge, the tufts were directed toward the slipstream. Inside the slipstream, tuft inclination after initial stall was toward the slipstream centerline.

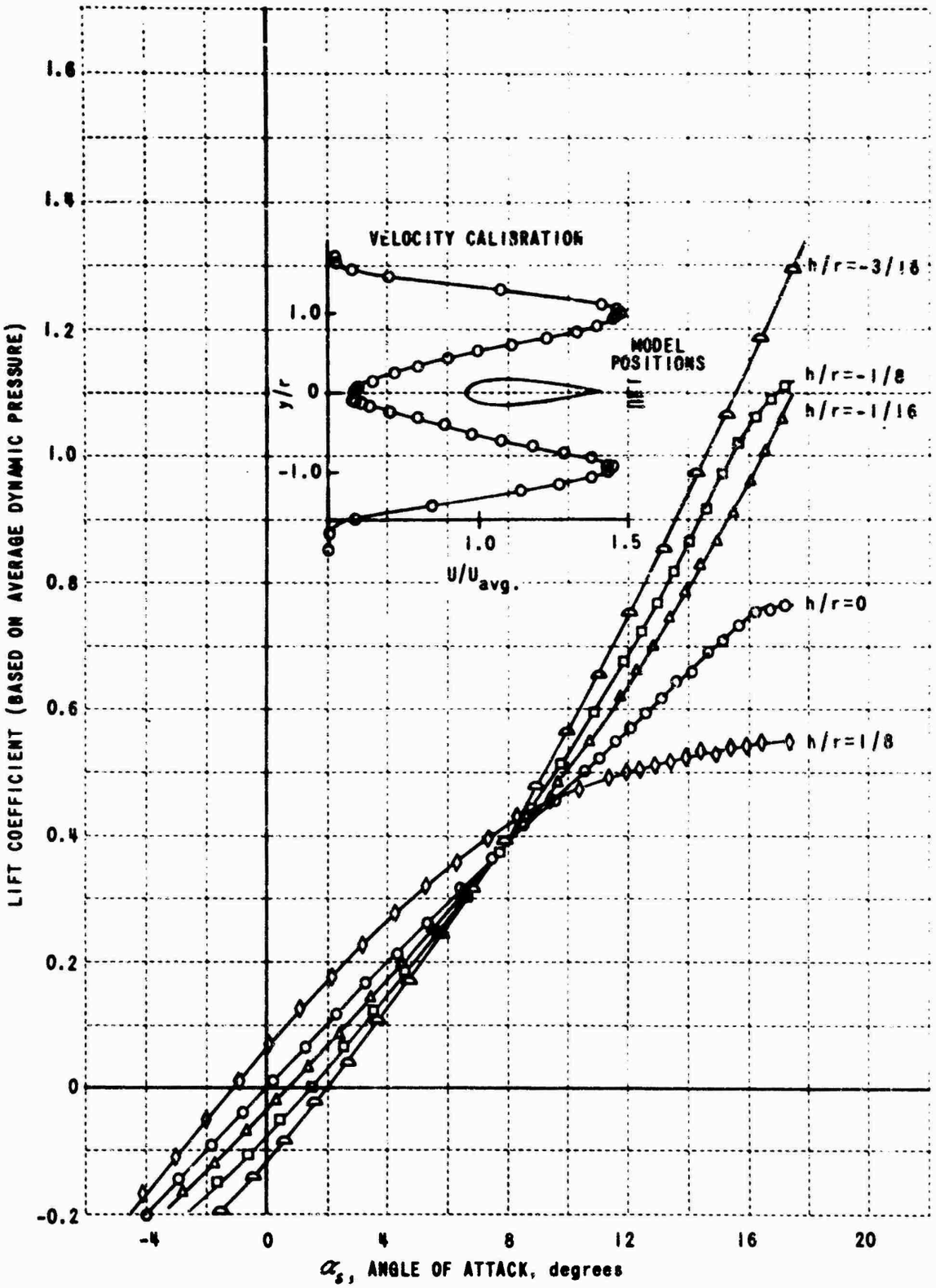

Figure 1. SECTION LIFT COEFFICIENT BASED ON AVERAGE DYNAMIC PRESSURE IN A TWO-DIMENSIONAL NONUNIFORM SHEARED FLOW

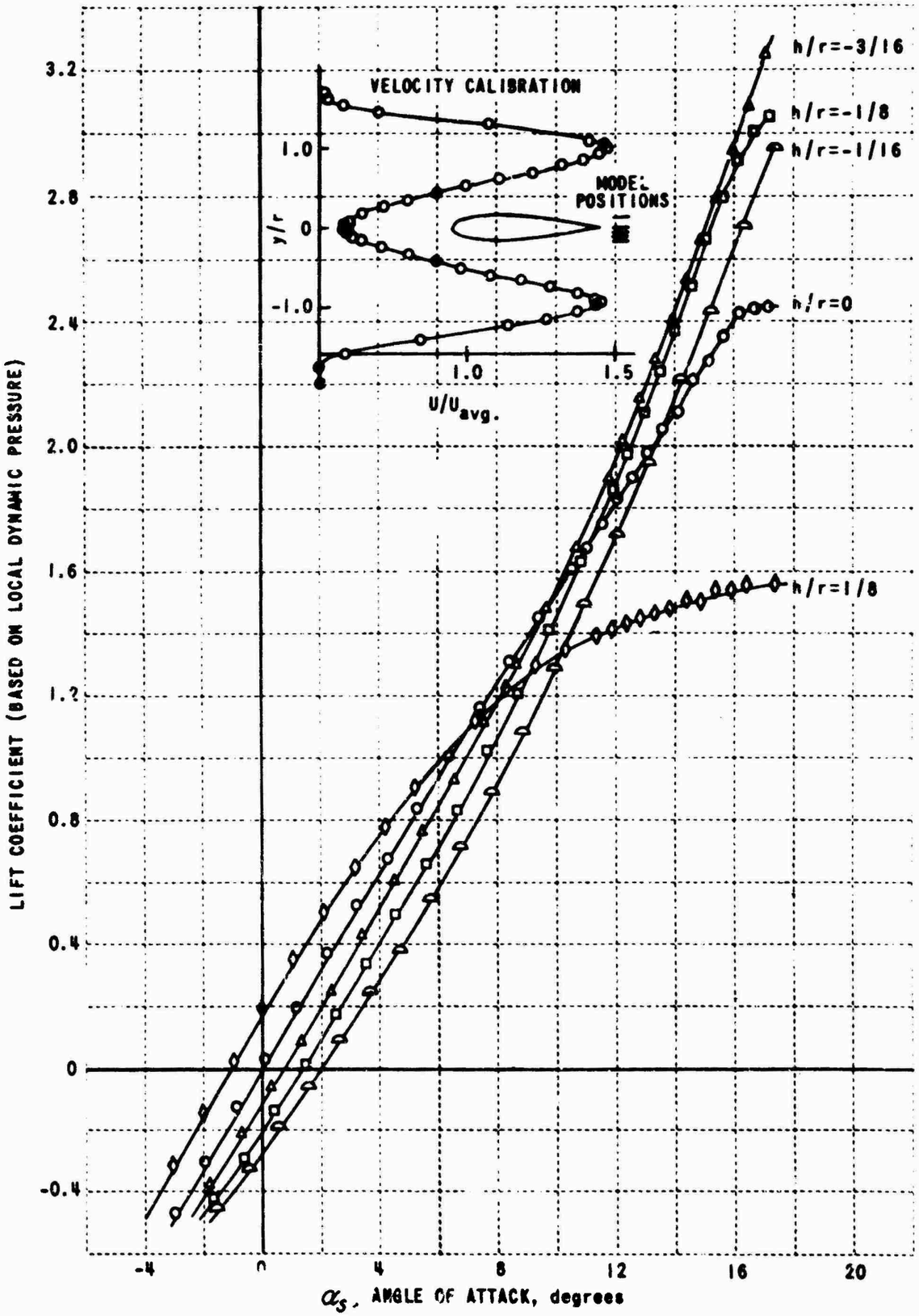

Figure 2. SECTION LIFT COEFFICIENT BASED ON LOCAL DYNAMIC PRESSURE IN A TWO-DIMENSIONAL NONUNIFORM SHEARED FLOW

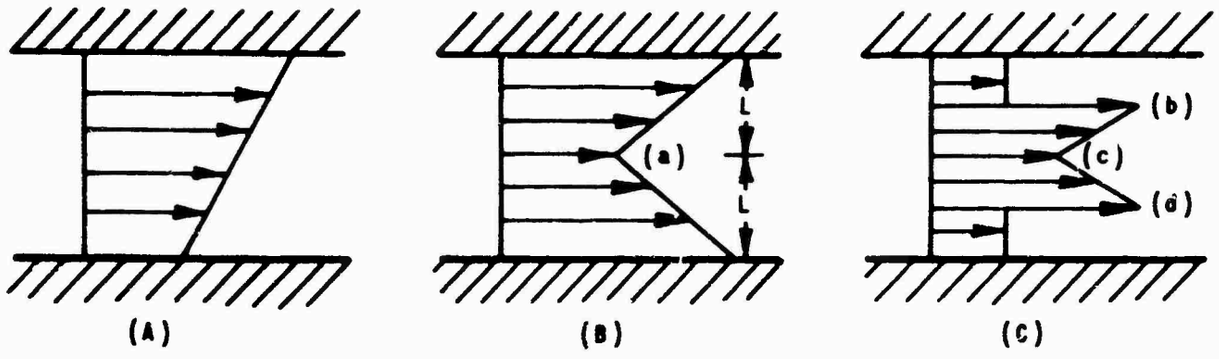

Figure 3. TYPICAL VELOCITY PROFILES SUITABLE FOR ANALYTICAL PROGRAM

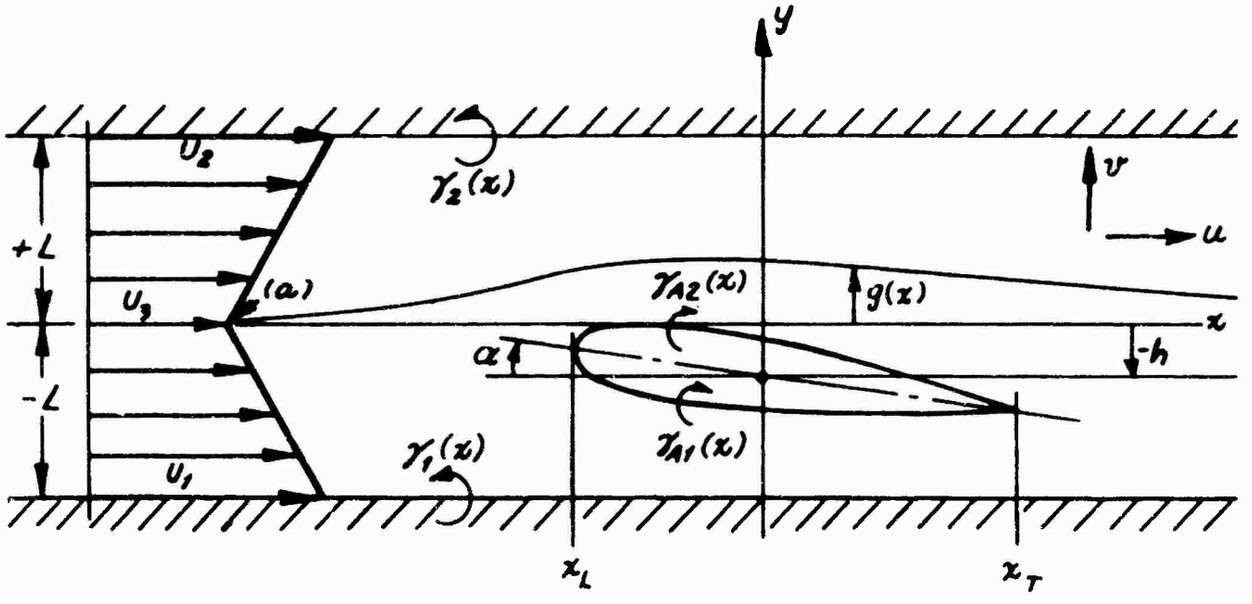

Figure 4. SCHEMATIC OF FLOW MODEL

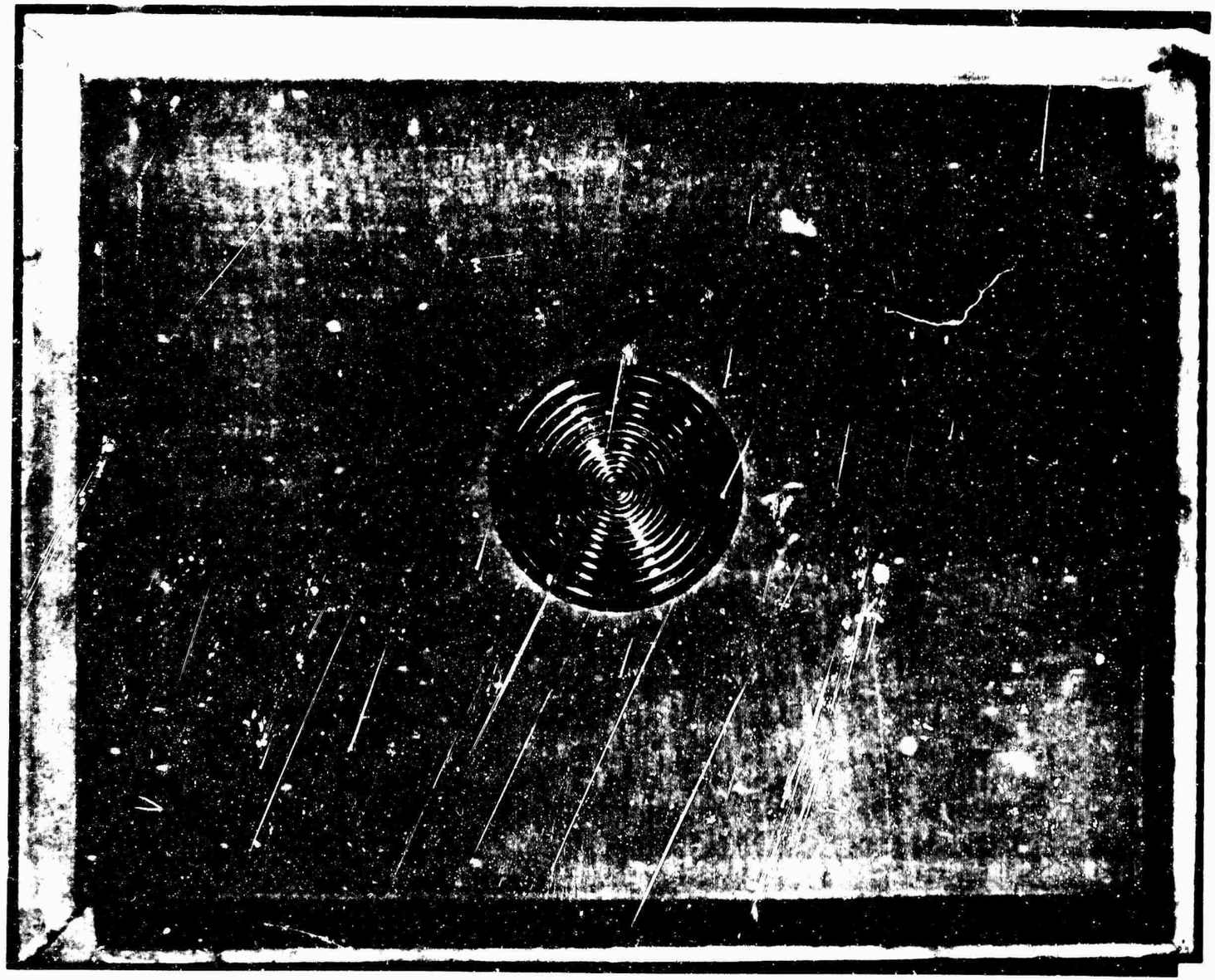

Figure 5. UPSTREAM SIDE OF AXISYMMETRIC SHEAR SCREEN

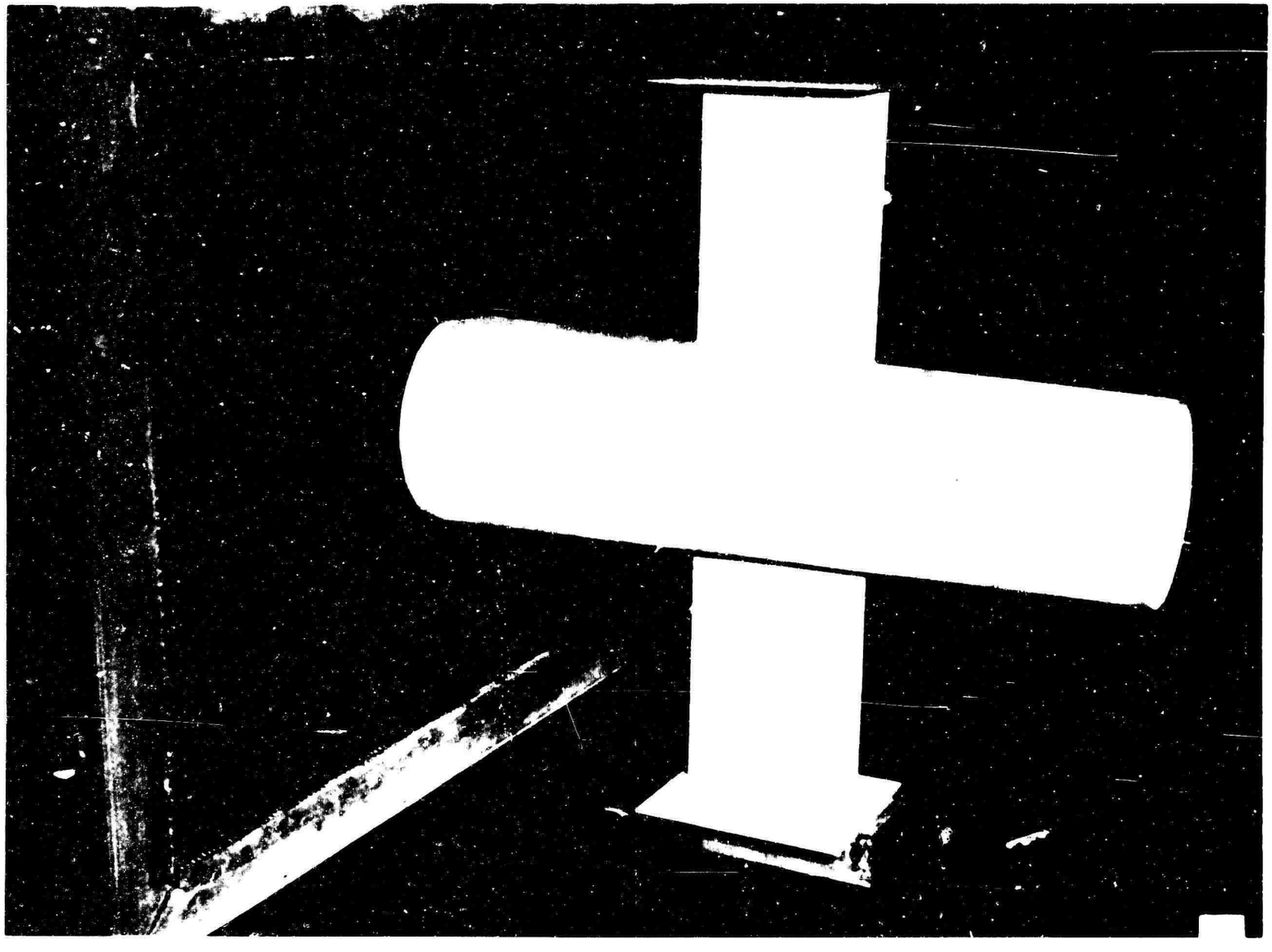

Figure 6. DOWNSTREAM SIDE OF AXISYMMETRIC SHEAR SCREEN WITH DUCT

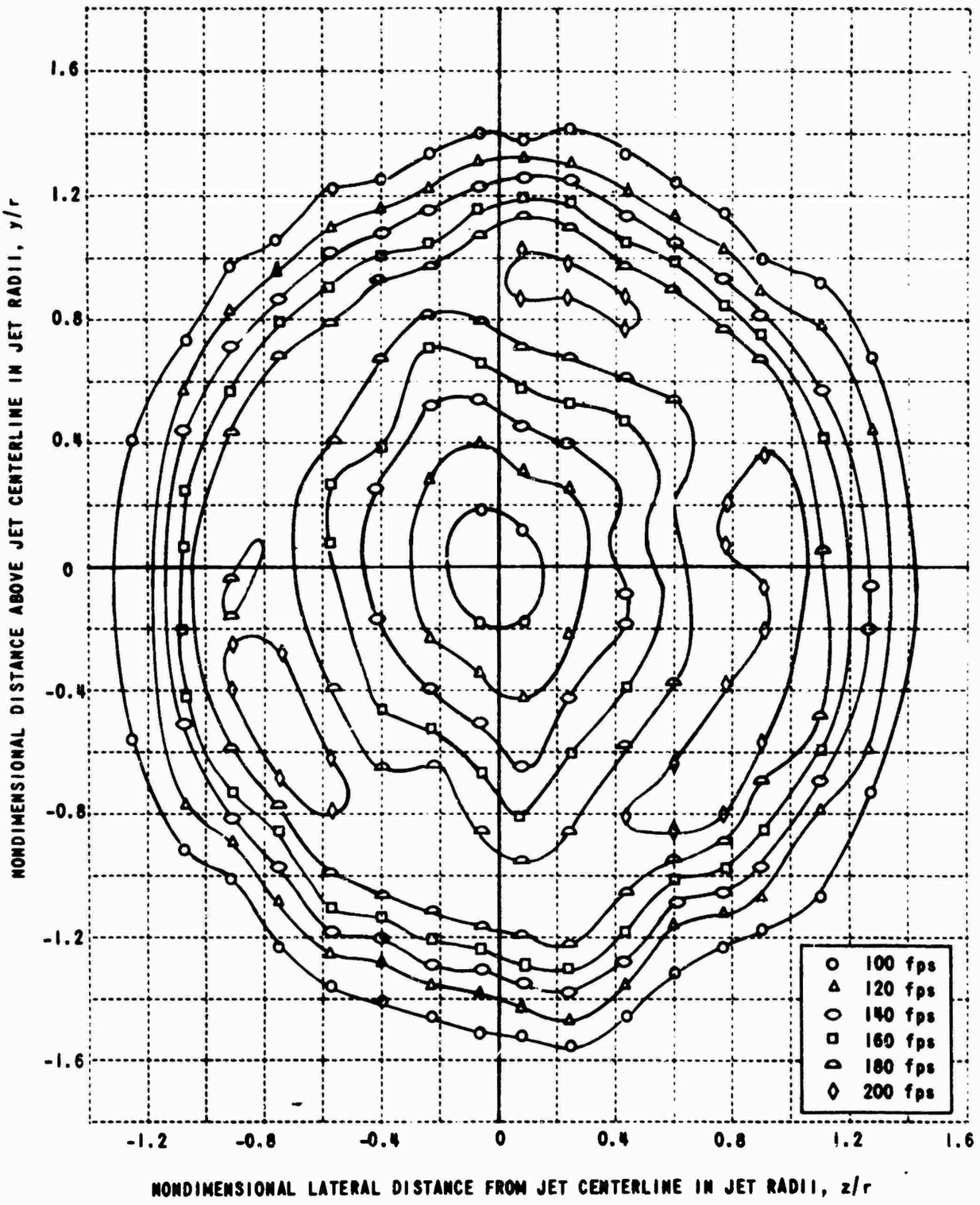

Figure 7. SHEARED FLOW ISOVELOCITY CONTOURS AT MODEL MIDCHORD STATION IN TEST SECTION, LOOKING UPSTREAM, HIGH q

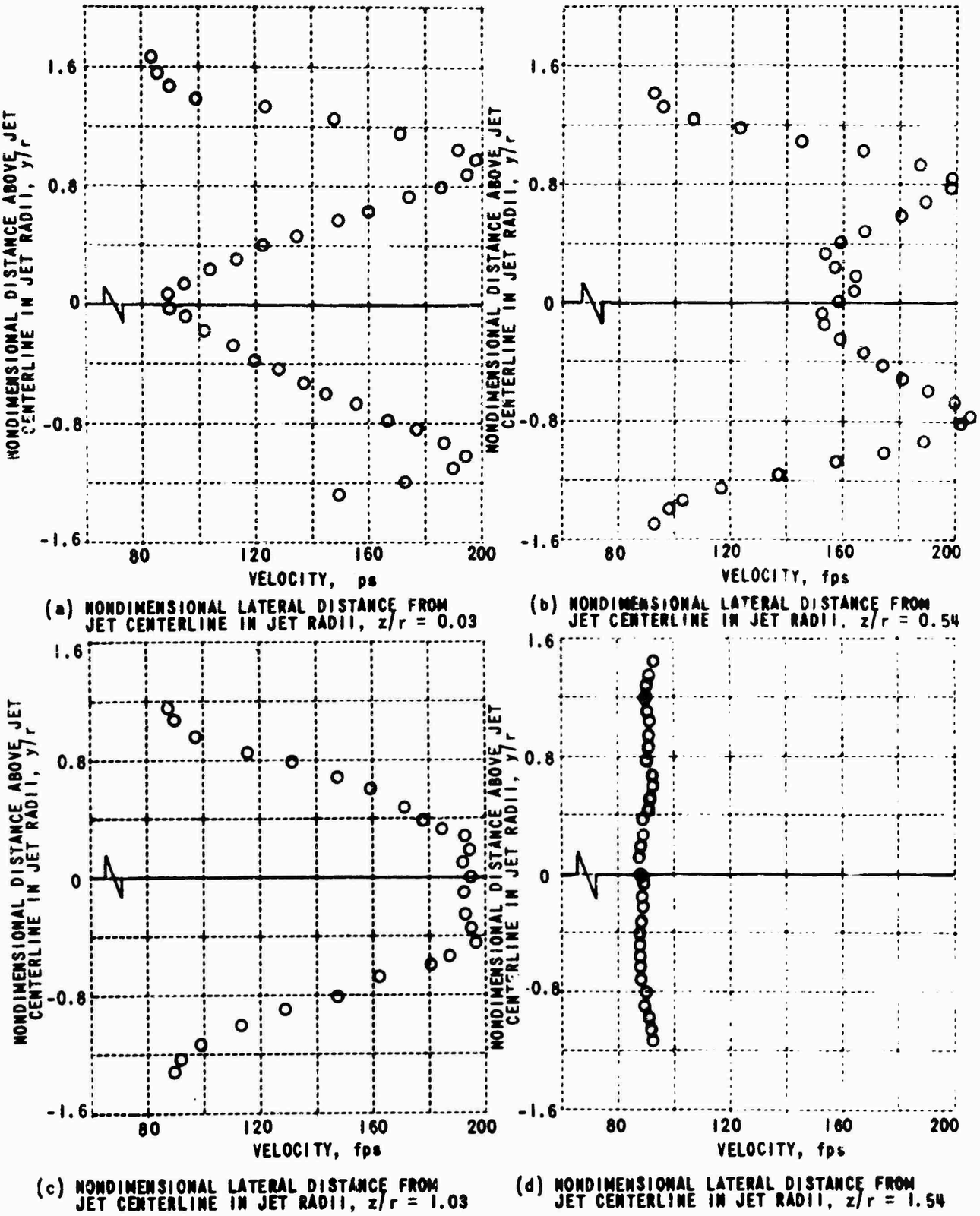

(a) NONDIMENSIONAL LATERAL DISTANCE FROM JET CENTERLINE IN JET RADII, z/r = 0.03

(b) NONDIMENSIONAL LATERAL DISTANCE FROM JET CENTERLINE IN JET RADII, z/r = 0.54

(c) NONDIMENSIONAL LATERAL DISTANCE FROM JET CENTERLINE IN JET RADII, z/r = 1.03

(d) NONDIMENSIONAL LATERAL DISTANCE FROM JET CENTERLINE IN JET RADII, z/r = 1.54

Figure 8. SHEARED FLOW VELOCITY DISTRIBUTIONS, HIGH q

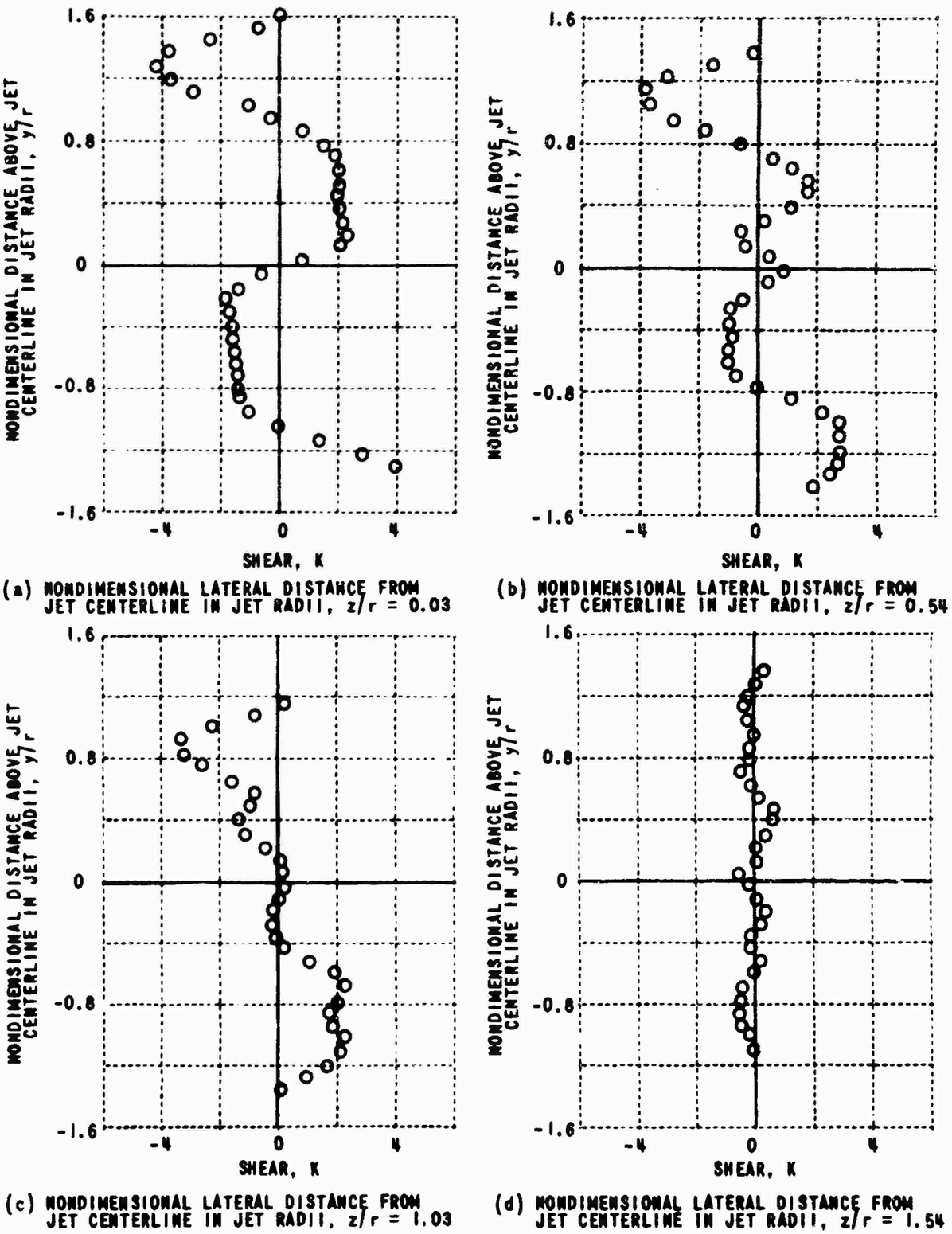

(a) NONDIMENSIONAL LATERAL DISTANCE FROM JET CENTERLINE IN JET RADII, z/r = 0.03

(b) NONDIMENSIONAL LATERAL DISTANCE FROM JET CENTERLINE IN JET RADII, z/r = 0.54

(c) NONDIMENSIONAL LATERAL DISTANCE FROM JET CENTERLINE IN JET RADII, z/r = 1.03

(d) NONDIMENSIONAL LATERAL DISTANCE FROM JET CENTERLINE IN JET RADII, z/r = 1.54

Figure 9. DISTRIBUTION OF SHEAR PARAMETER K, HIGH q

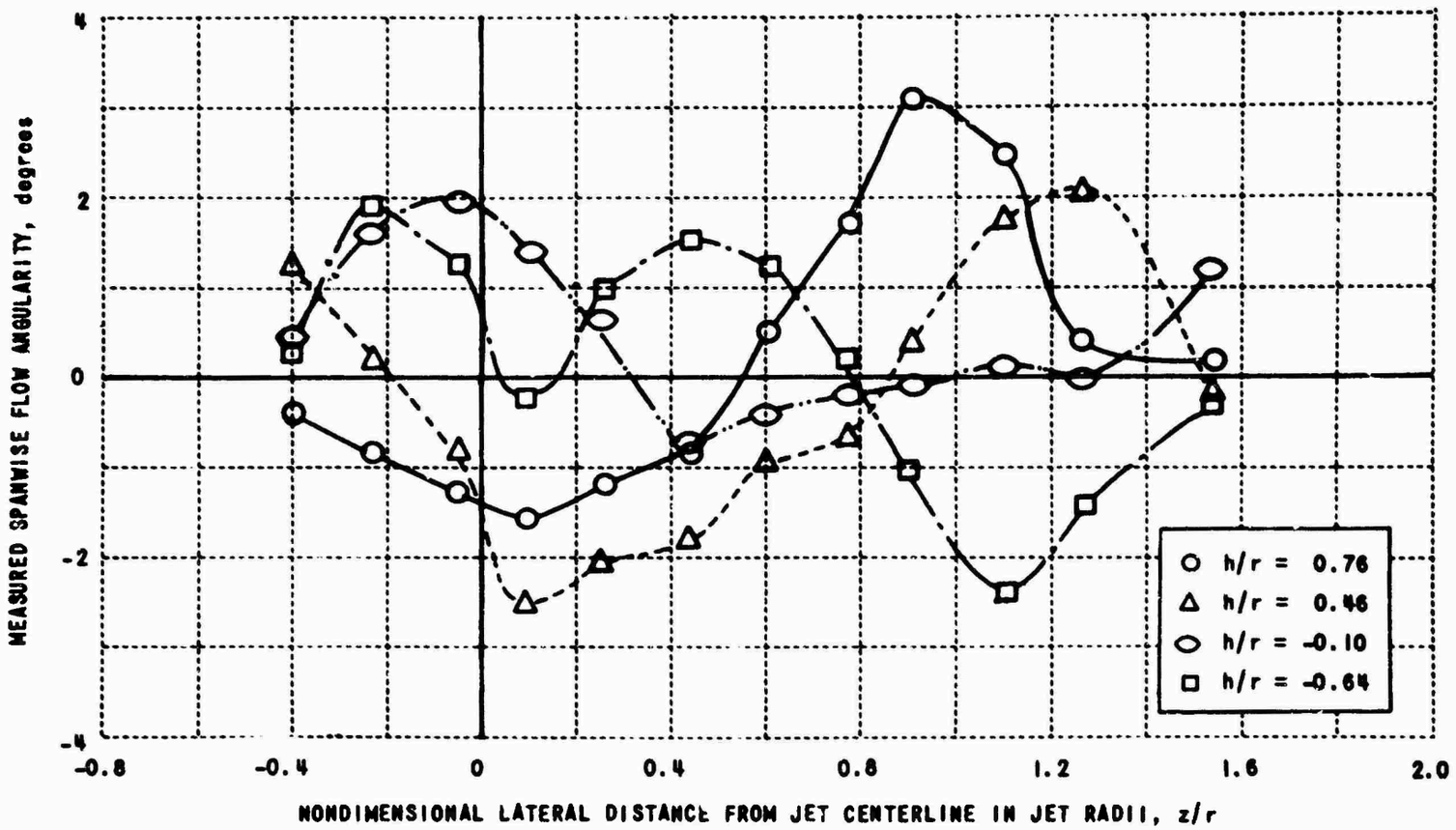

Figure 10. EXPERIMENTAL SPANWISE DISTRIBUTION OF FREE-STREAM FLOW ANGULARITY

Figure 11. WIND TUNNEL WING MODEL SUPPORT AND MODEL

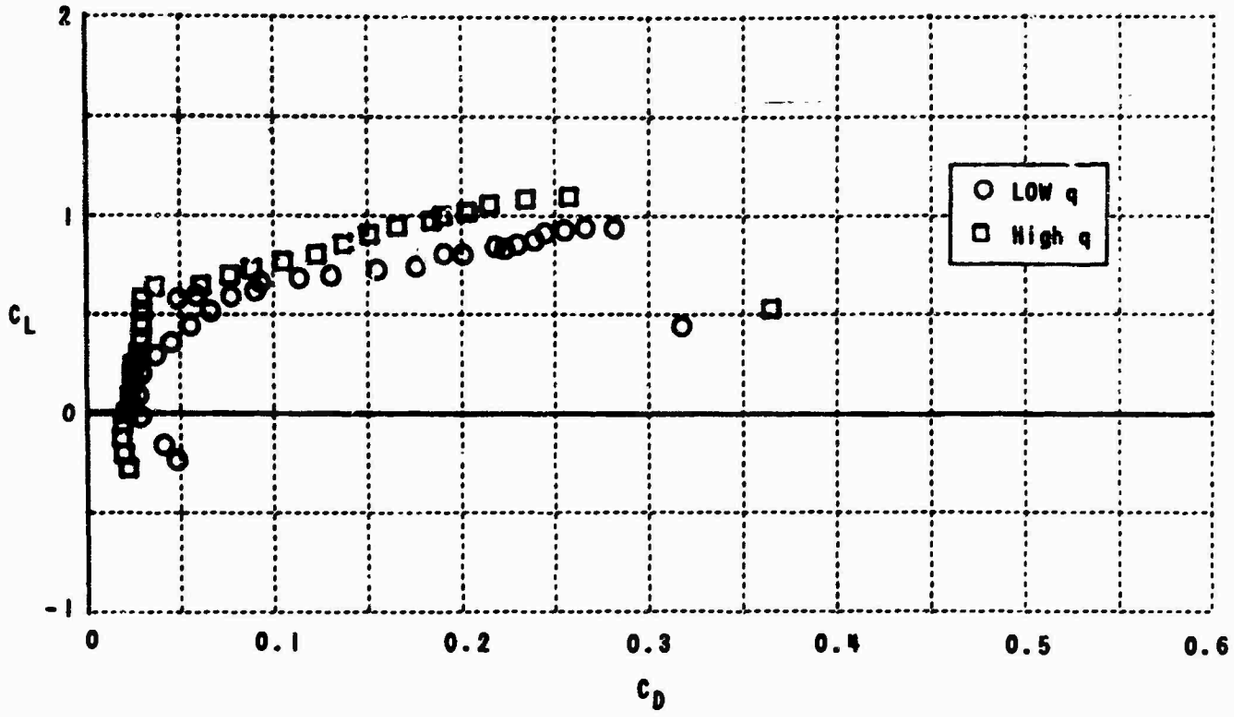

(a) NONDIMENSIONAL HEIGHT OF WING MIDCHORD ABOVE JET CENTERLINE IN JET RADII, $h/r = 0.76$

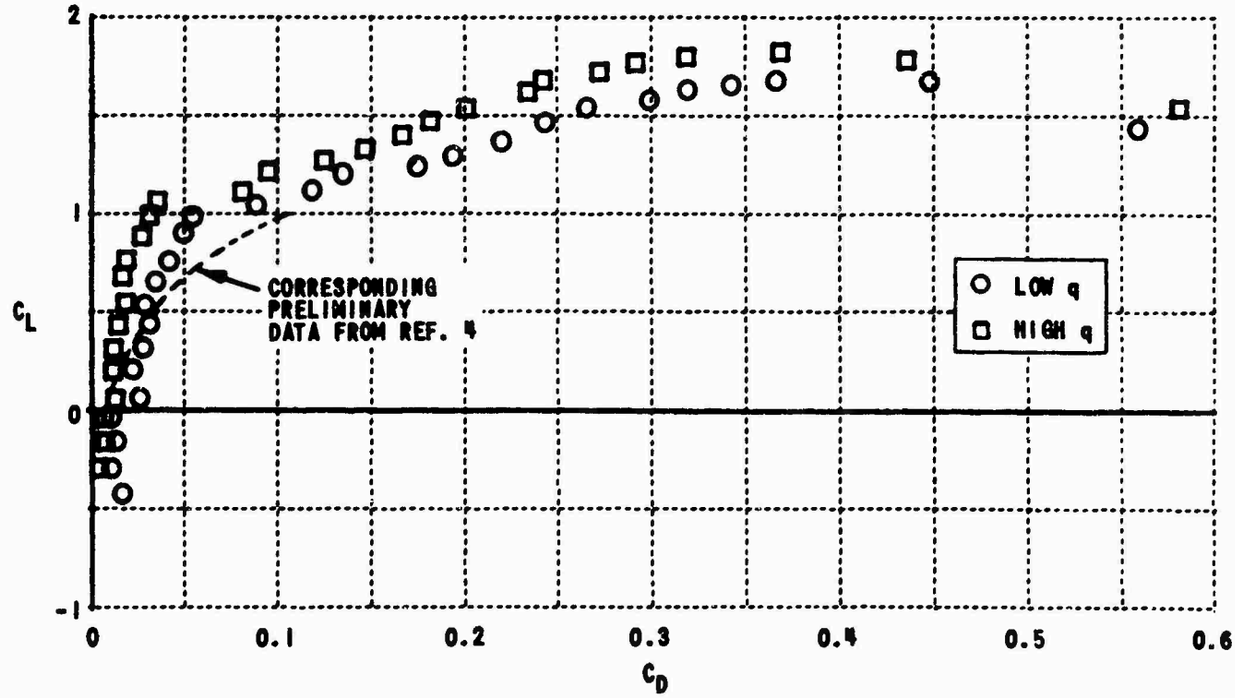

(b) NONDIMENSIONAL HEIGHT OF WING MIDCHORD ABOVE JET CENTERLINE IN JET RADII, $h/r = 0.46$

Figure 12. SECTION LIFT COEFFICIENTS vs. SECTION DRAG COEFFICIENT, $z/r = 0.03$

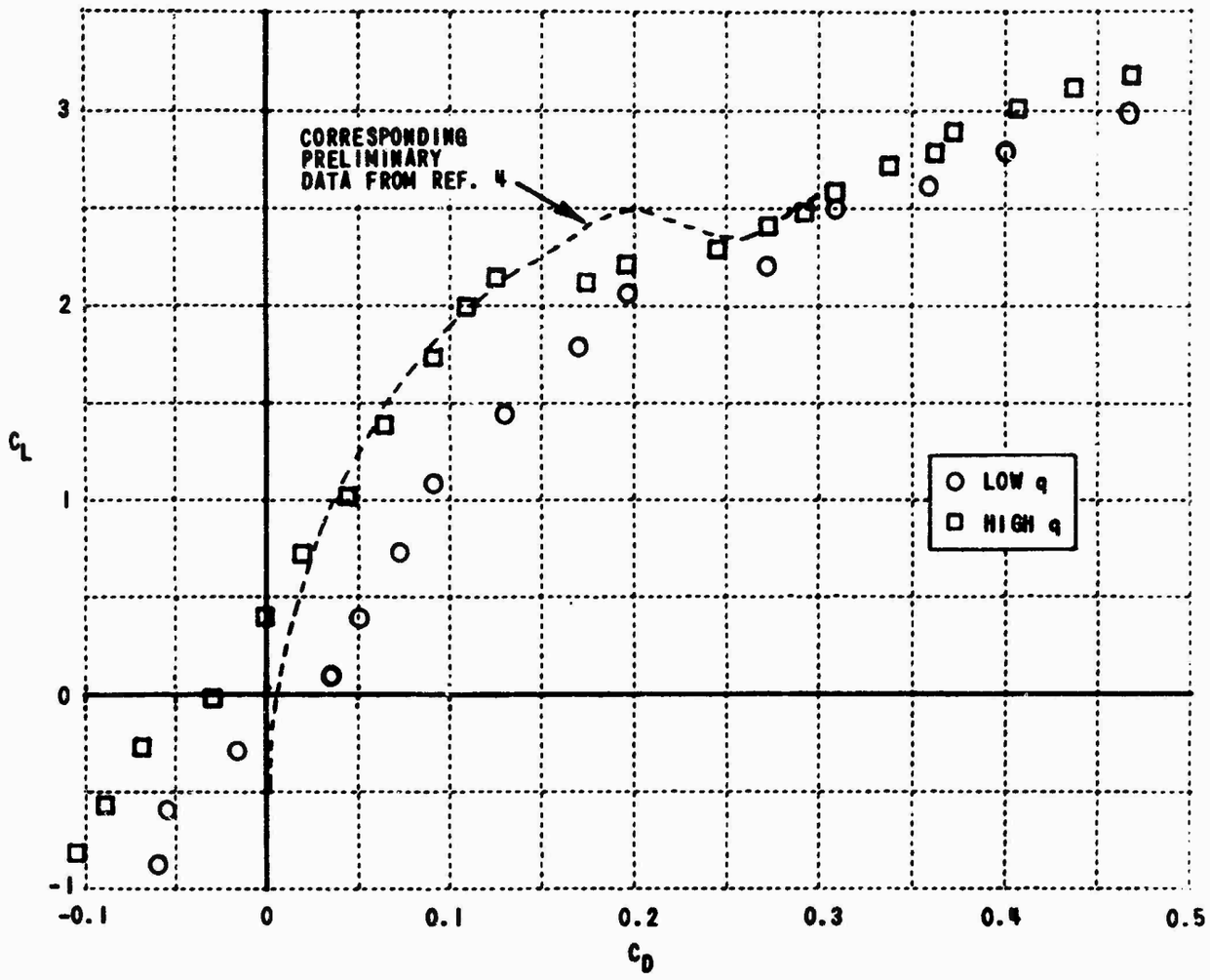

(c) NONDIMENSIONAL HEIGHT OF WING MIDCHORD ABOVE JET CENTERLINE IN JET RADII, h/r = -0.10

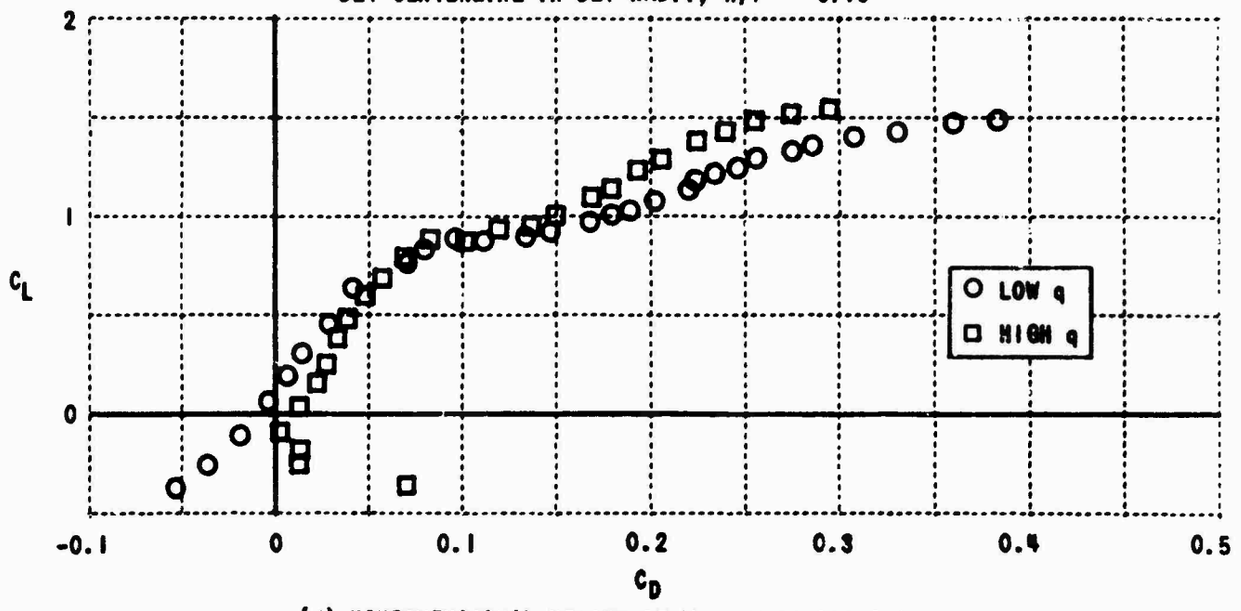

(d) NONDIMENSIONAL HEIGHT OF WING MIDCHORD ABOVE JET CENTERLINE IN JET RADII, h/r = -0.64

Figure 12. SECTION LIFT COEFFICIENTS vs. SECTION DRAG COEFFICIENT, z/r = 0.03

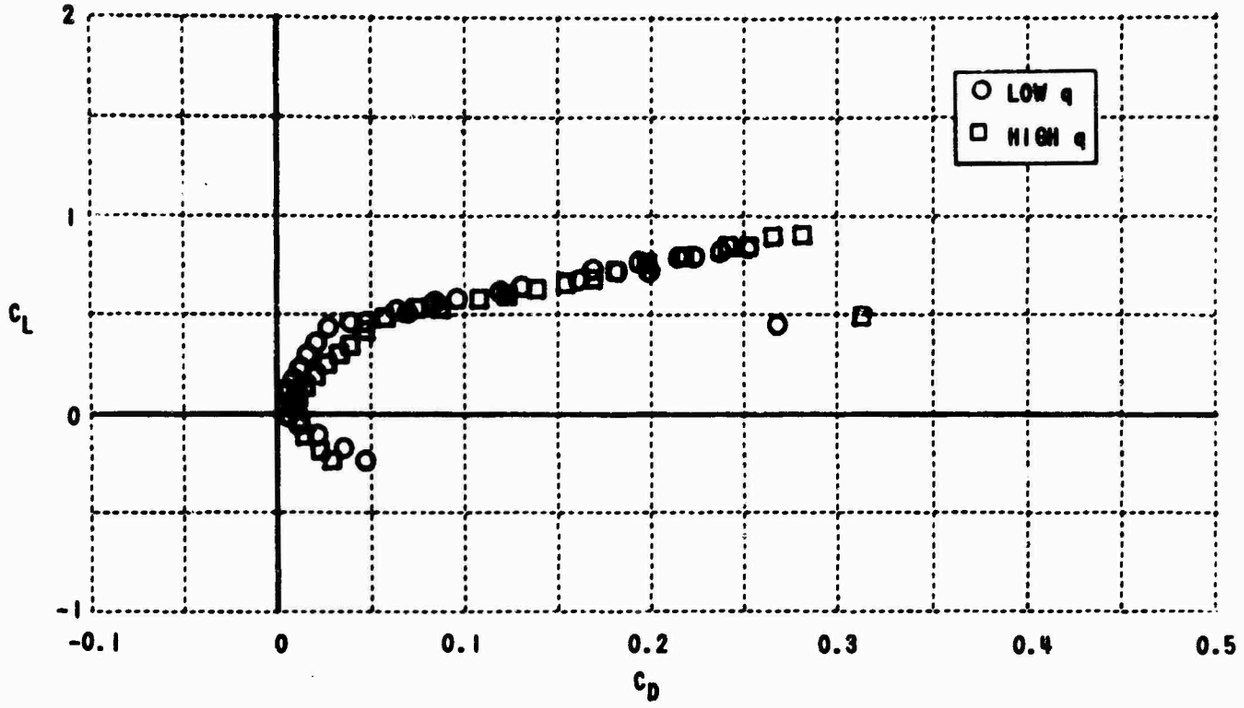

(a) NONDIMENSIONAL HEIGHT OF WING MIDCHORD ABOVE JET CENTERLINE IN JET RADII, h/r = 0.76

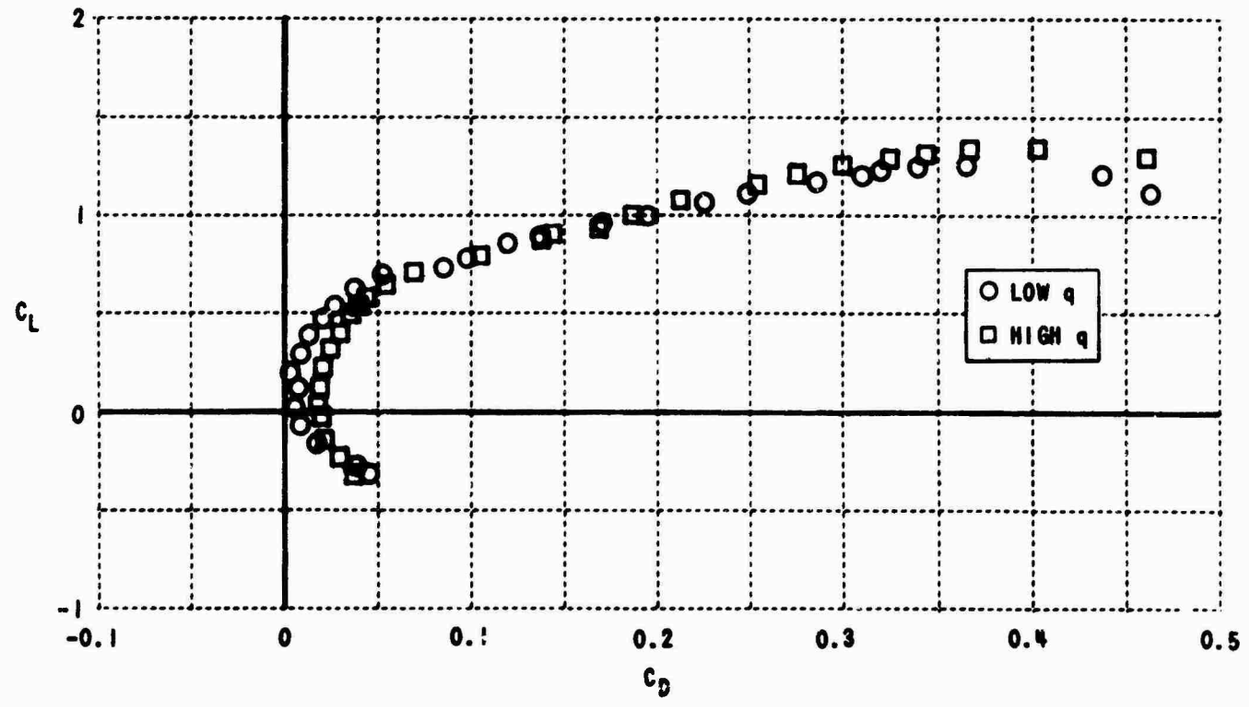

(b) NONDIMENSIONAL HEIGHT OF WING MIDCHORD ABOVE JET CENTERLINE IN JET RADII, h/r = 0.46

Figure 13. SECTION LIFT COEFFICIENTS vs. SECTION DRAG COEFFICIENT, z/r = 0.54

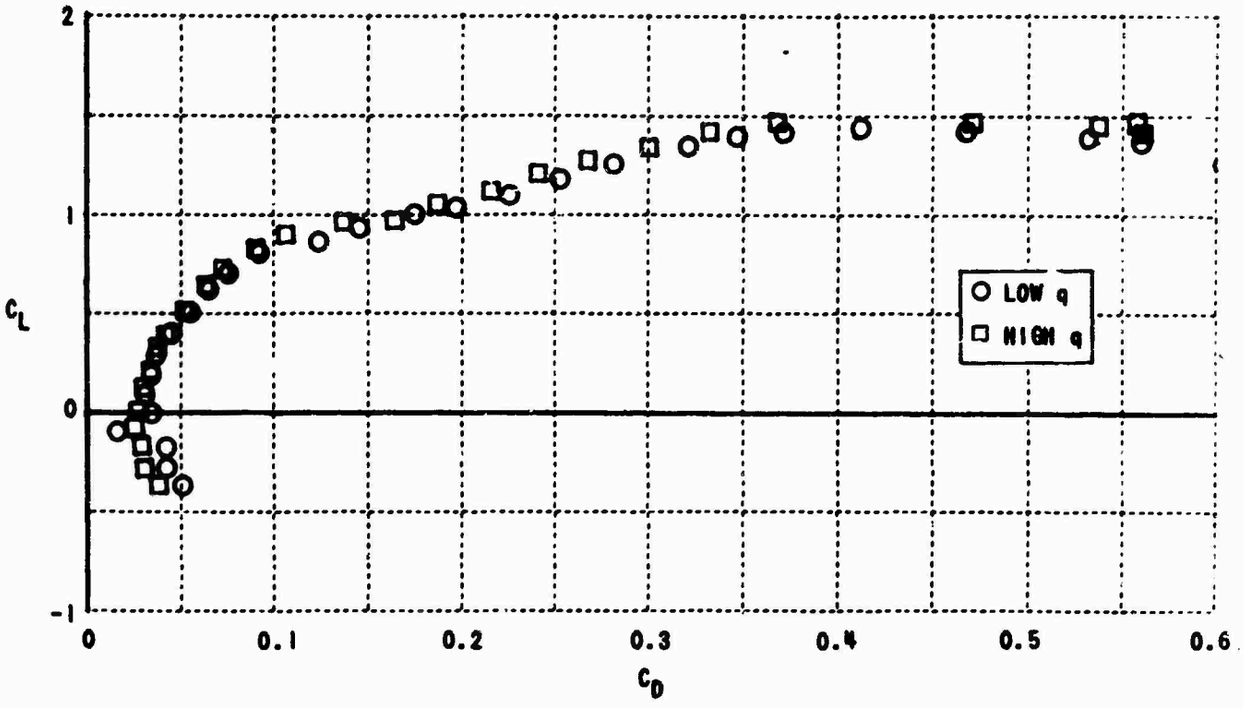

(c) NONDIMENSIONAL HEIGHT OF WING MIDCHORD ABOVE JET CENTERLINE IN JET RADII, h/r = -0.10

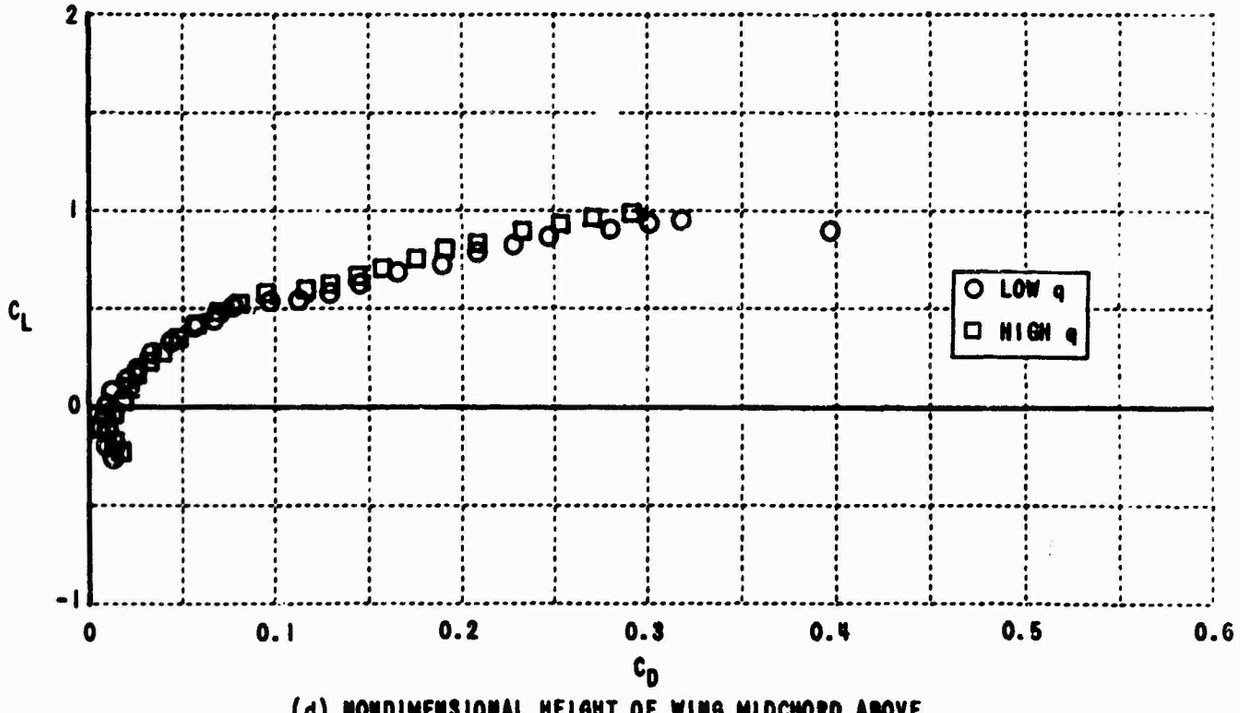

(d) NONDIMENSIONAL HEIGHT OF WING MIDCHORD ABOVE JET CENTERLINE IN JET RADII, h/r = -0.64

Figure 13. SECTION LIFT COEFFICIENTS vs. SECTION DRAG COEFFICIENT, z/r = 0.54

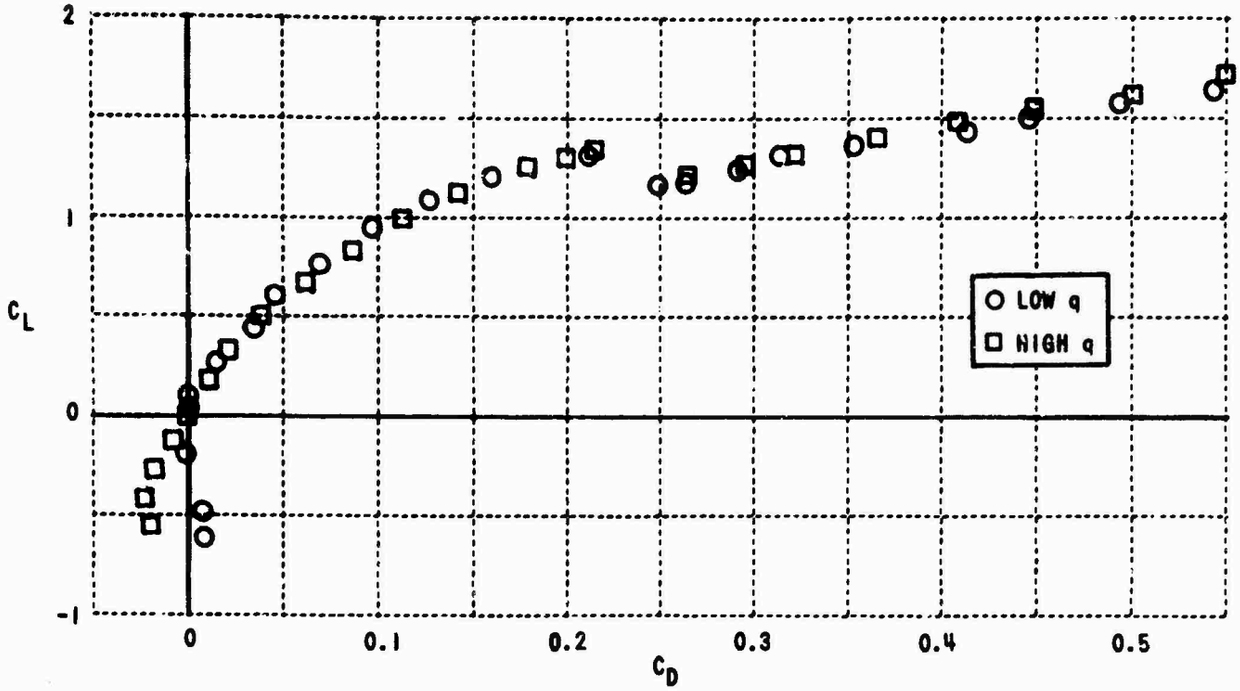

(a) NONDIMENSIONAL HEIGHT OF WING MIDCHORD ABOVE JET CENTERLINE IN JET RADII, $h/r = 0.76$

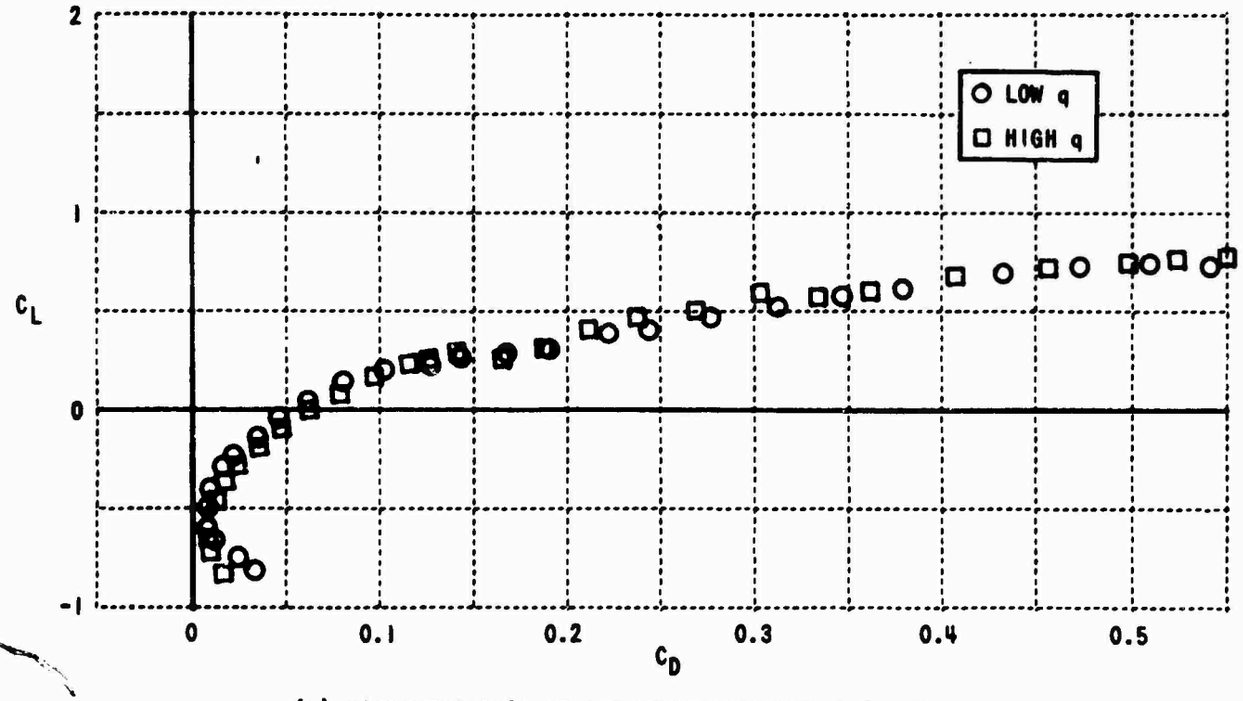

(b) NONDIMENSIONAL HEIGHT OF WING MIDCHORD ABOVE JET CENTERLINE IN JET RADII, $h/r = 0.46$

Figure 14. SECTION LIFT COEFFICIENTS vs. SECTION DRAG COEFFICIENT, $z/r = 1.03$

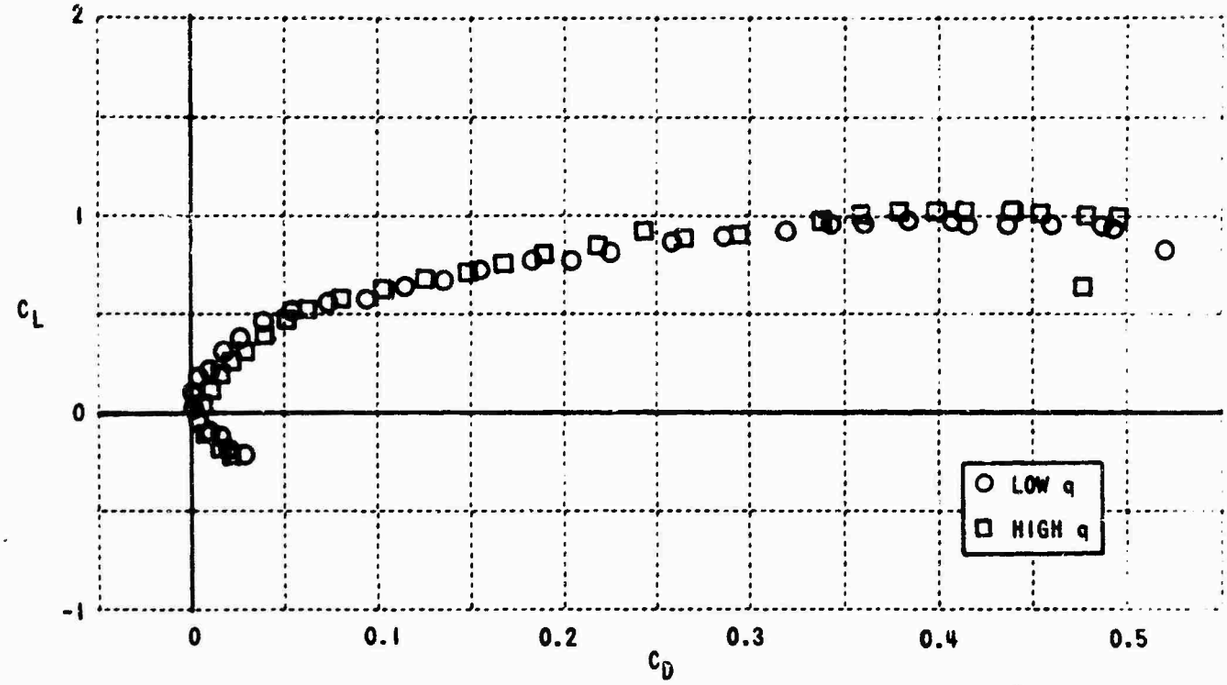

(c) NONDIMENSIONAL HEIGHT OF WING MIDCHORD ABOVE JET CENTERLINE IN JET RADII, h/r = -0.10

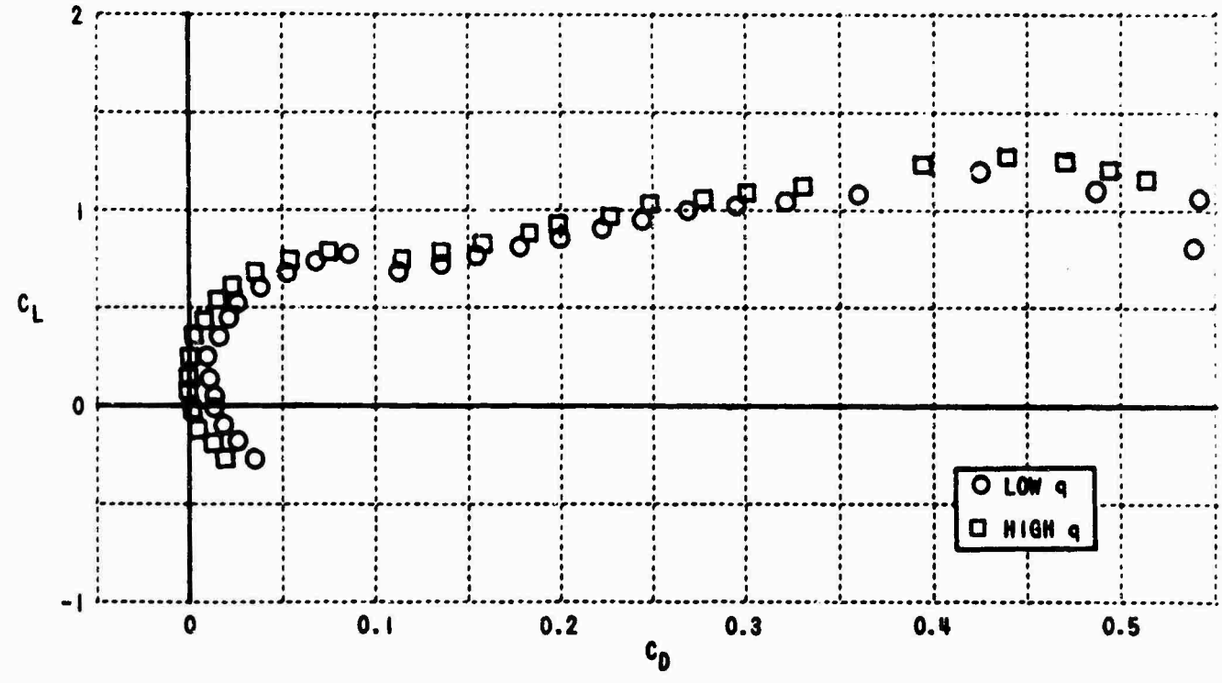

(d) NONDIMENSIONAL HEIGHT OF WING MIDCHORD ABOVE JET CENTERLINE IN JET RADII, h/r = -0.64

Figure 14. SECTION LIFT COEFFICIENTS vs. SECTION DRAG COEFFICIENT, z/r = 1.03

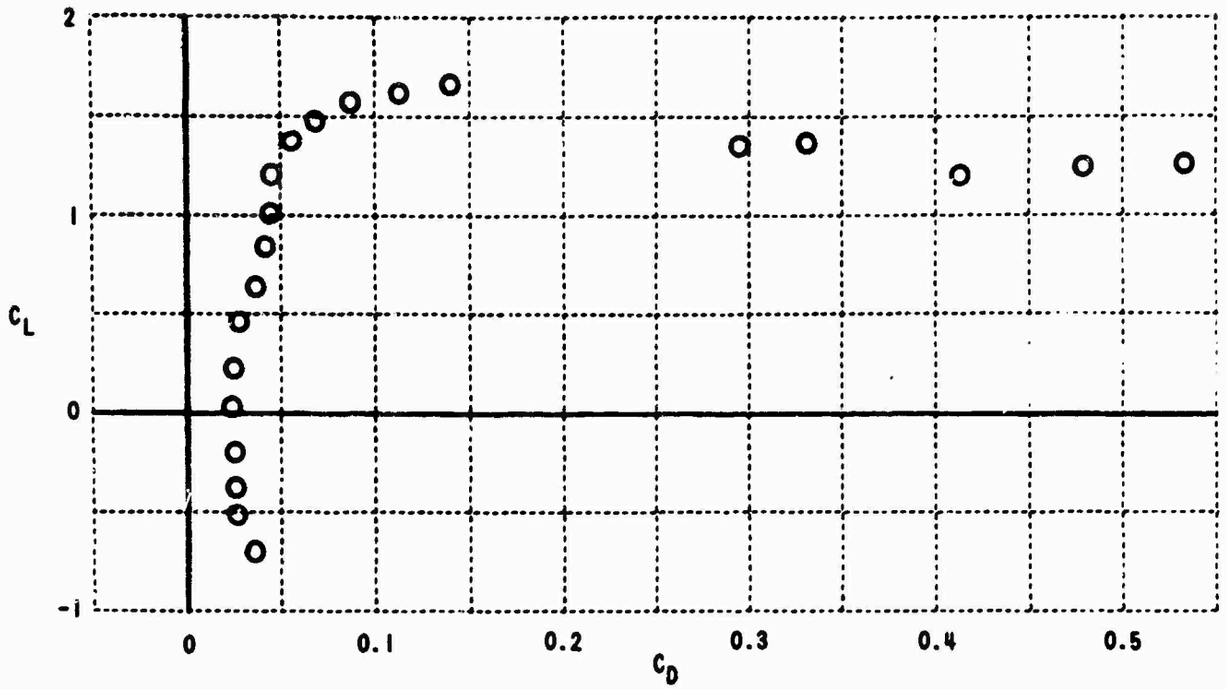

(a) NONDIMENSIONAL HEIGHT OF WING MIDCHORD ABOVE JET CENTERLINE IN JET RADII, h/r = 0.76

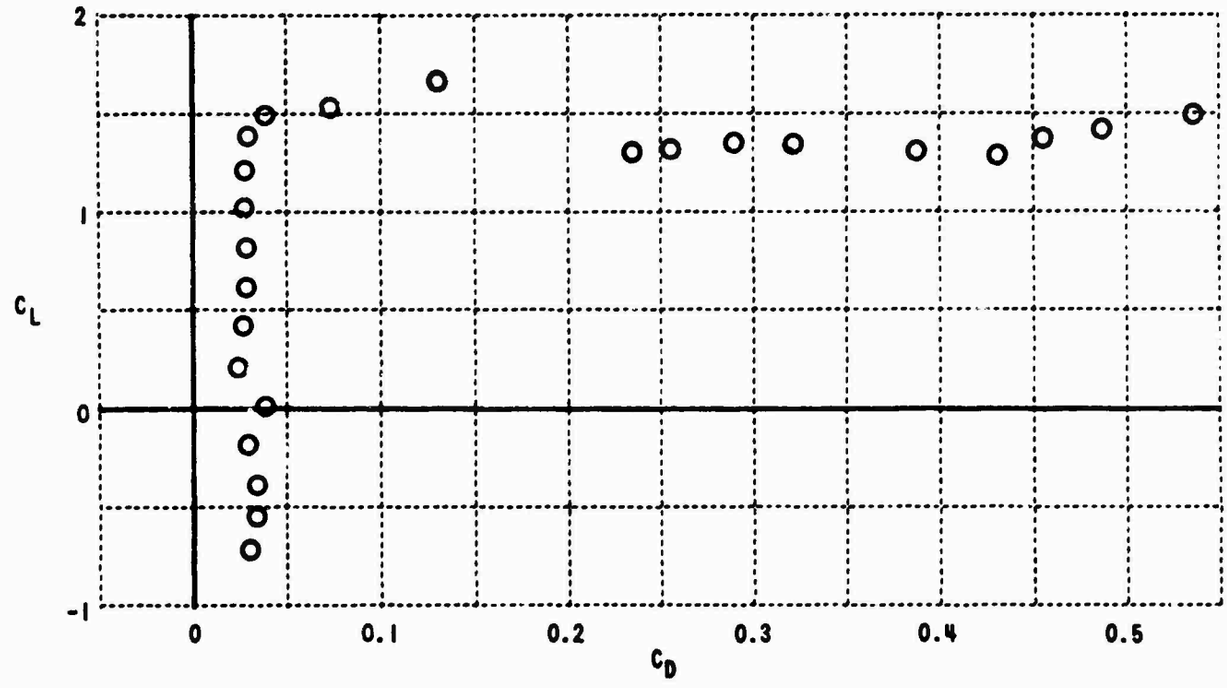

(b) NONDIMENSIONAL HEIGHT OF WING MIDCHORD ABOVE JET CENTERLINE IN JET RADII, h/r = 0.46

Figure 15. SECTION LIFT COEFFICIENTS vs. SECTION DRAG COEFFICIENT, LOW q, z/r = 1.54

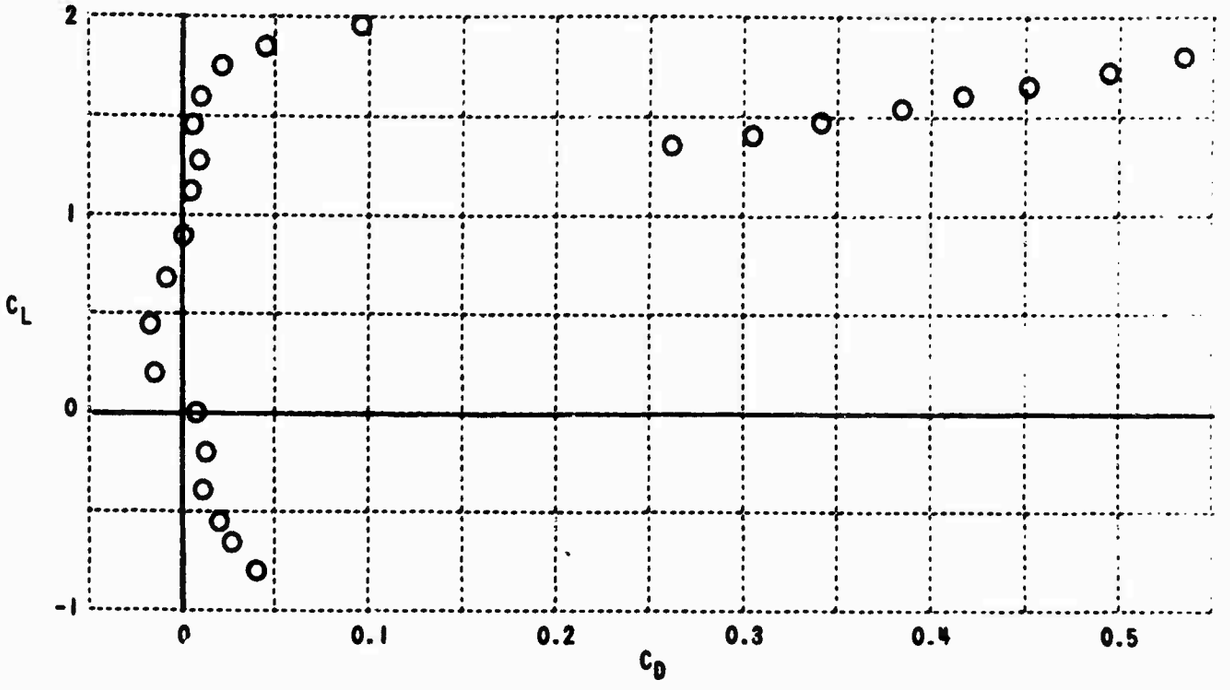

(c) NONDIMENSIONAL HEIGHT OF WING MIDCHORD ABOVE JET CENTERLINE IN JET RADII, $h/r = -0.10$

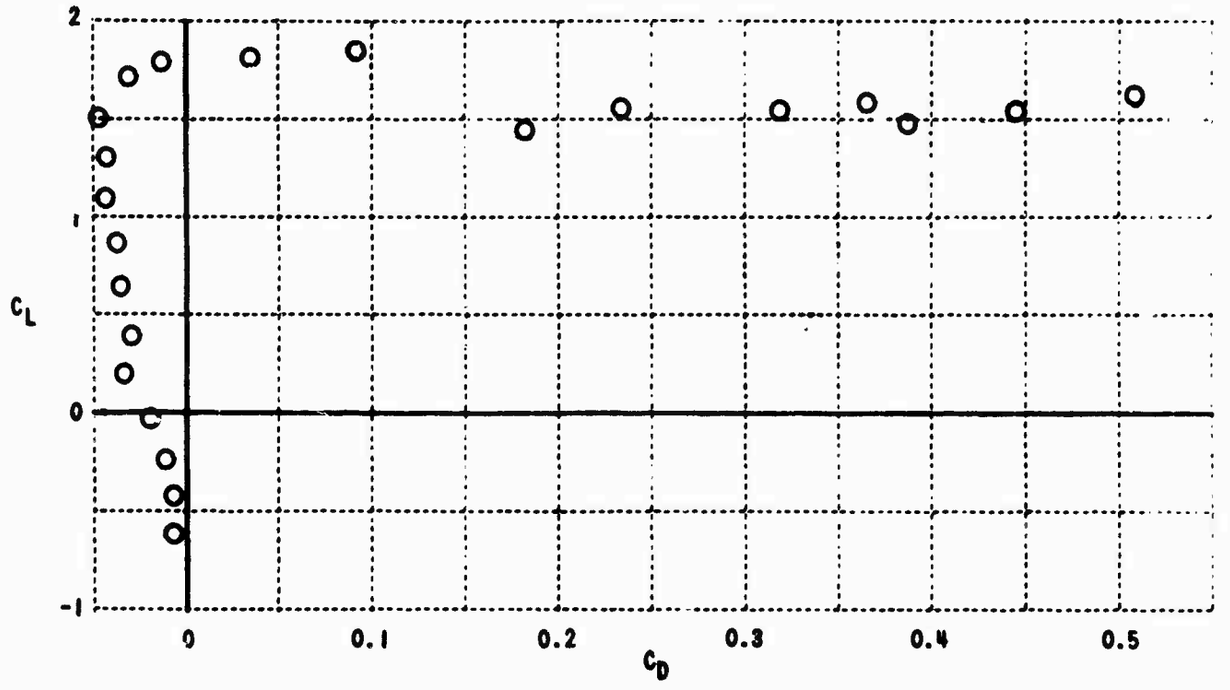

(d) NONDIMENSIONAL HEIGHT OF WING MIDCHORD ABOVE JET CENTERLINE IN JET RADII, $h/r = -0.64$

Figure 15. SECTION LIFT COEFFICIENTS vs. SECTION DRAG COEFFICIENT, LOW q, $z/r = 1.54$

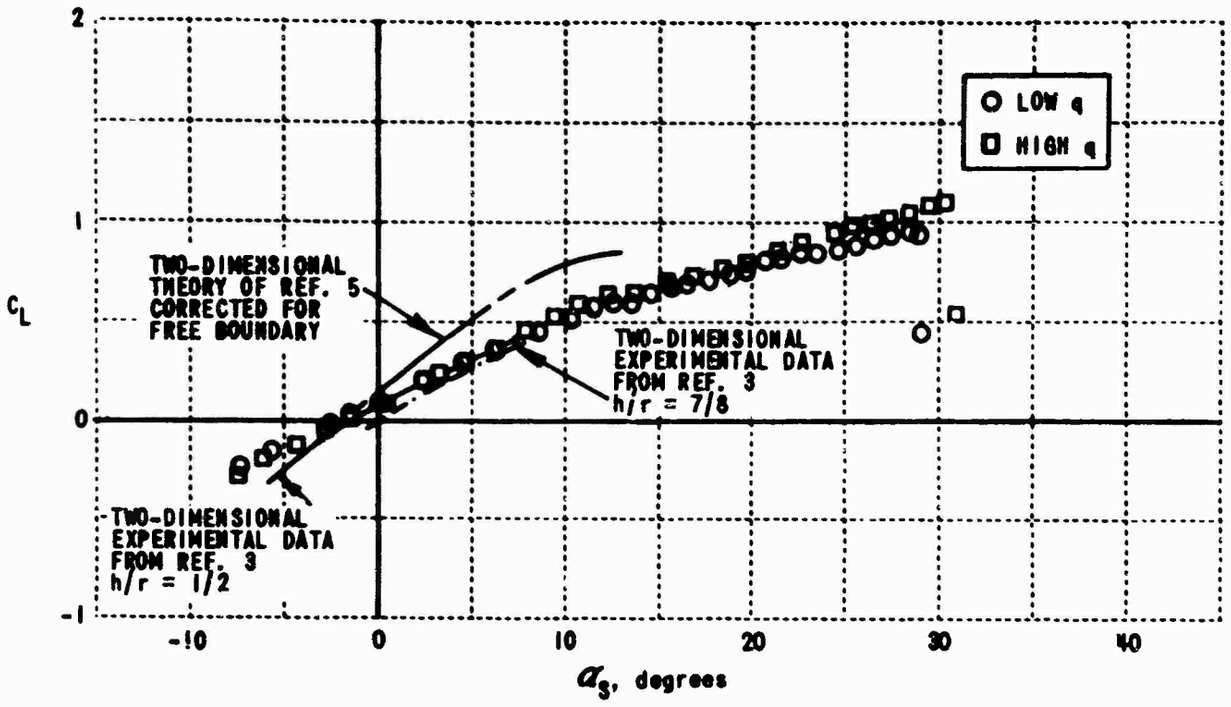

(a) NONDIMENSIONAL HEIGHT OF WING MIDCHORD ABOVE JET CENTERLINE IN JET RADII, h/r = 0.76

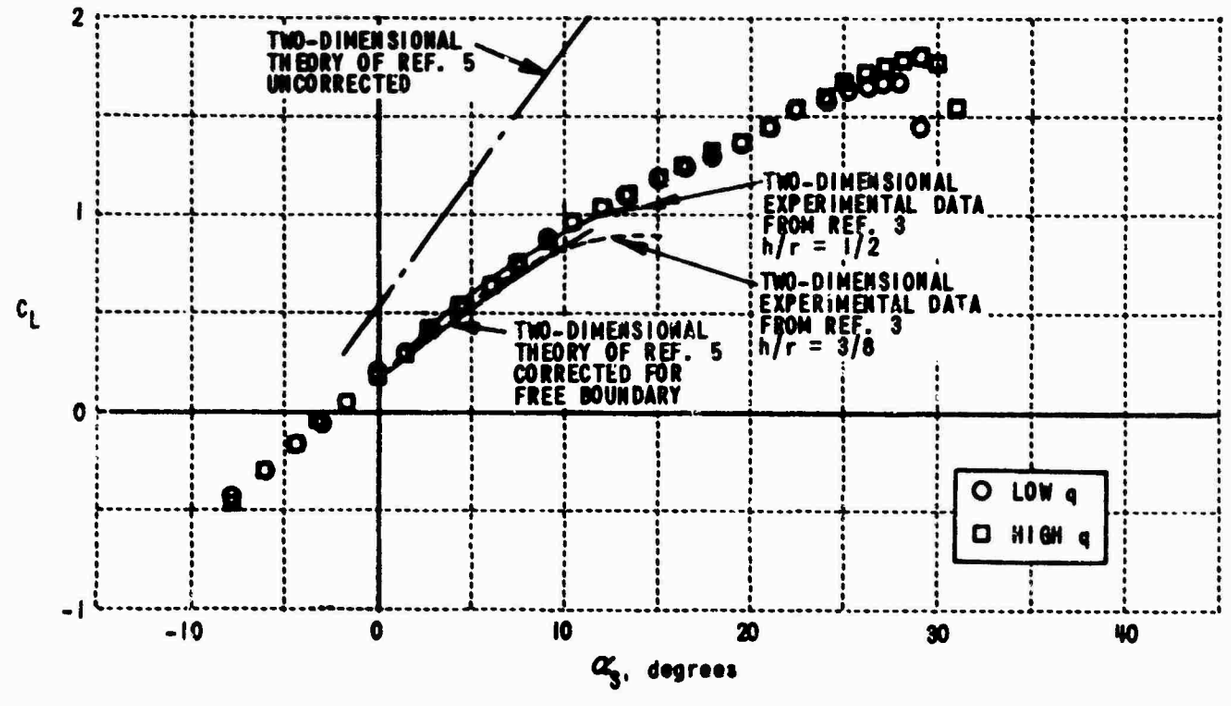

(b) NONDIMENSIONAL HEIGHT OF WING MIDCHORD ABOVE JET CENTERLINE IN JET RADII, h/r = 0.46

Figure 16. SECTION LIFT COEFFICIENTS vs. SECTION ANGLE OF ATTACK, z/r = 0.03

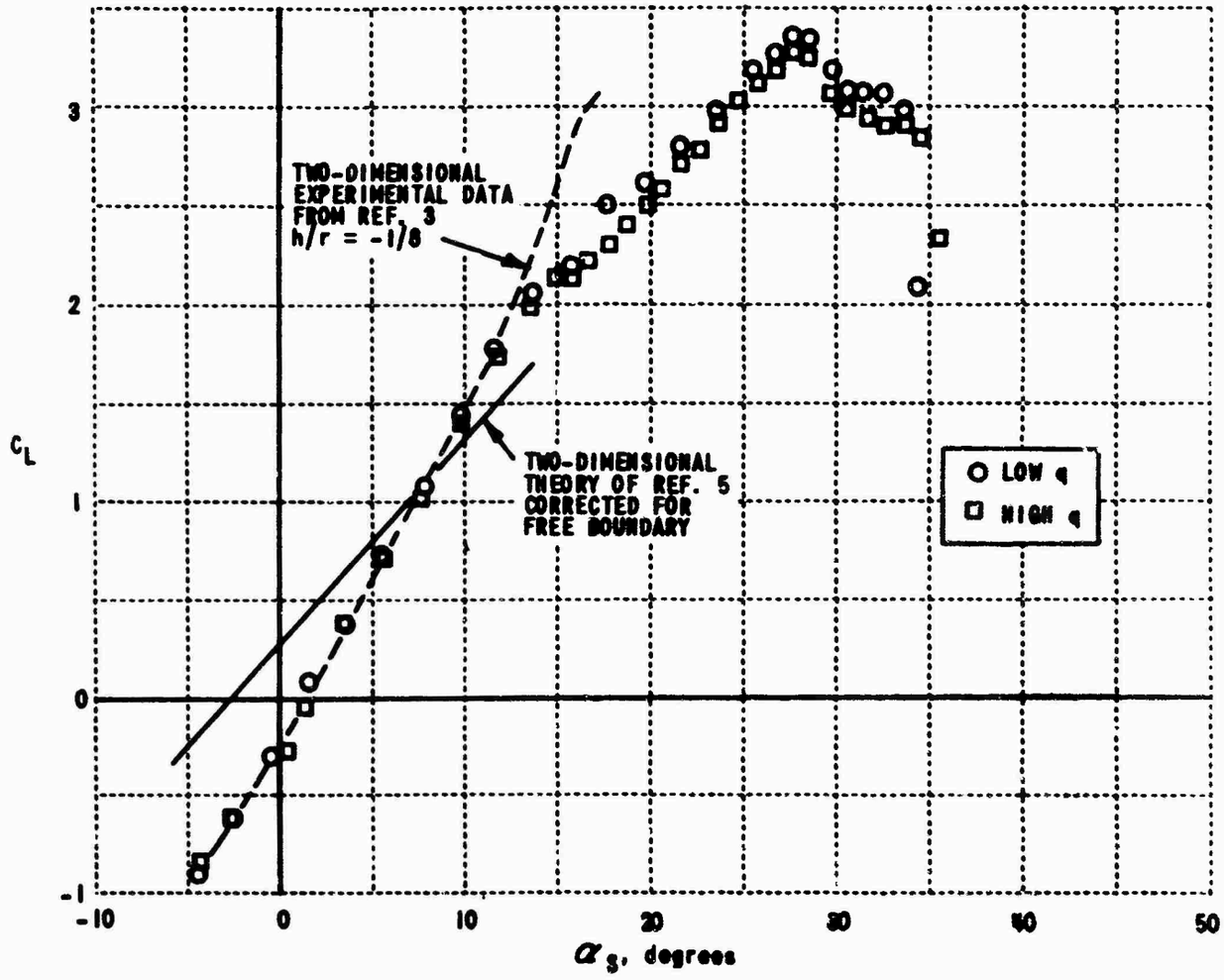

(c) NONDIMENSIONAL HEIGHT OF WING MIDCHORD ABOVE JET CENTERLINE IN JET RADII, h/r = -0.10

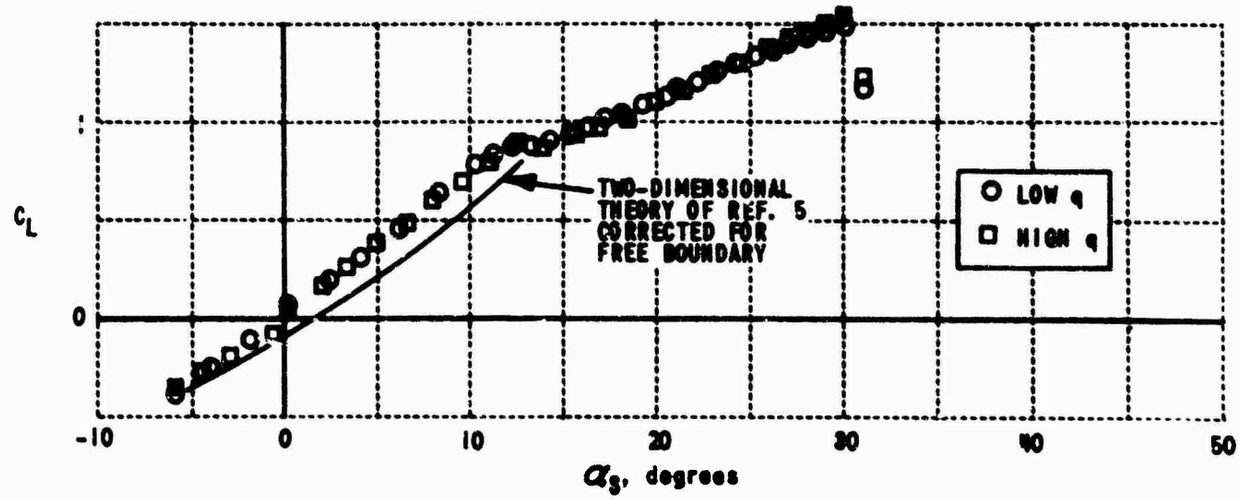

(d) NONDIMENSIONAL HEIGHT OF WING MIDCHORD ABOVE JET CENTERLINE IN JET RADII, h/r = -0.06

Figure 16. SECTION LIFT COEFFICIENTS vs. SECTION ANGLE OF ATTACK, z/r = 0.03

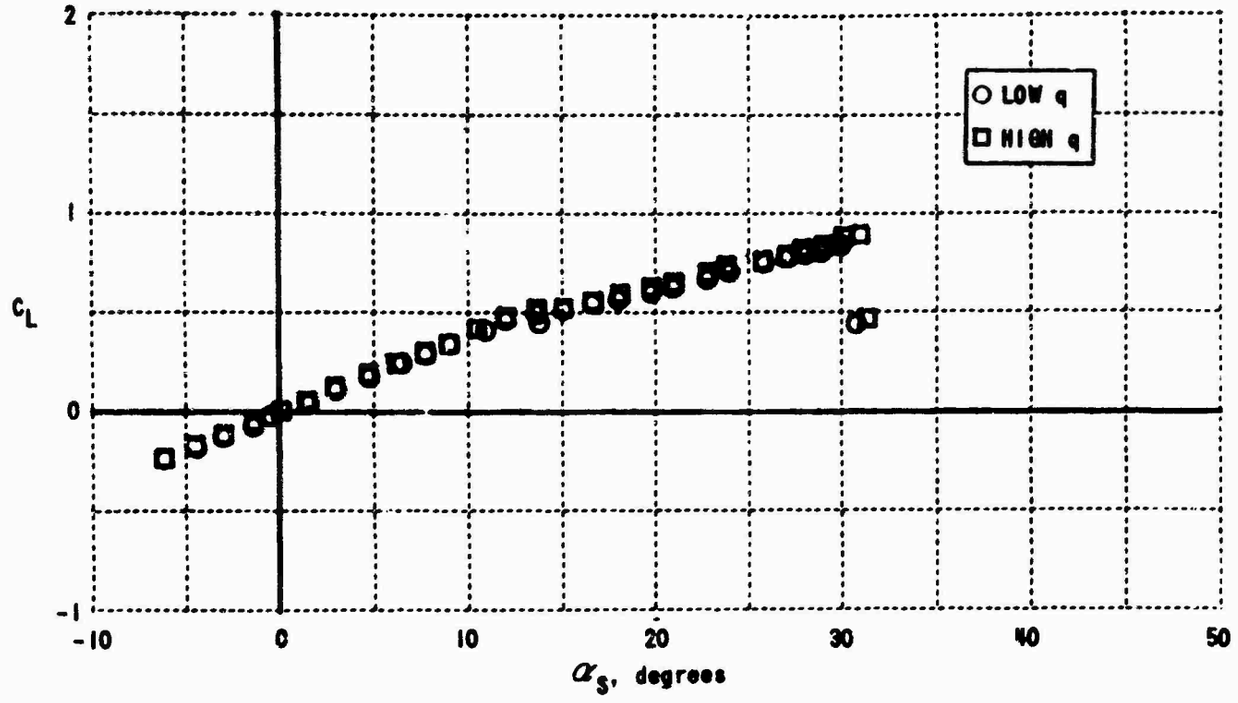

(a) NONDIMENSIONAL HEIGHT OF WING MIDCHORD ABOVE JET CENTERLINE IN JET RADII, h/r = 0.76

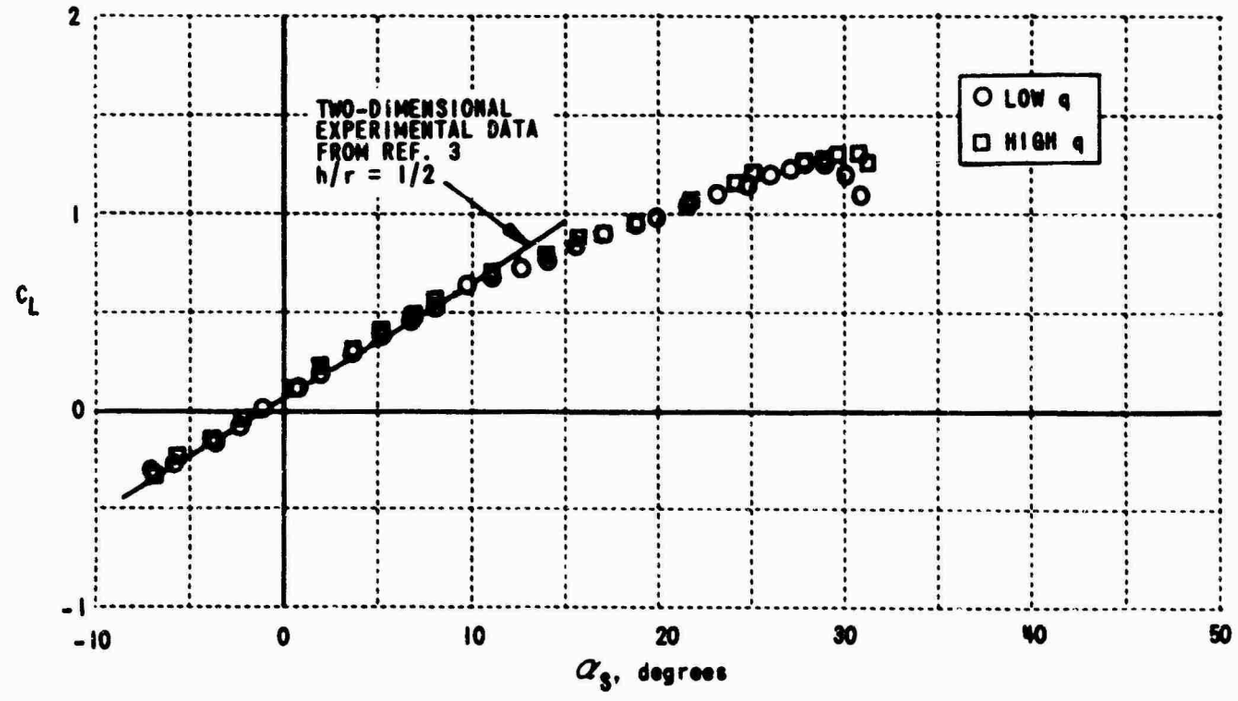

(b) NONDIMENSIONAL HEIGHT OF WING MIDCHORD ABOVE JET CENTERLINE IN JET RADII, h/r = 0.46

Figure 17. SECTION LIFT COEFFICIENTS vs. SECTION ANGLE OF ATTACK, z/r = 0.54

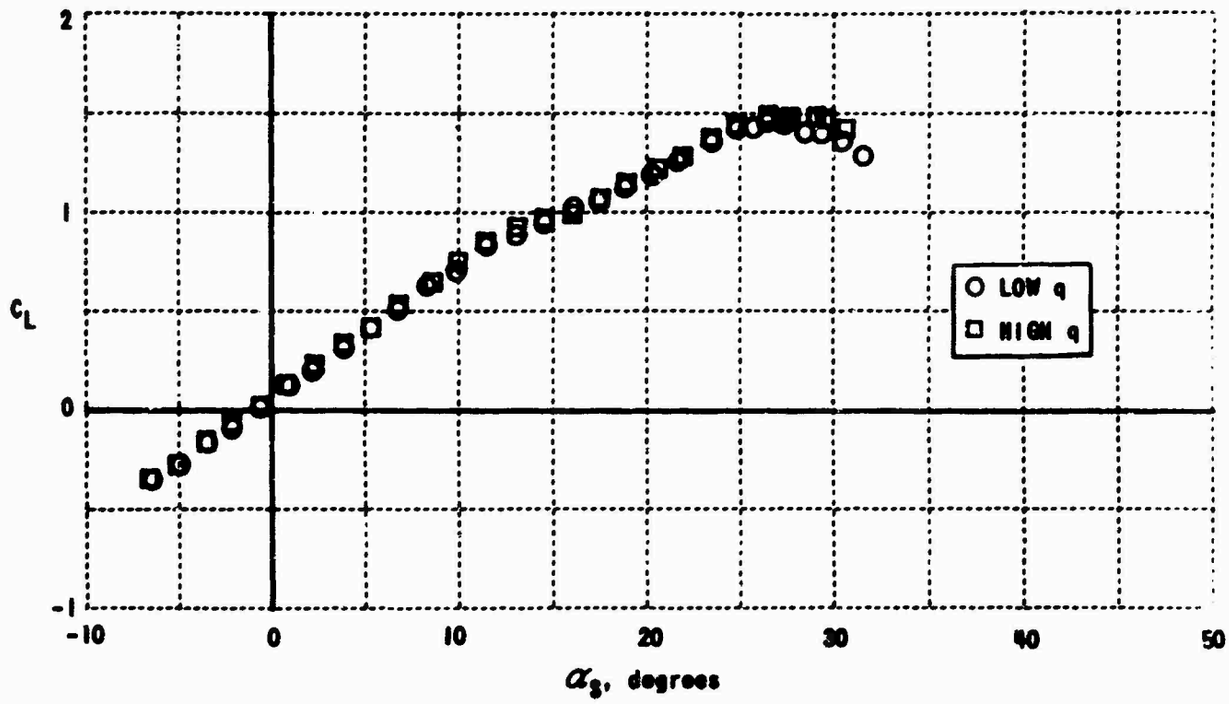

(c) NONDIMENSIONAL HEIGHT OF WING MIDCHORD ABOVE JET CENTERLINE IN JET RADII, h/r = -0.10

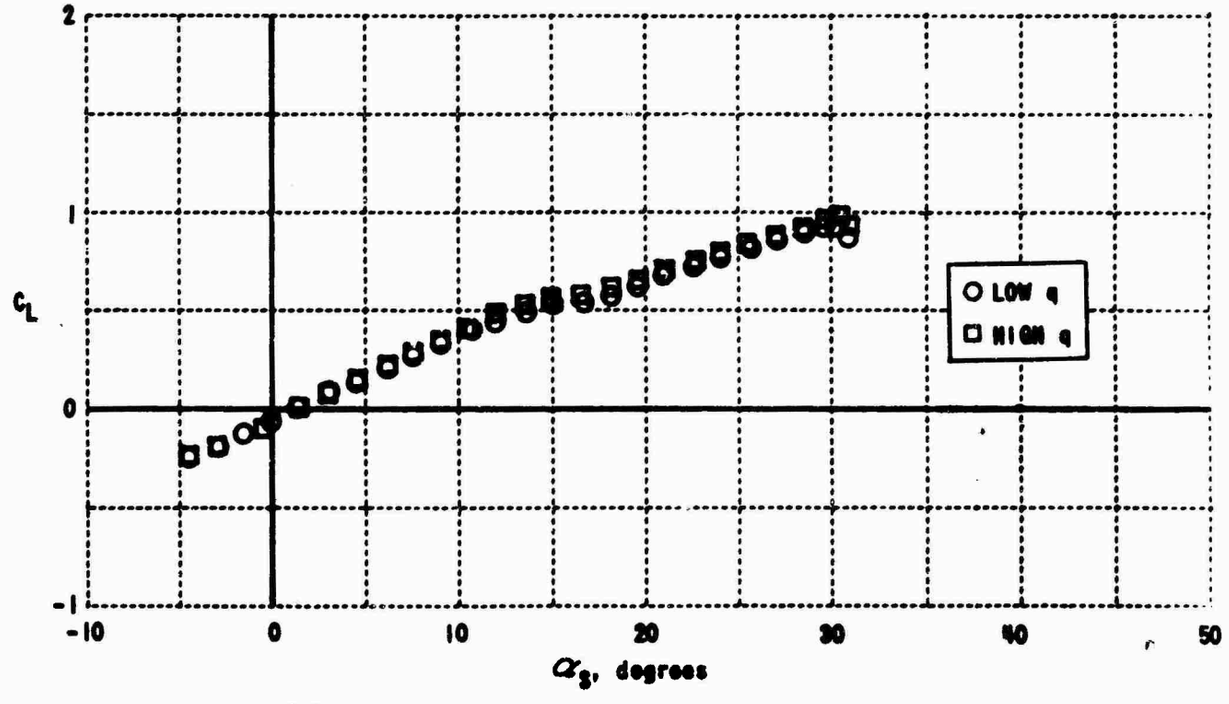

(d) NONDIMENSIONAL HEIGHT OF WING MIDCHORD ABOVE JET CENTERLINE IN JET RADII, h/r = -0.64

Figure 17. SECTION LIFT COEFFICIENTS vs. SECTION ANGLE OF ATTACK, z/r = 0.54

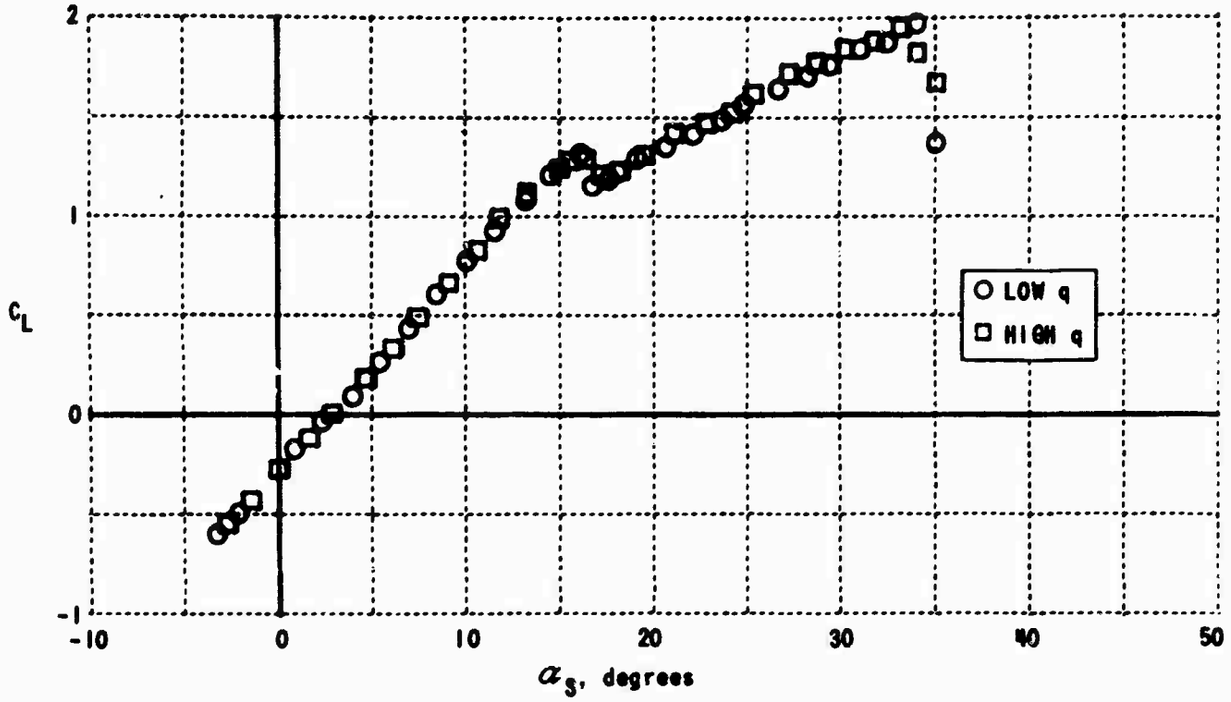

(a) NONDIMENSIONAL HEIGHT OF WING MIDCHORD ABOVE JET CENTERLINE IN JET RADII, h/r = 0.76

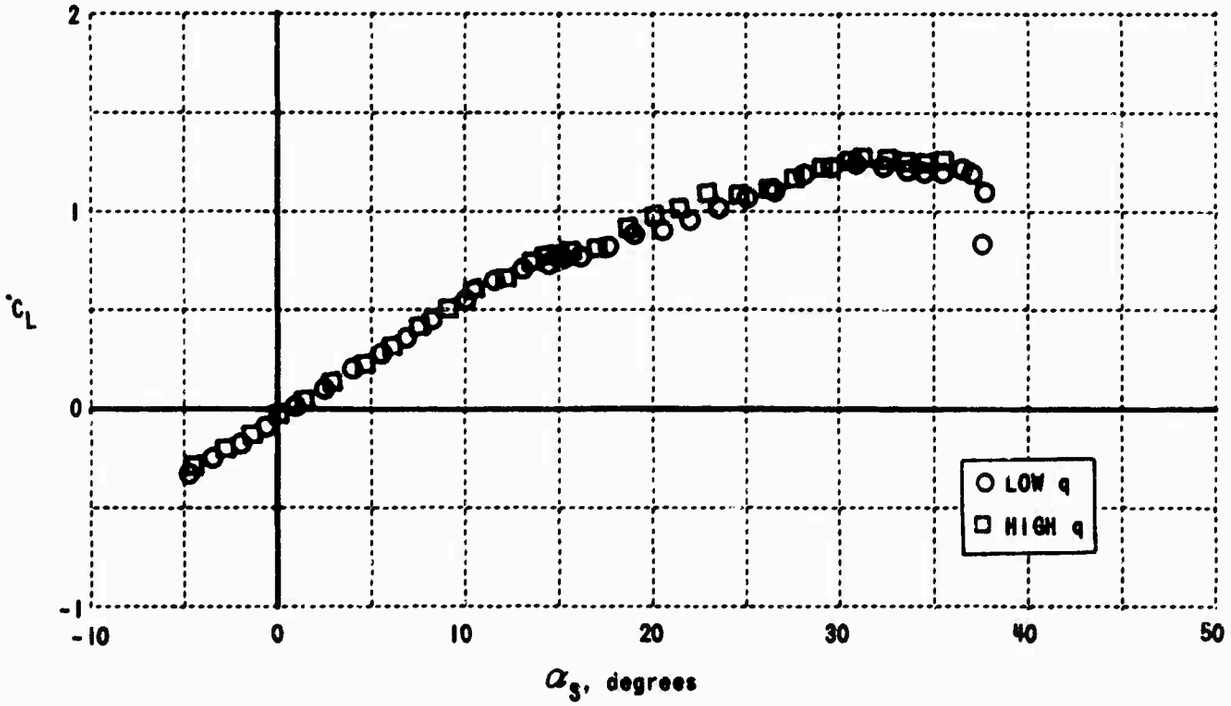

(b) NONDIMENSIONAL HEIGHT OF WING MIDCHORD ABOVE JET CENTERLINE IN JET RADII, h/r = 0.46

Figure 18. SECTION LIFT COEFFICIENTS vs. SECTION ANGLE OF ATTACK, z/r = 1.03

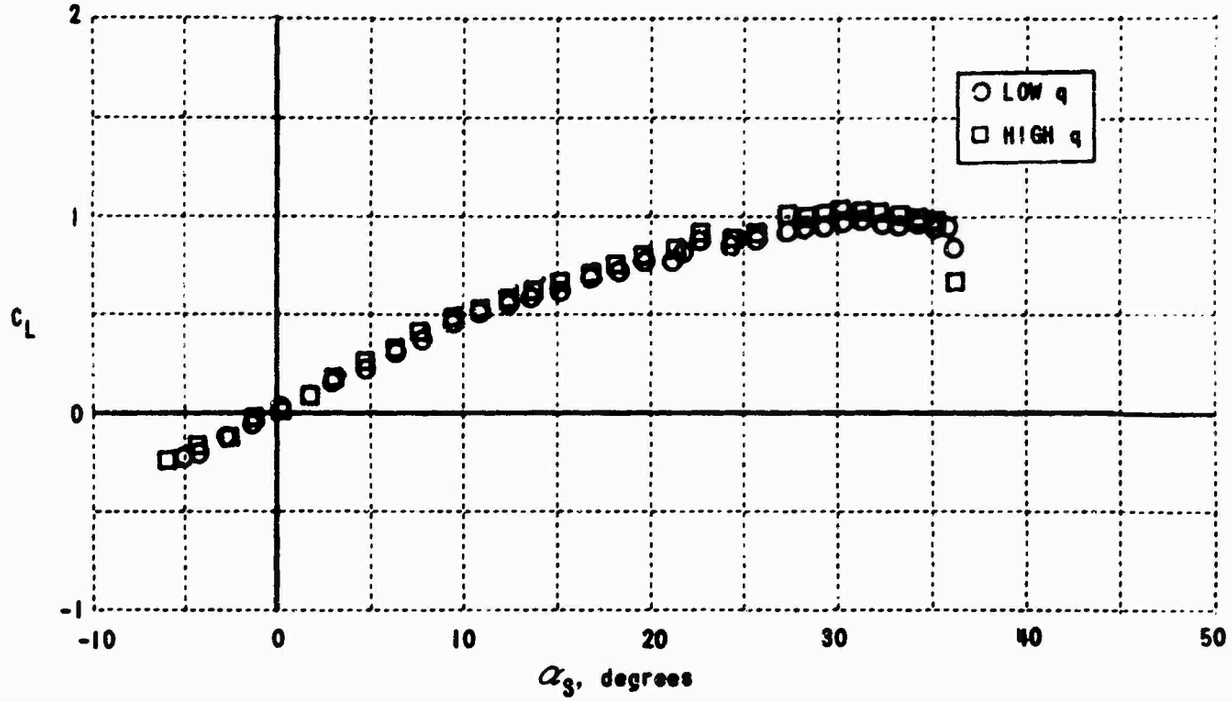

(c) NONDIMENSIONAL HEIGHT OF WING MIDCHORD ABOVE JET CENTERLINE IN JET RADII, h/r = -0.10

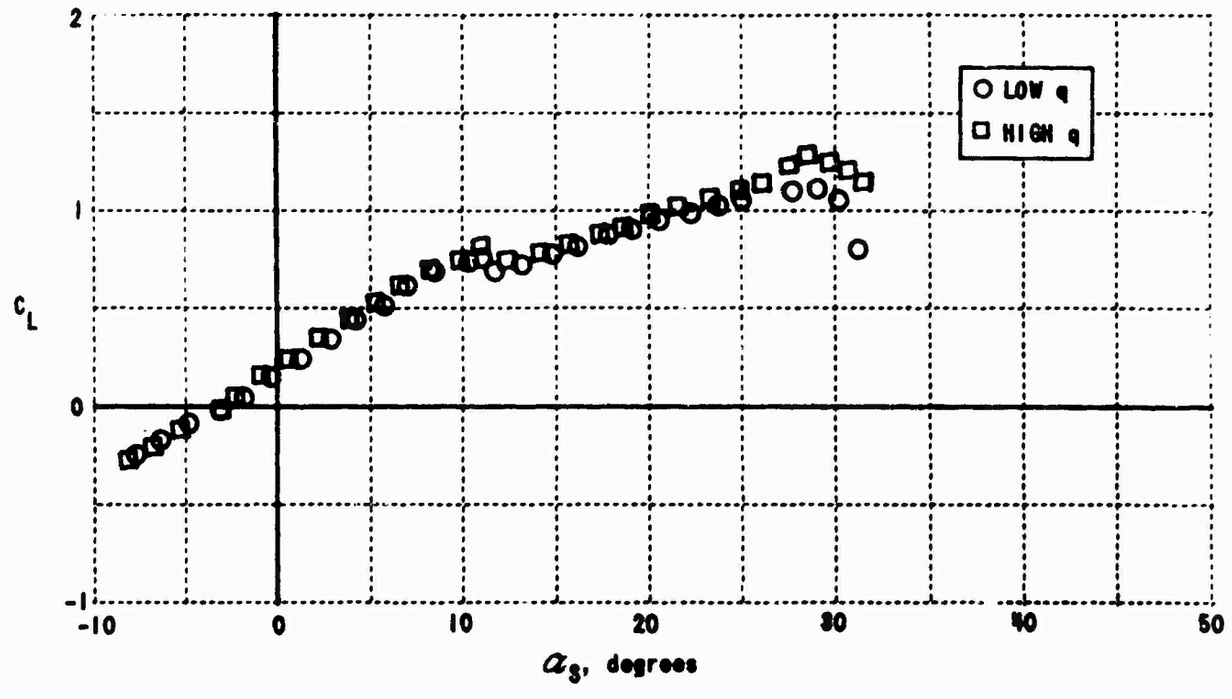

(d) NONDIMENSIONAL HEIGHT OF WING MIDCHORD ABOVE JET CENTERLINE IN JET RADII, h/r = -0.64

Figure 18. SECTION LIFT COEFFICIENTS vs. SECTION ANGLE OF ATTACK, z/r = 1.03

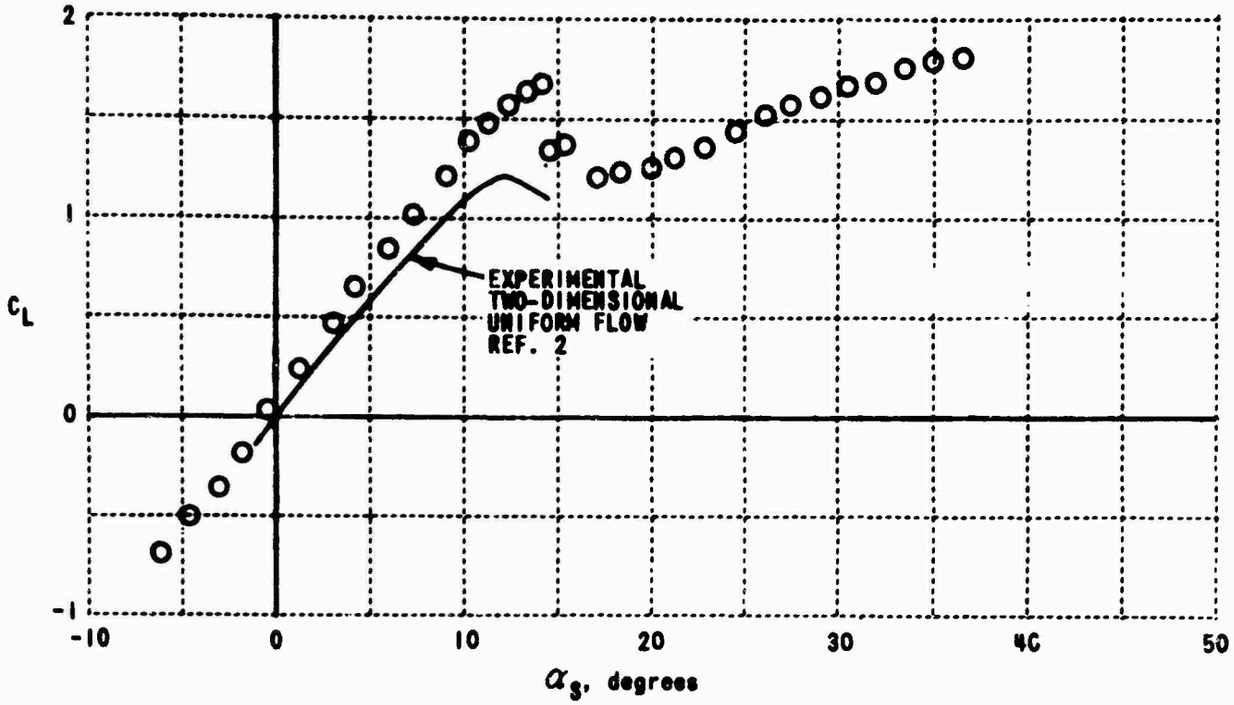

(a) NONDIMENSIONAL HEIGHT OF WING MIDCHORD ABOVE JET CENTERLINE IN JET RADII, $h/r = 0.76$

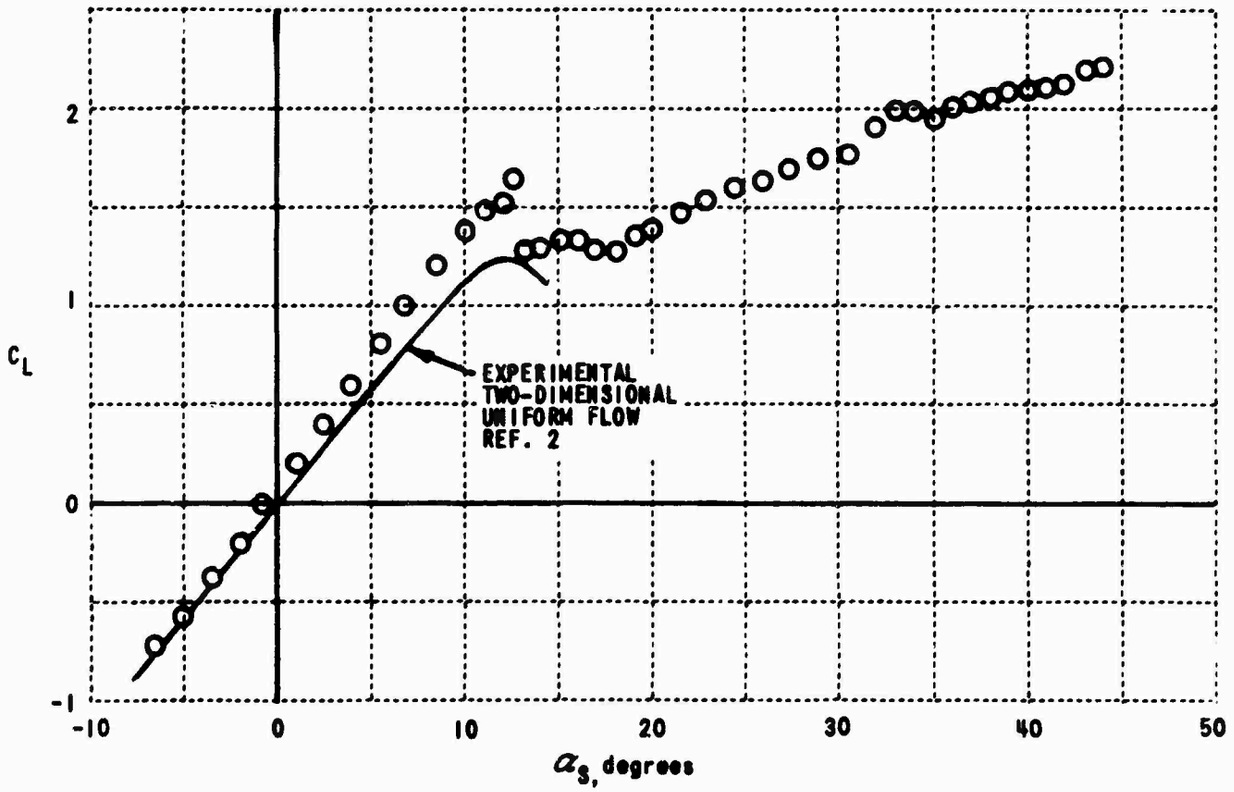

(b) NONDIMENSIONAL HEIGHT OF WING MIDCHORD ABOVE JET CENTERLINE IN JET RADII, $h/r = 0.46$

Figure 19. SECTION LIFT COEFFICIENTS vs. SECTION ANGLE OF ATTACK, LOW q, $z/r = 1.54$

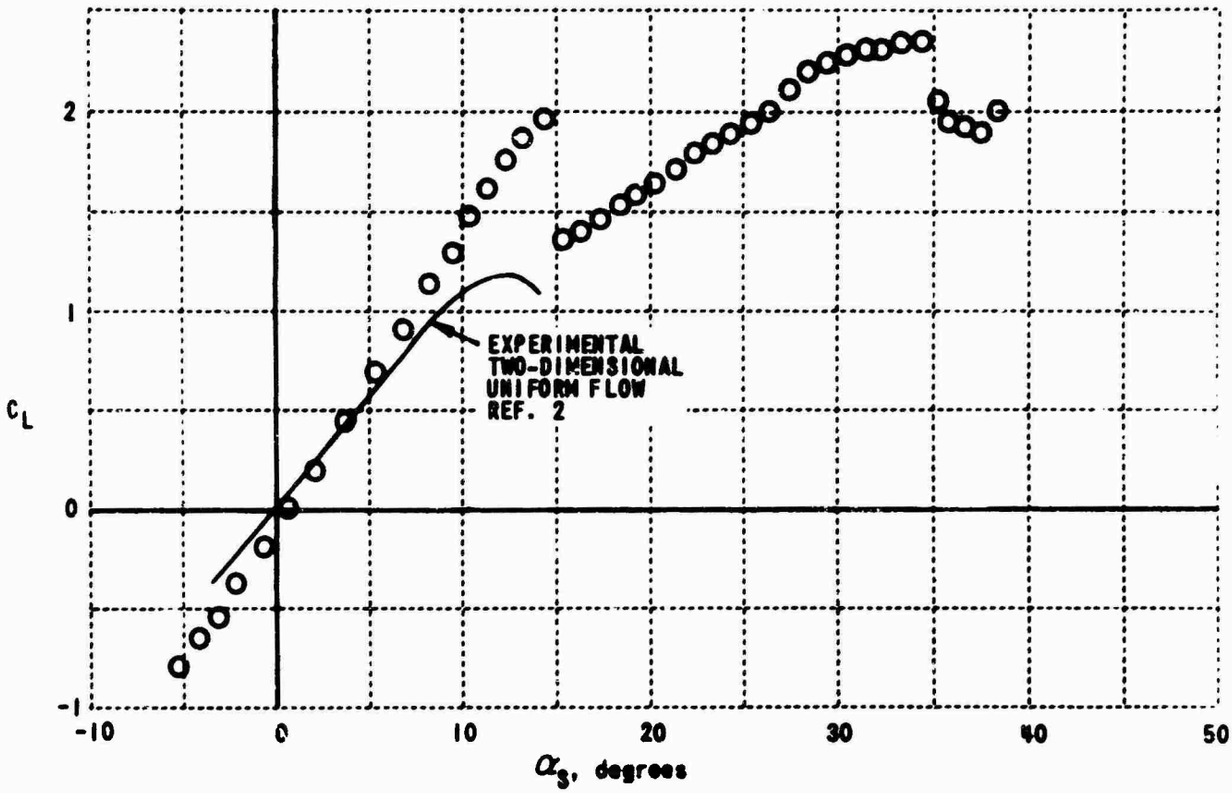

(c) NONDIMENSIONAL HEIGHT OF WING MIDCHORD ABOVE JET CENTERLINE IN JET RADII, $h/r = -0.10$

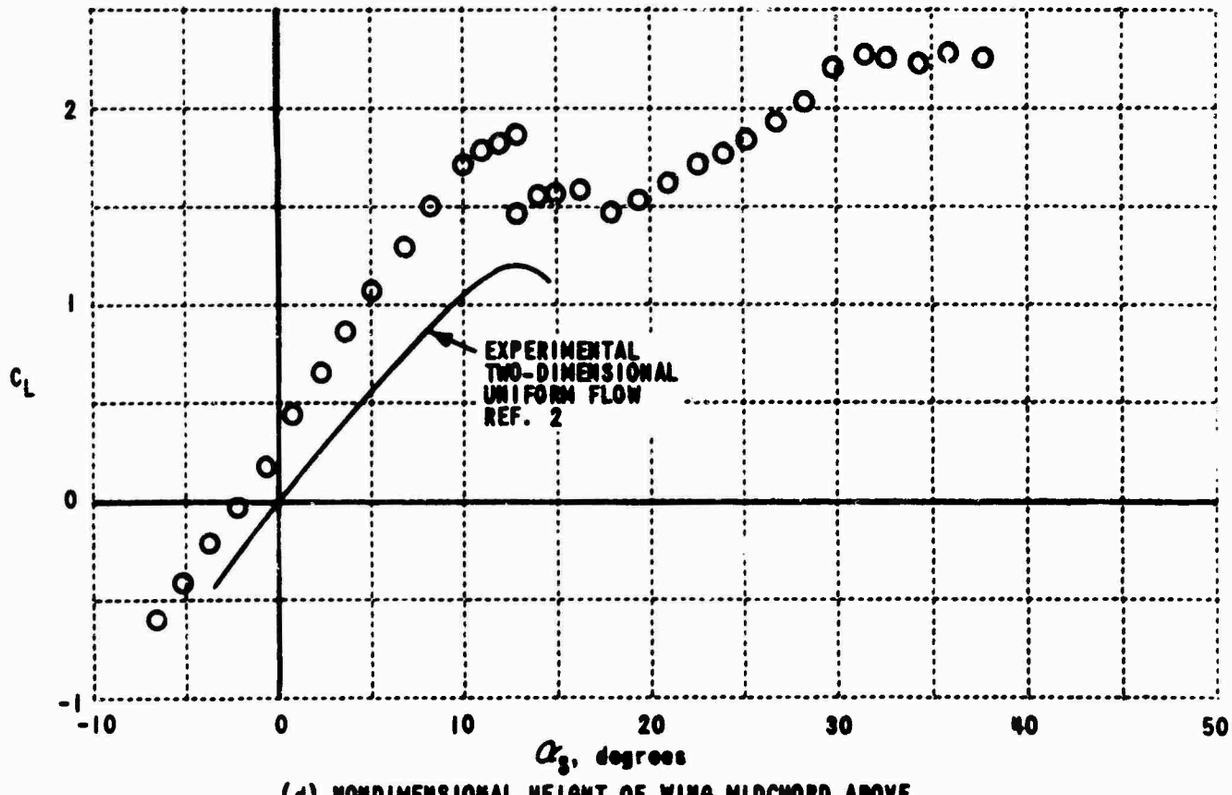

(d) NONDIMENSIONAL HEIGHT OF WING MIDCHORD ABOVE JET CENTERLINE IN JET RADII, $h/r = -0.64$

Figure 19. SECTION LIFT COEFFICIENTS vs. SECTION ANGLE OF ATTACK, LOW q, $z/r = 1.54$

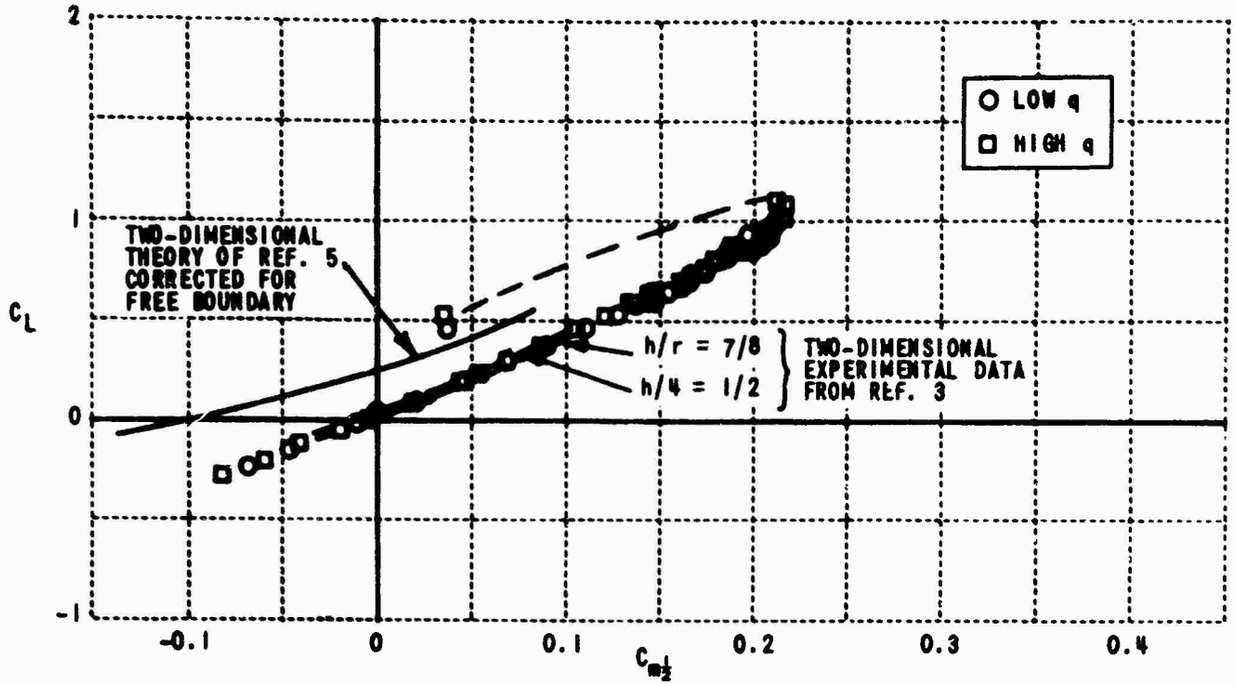

(a) NONDIMENSIONAL HEIGHT OF WING MIDCHORD ABOVE JET CENTERLINE IN JET RADII, h/r = 0.76

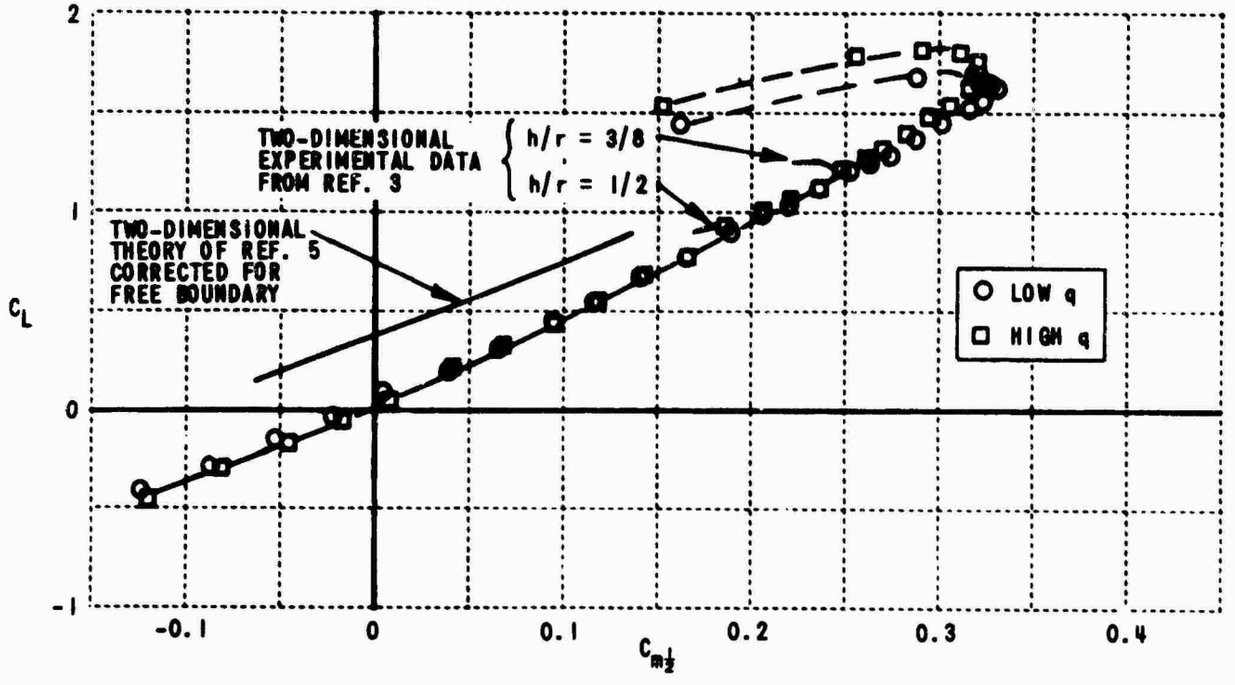

(b) NONDIMENSIONAL HEIGHT OF WING MIDCHORD ABOVE JET CENTERLINE IN JET RADII, h/r = 0.46

Figure 20. SECTION LIFT COEFFICIENTS vs. SECTION MOMENT COEFFICIENT, z/r = 0.03

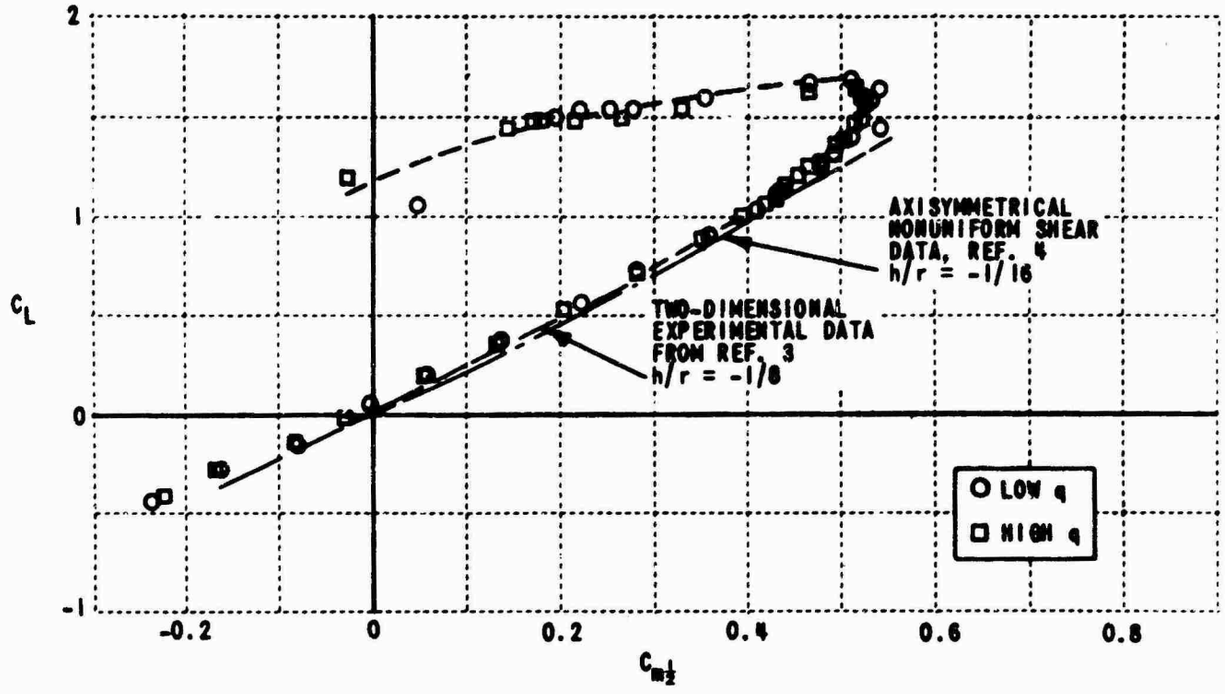

(c) NONDIMENSIONAL HEIGHT OF WING MIDCHORD ABOVE JET CENTERLINE IN JET RADII, h/r = -0.10

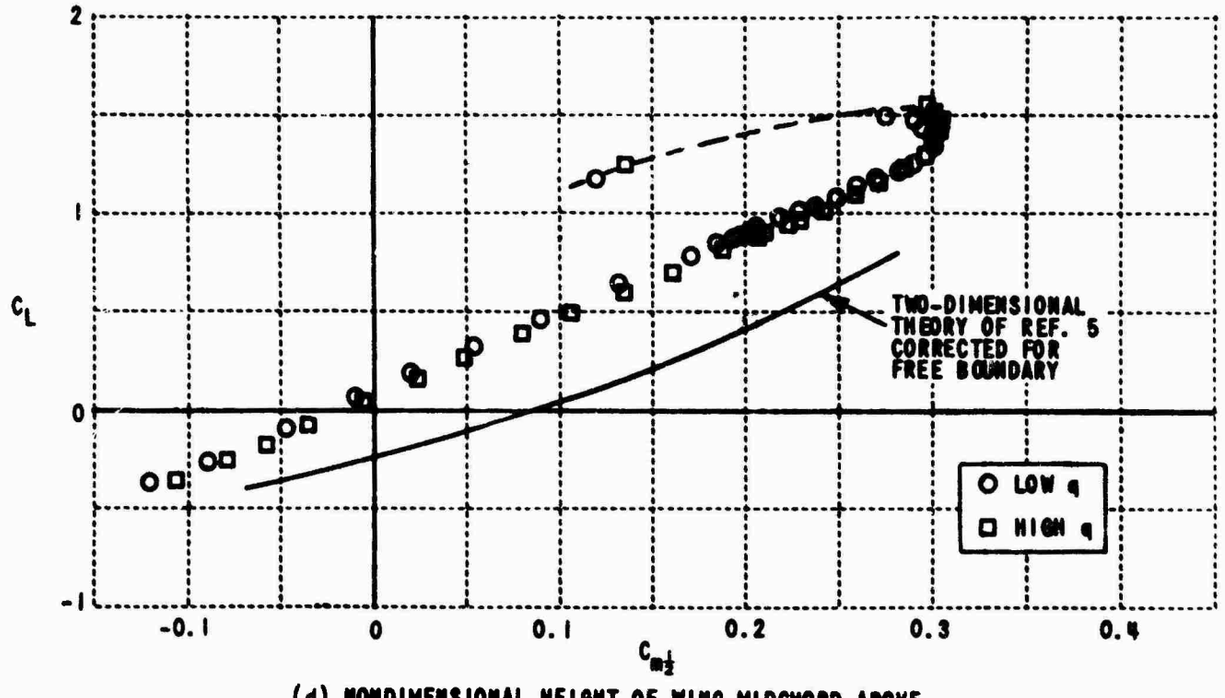

(d) NONDIMENSIONAL HEIGHT OF WING MIDCHORD ABOVE JET CENTERLINE IN JET RADII, h/r = -0.64

Figure 20. SECTION LIFT COEFFICIENTS vs. SECTION MOMENT COEFFICIENT, z/r = 0.03

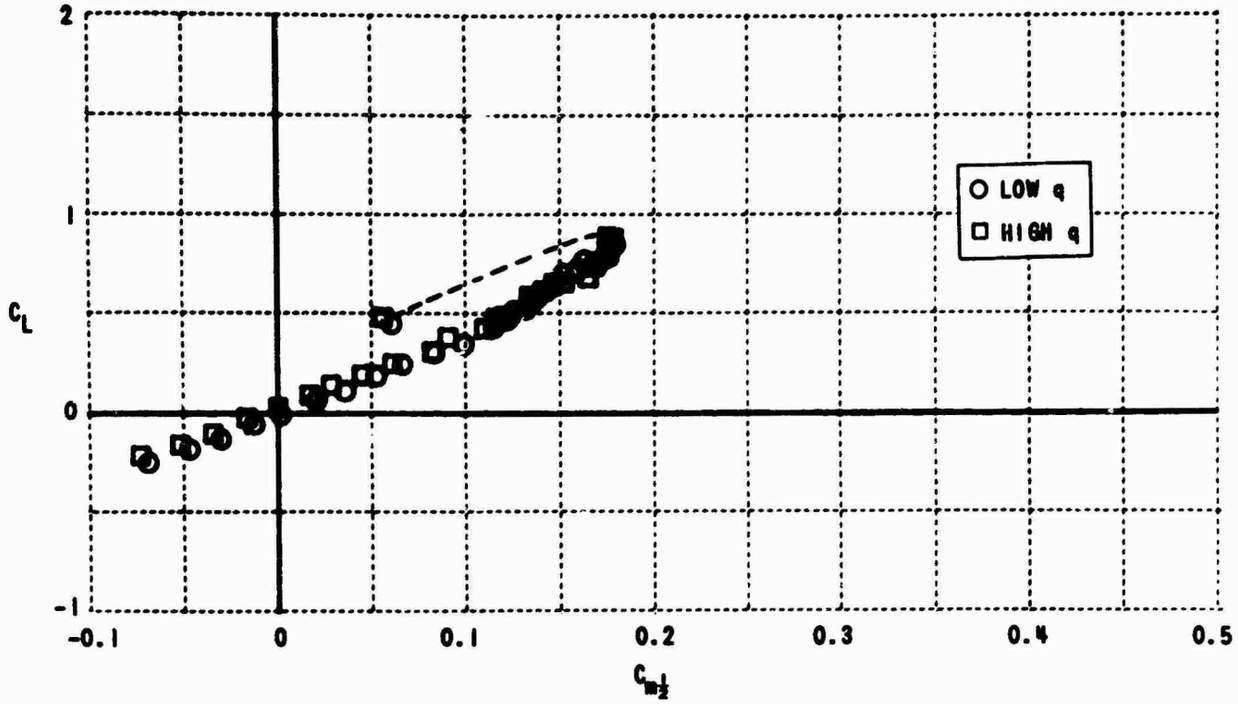

(a) NONDIMENSIONAL HEIGHT OF WING MIDCHORD ABOVE JET CENTERLINE IN JET RADII, $h/r = 0.76$

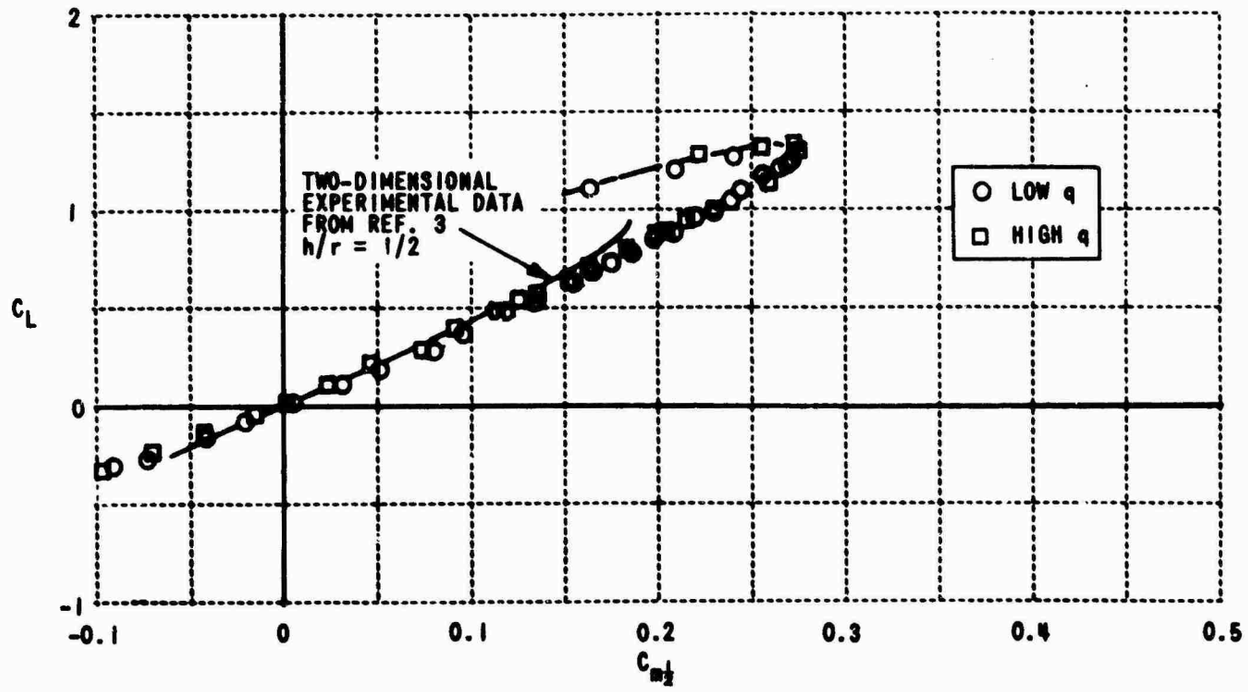

(b) NONDIMENSIONAL HEIGHT OF WING MIDCHORD ABOVE JET CENTERLINE IN JET RADII, $h/r = 0.46$

Figure 21. SECTION LIFT COEFFICIENTS vs. SECTION MOMENT COEFFICIENT, $z/r = 0.54$

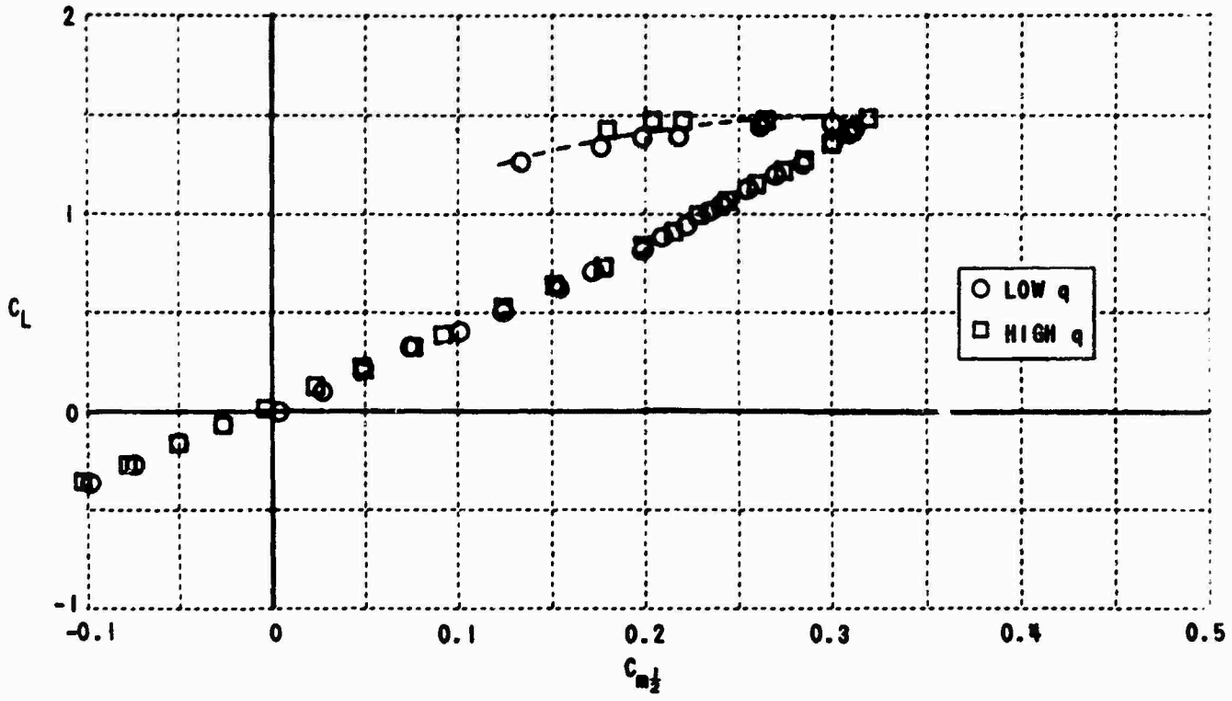

(c) NONDIMENSIONAL HEIGHT OF WING MIDCHORD ABOVE JET CENTERLINE IN JET RADII, h/r = -0.10

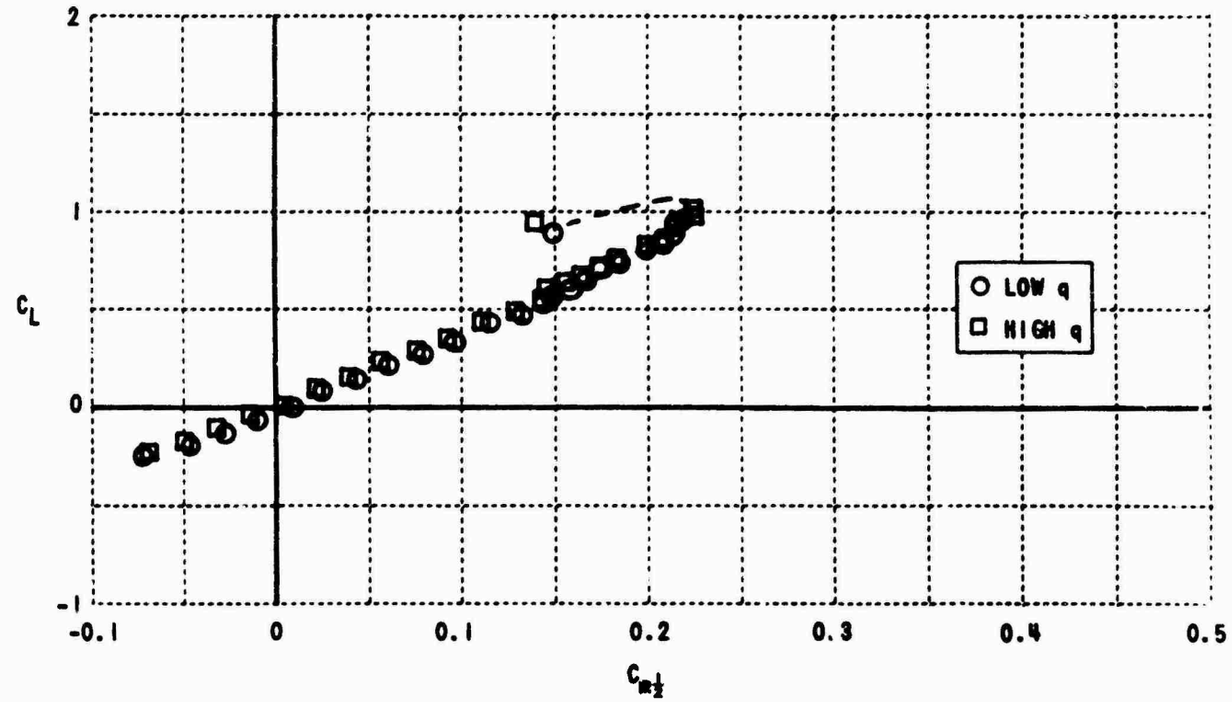

(d) NONDIMENSIONAL HEIGHT OF WING MIDCHORD ABOVE JET CENTERLINE IN JET RADII, h/r = -0.64

Figure 21. SECTION LIFT COEFFICIENTS vs. SECTION MOMENT COEFFICIENT, z/r = 0.54

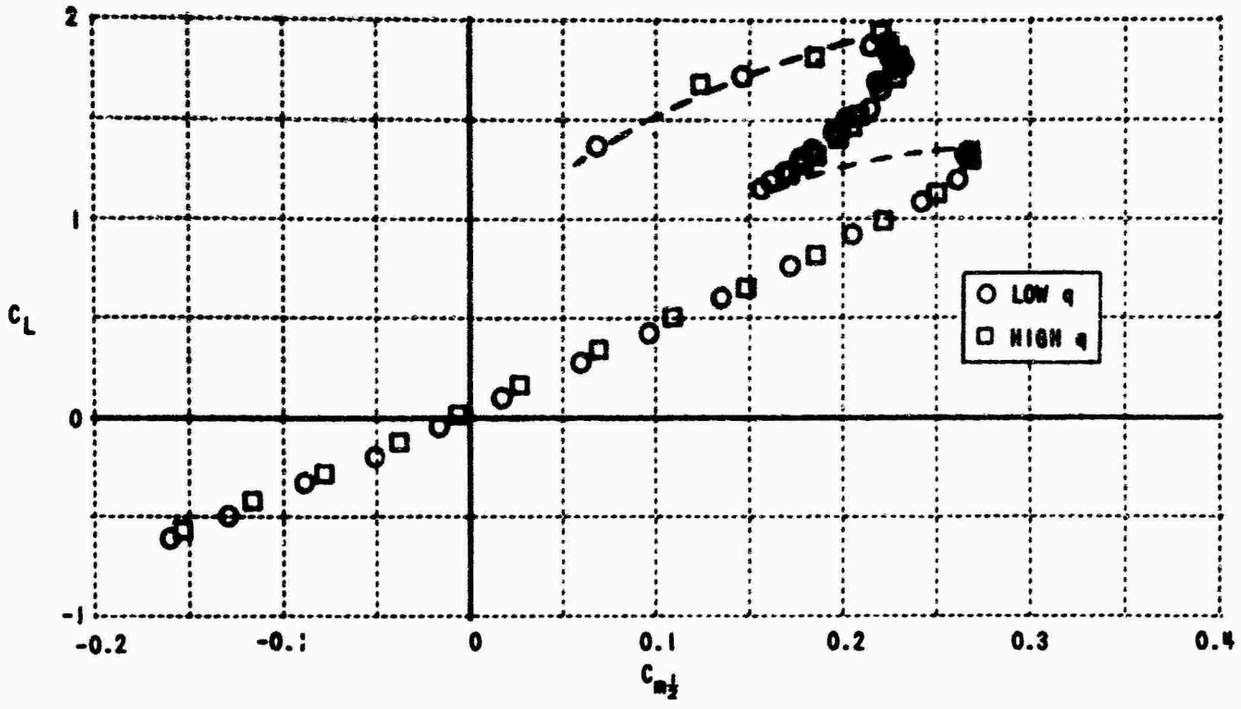

(a) NONDIMENSIONAL HEIGHT OF WING MIDCHORD ABOVE JET CENTERLINE IN JET RADII, h/r = 0.76

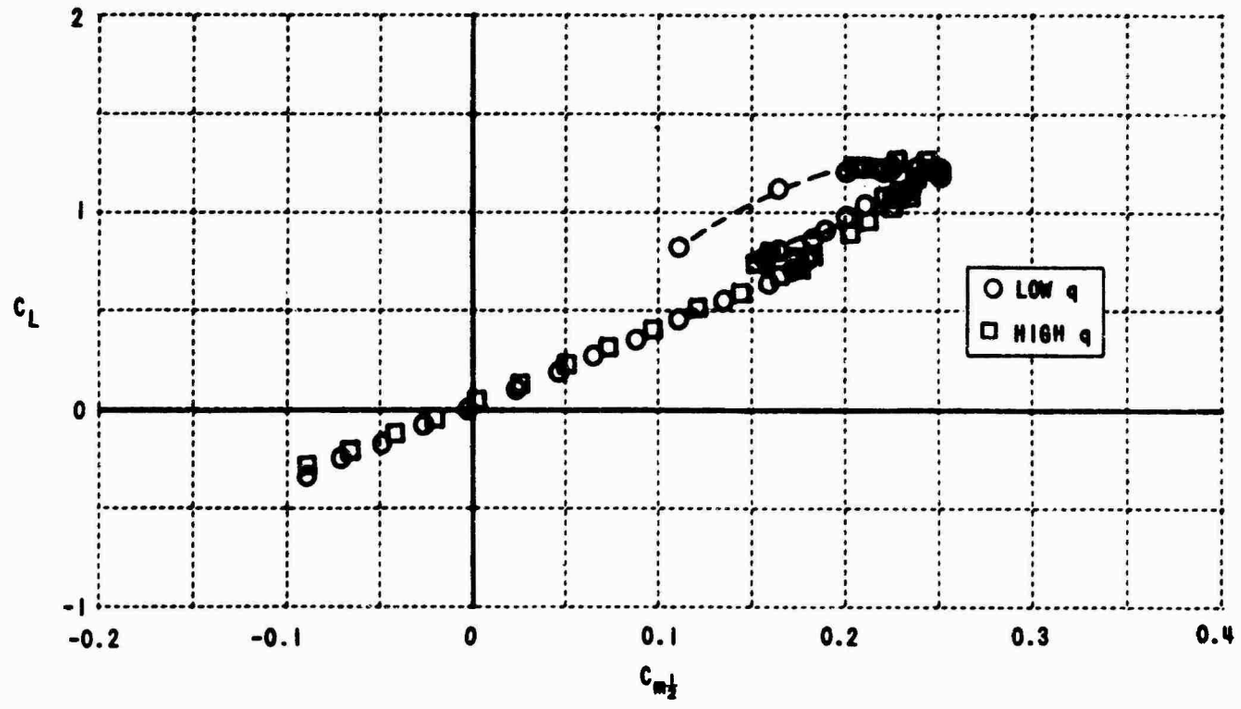

(b) NONDIMENSIONAL HEIGHT OF WING MIDCHORD ABOVE JET CENTERLINE IN JET RADII, h/r = 0.46

Figure 22. SECTION LIFT COEFFICIENTS vs. SECTION MOMENT COEFFICIENT, z/r = 1.03

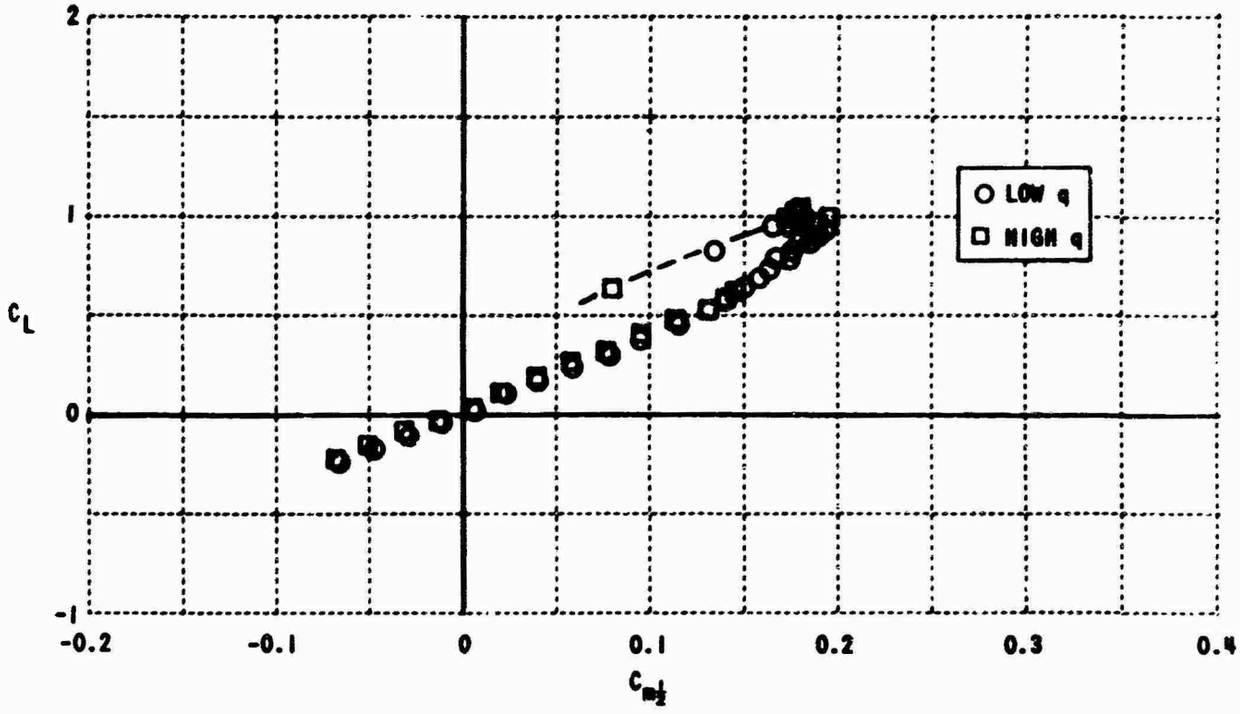

(c) NONDIMENSIONAL HEIGHT OF WING MIDCHORD ABOVE JET CENTERLINE IN JET RADII, h/r = -0.10

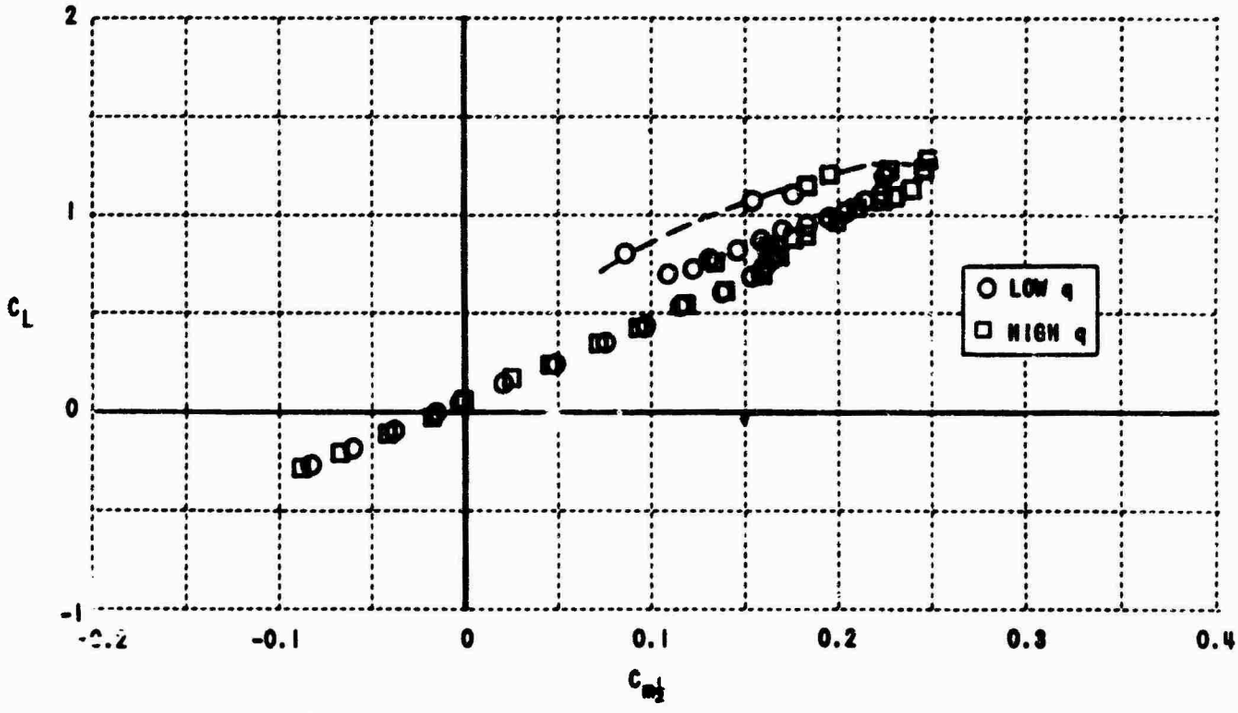

(d) NONDIMENSIONAL HEIGHT OF WING MIDCHORD ABOVE JET CENTERLINE IN JET RADII, h/r = -0.64

Figure 22. SECTION LIFT COEFFICIENTS vs. SECTION MOMENT COEFFICIENT, z/r = 1.03

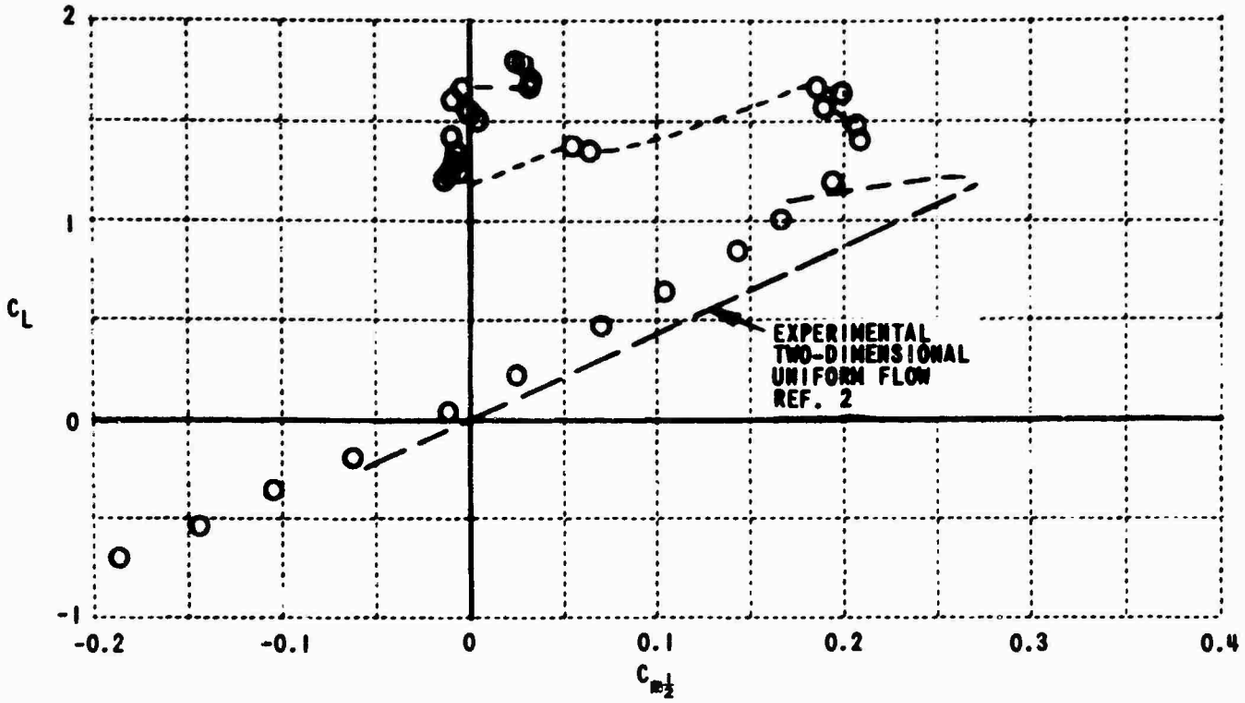

(a) NONDIMENSIONAL HEIGHT OF WING MIDCHORD ABOVE JET CENTERLINE IN JET RADII, $h/r = 0.76$

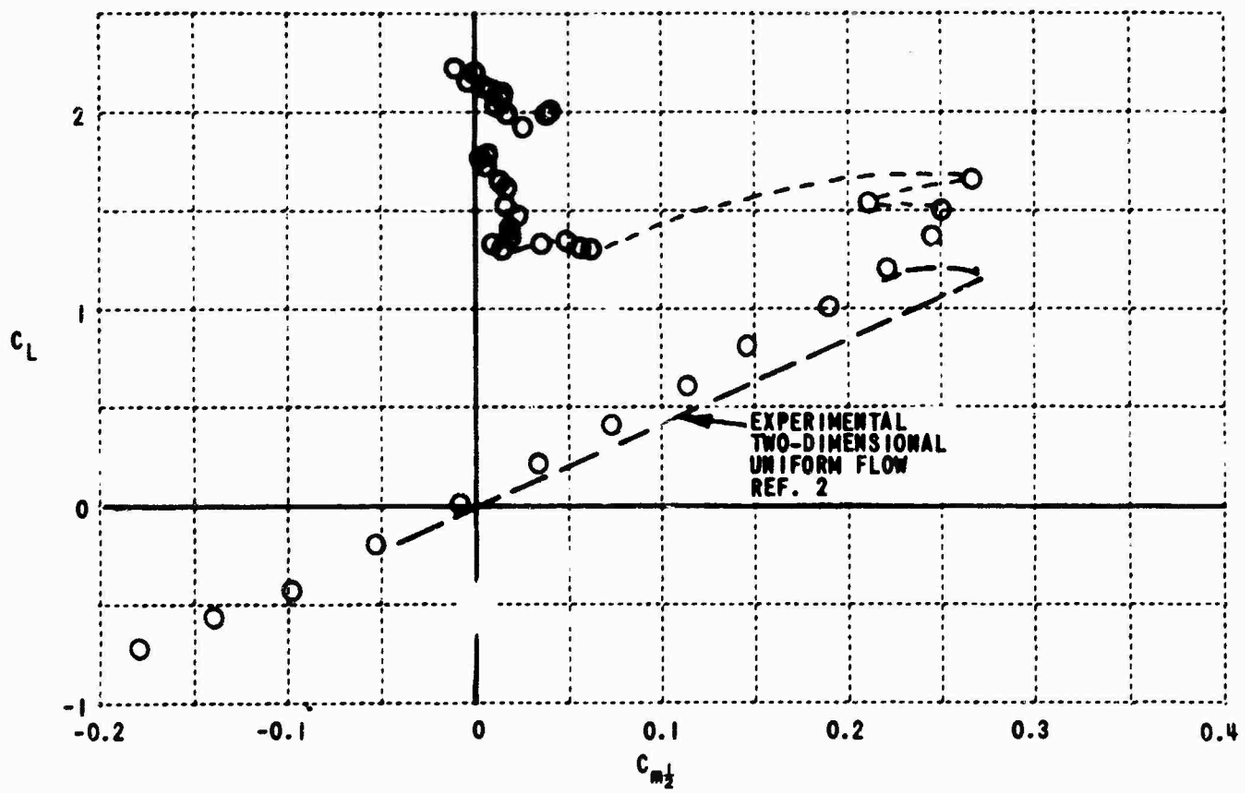

(b) NONDIMENSIONAL HEIGHT OF WING MIDCHORD ABOVE JET CENTERLINE IN JET RADII, $h/r = 0.46$

Figure 23. SECTION LIFT COEFFICIENT vs. SECTION MOMENT COEFFICIENT, LOW q, $z/r = 1.54$

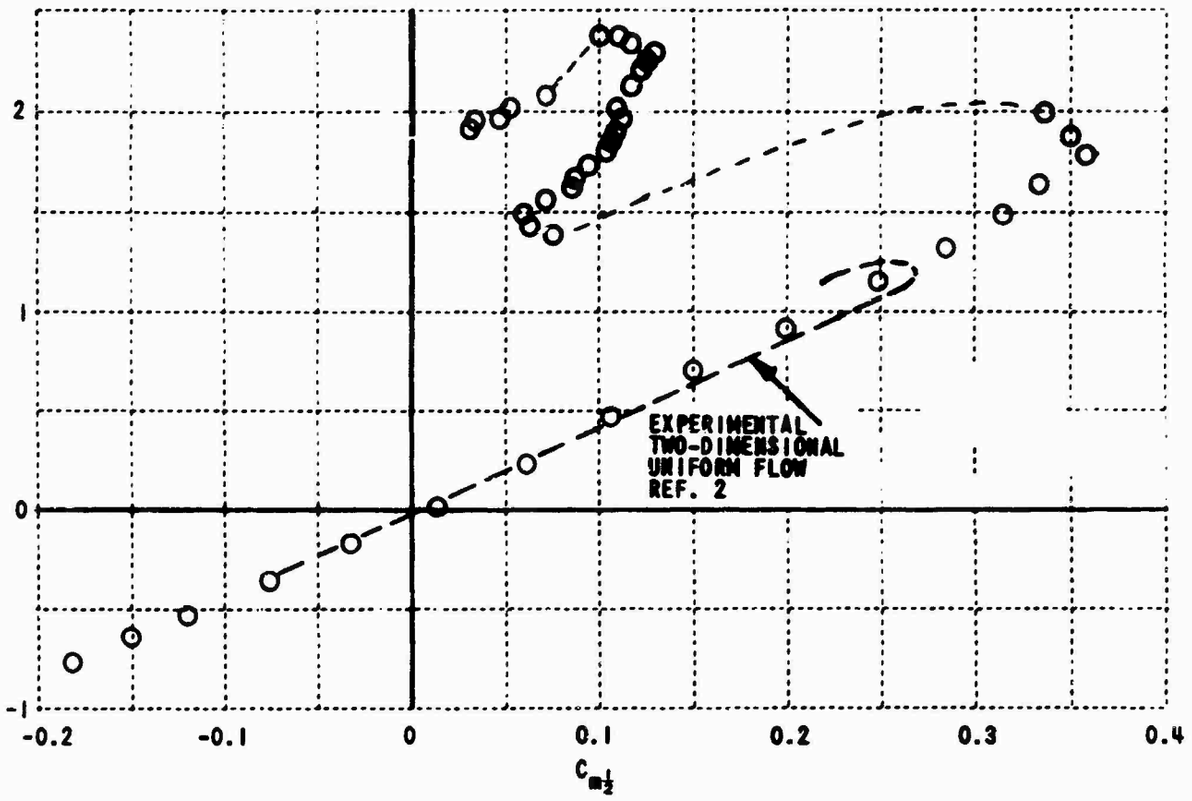

(c) NONDIMENSIONAL HEIGHT OF WING MIDCHORD ABOVE JET CENTERLINE IN JET RADII, $h/r = -0.10$

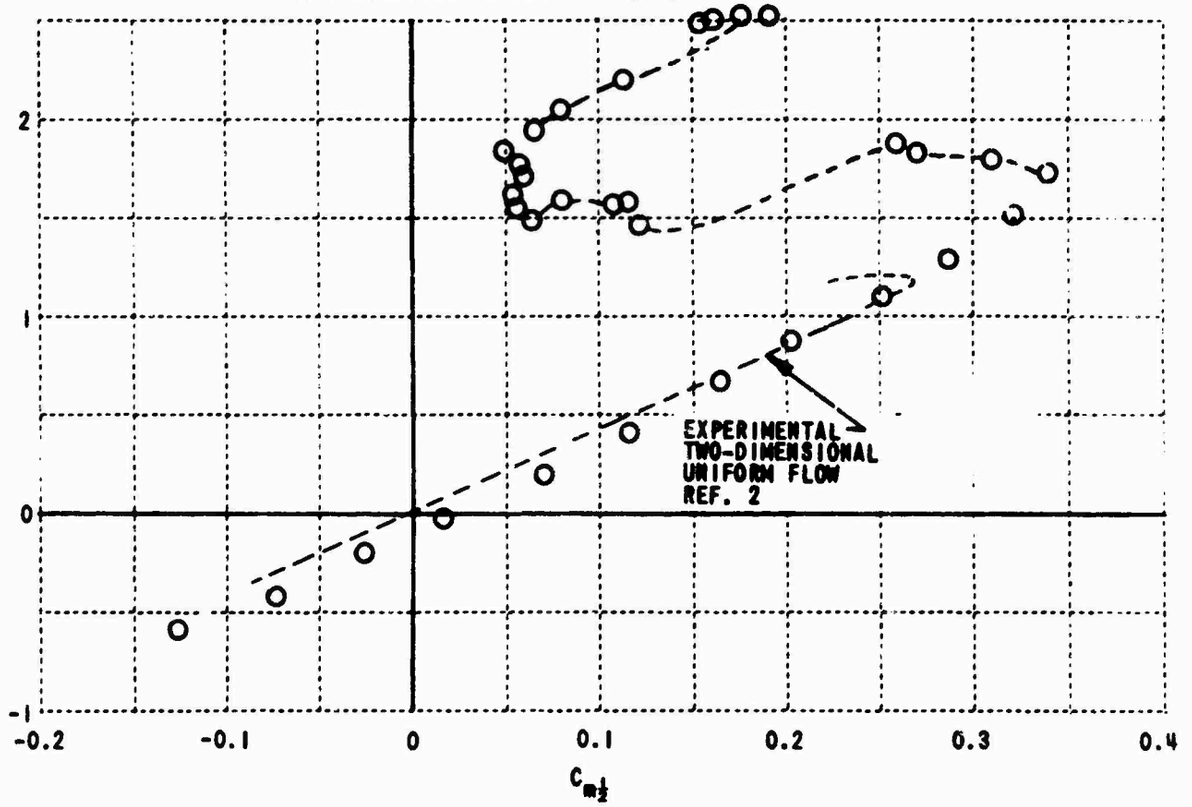

(d) NONDIMENSIONAL HEIGHT OF WING MIDCHORD ABOVE JET CENTERLINE IN JET RADII, $h/r = -0.64$

Figure 23. SECTION LIFT COEFFICIENTS vs. SECTION MOMENT COEFFICIENT, LOW q, $z/r = 1.54$

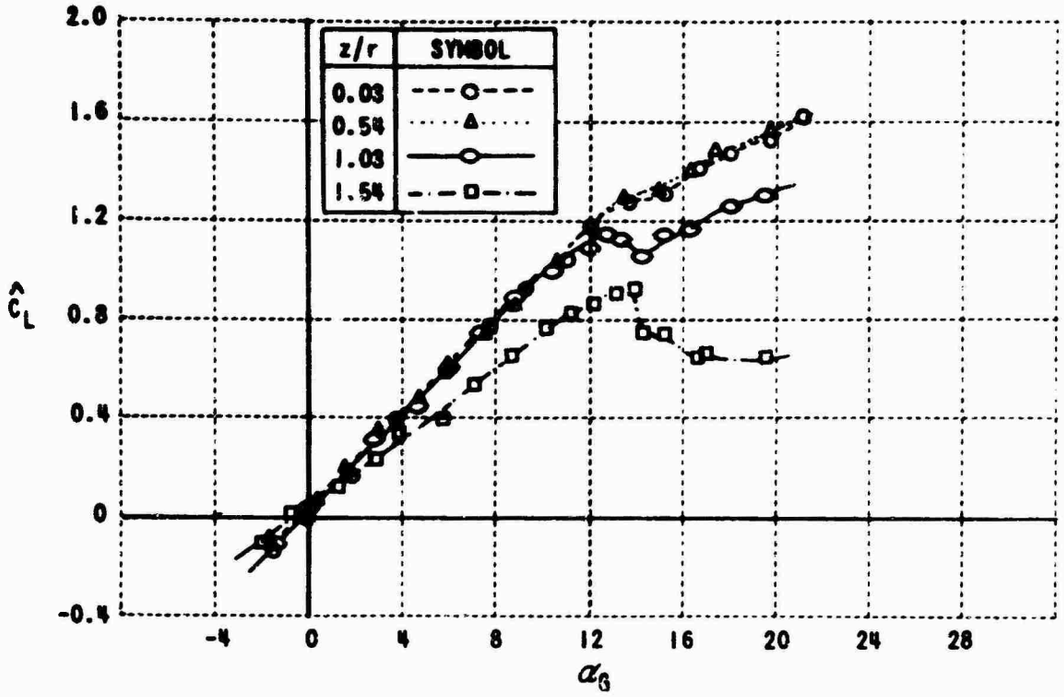

(a) NONDIMENSIONAL HEIGHT OF WING MIDCHORD ABOVE JET CENTERLINE IN JET RADII, h/r = 0.76

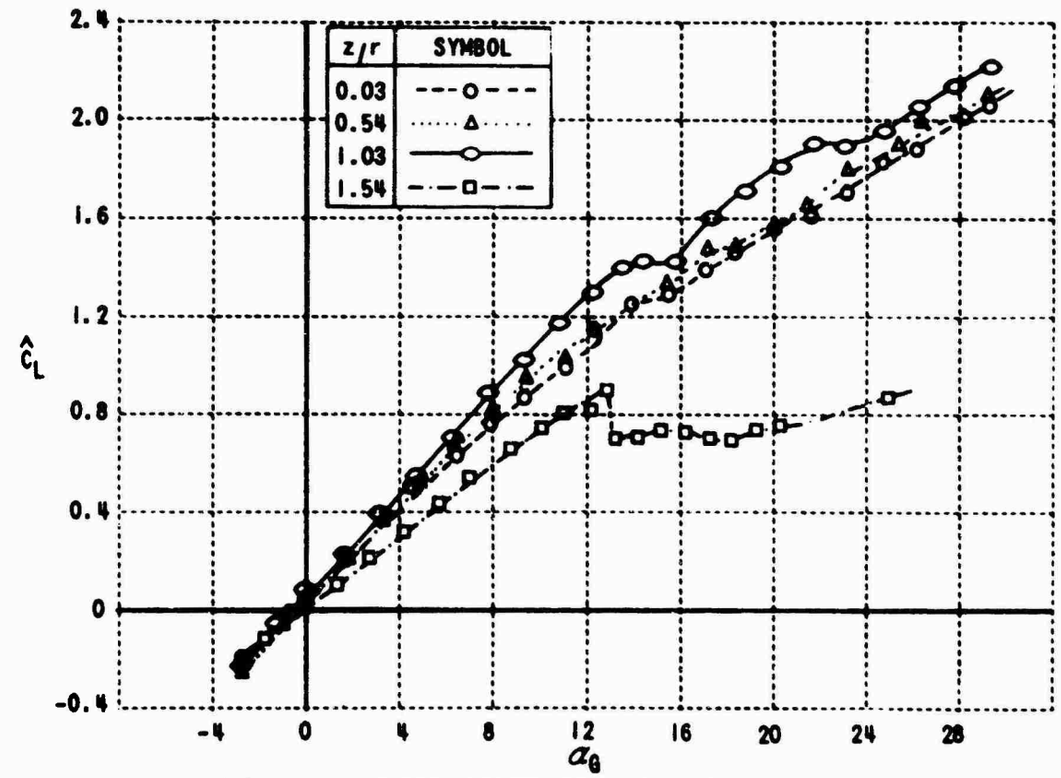

(b) NONDIMENSIONAL HEIGHT OF WING MIDCHORD ABOVE JET CENTERLINE IN JET RADII, h/r = 0.46

Figure 24. VARIATION OF $\hat{C}_L$ WITH GEOMETRIC ANGLE OF ATTACK AND z/r AT VARIOUS VALUES OF h/r

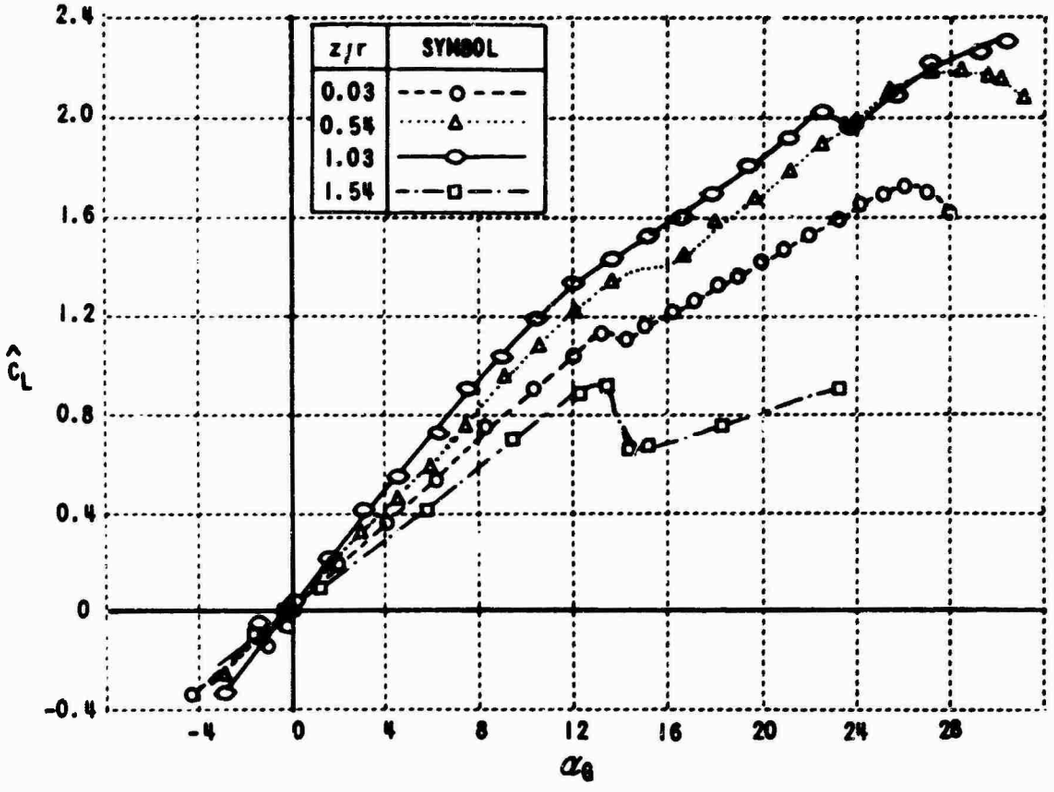

(c) NONDIMENSIONAL HEIGHT OF WING MIDCHORD ABOVE JET CENTERLINE IN JET RADII, h/r = -0.10

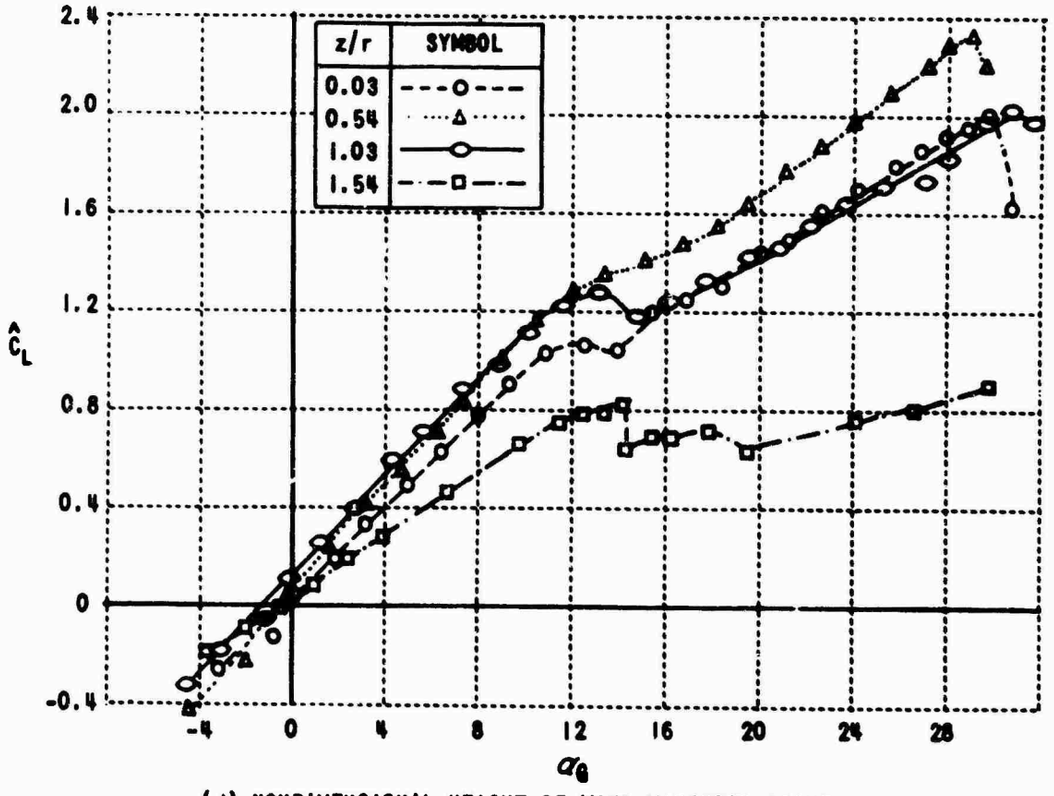

(d) NONDIMENSIONAL HEIGHT OF WING MIDCHORD ABOVE JET CENTERLINE IN JET RADII, h/r = -0.64

Figure 24. VARIATION OF $\hat{C}_L$ WITH GEOMETRIC ANGLE OF ATTACK AND z/r AT VARIOUS VALUES OF h/r

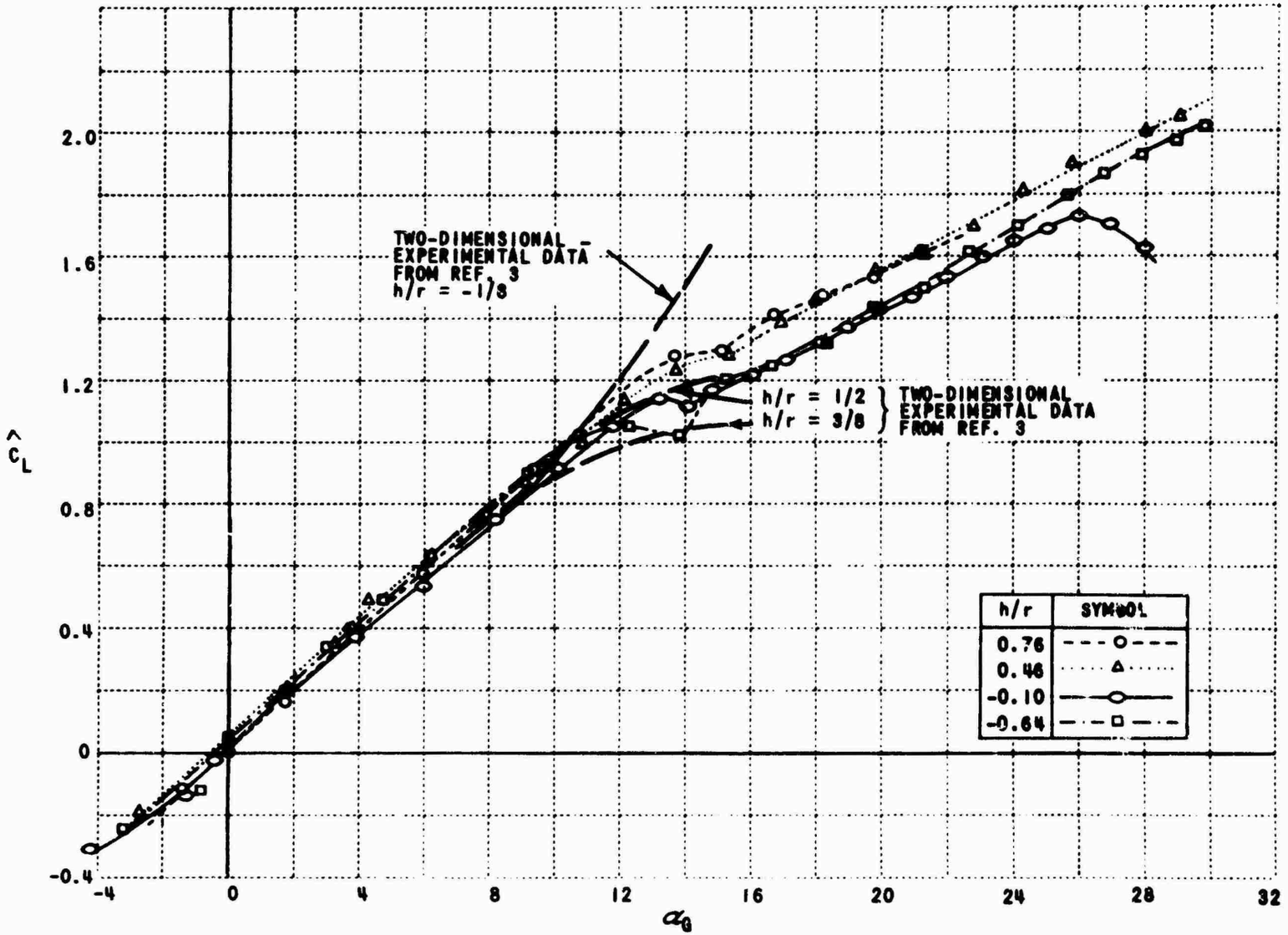

(a) NONDIMENSIONAL LATERAL DISTANCE FROM JET CENTERLINE IN JET RADII, z/r = 0.03

Figure 25. VARIATION OF $\hat{C}_L$ WITH GEOMETRIC ANGLE OF ATTACK AND h/r AT VARIOUS VALUES OF z/r

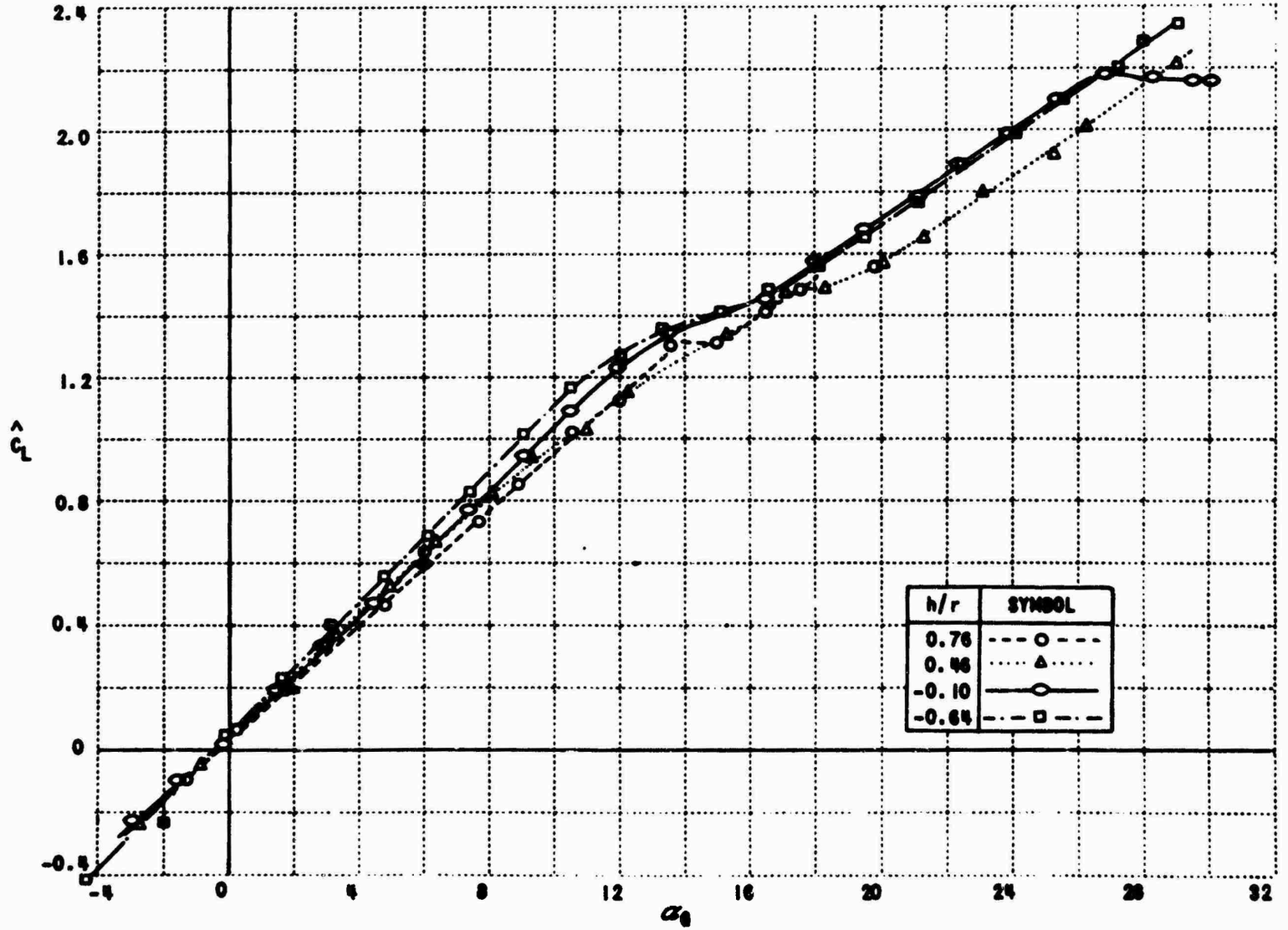

(b) NONDIMENSIONAL LATERAL DISTANCE FROM JET CENTERLINE IN JET RADII, z/r = 0.54

Figure 25. VARIATION OF $\hat{C}_L$ WITH GEOMETRIC ANGLE OF ATTACK AND h/r AT VARIOUS VALUES OF z/r

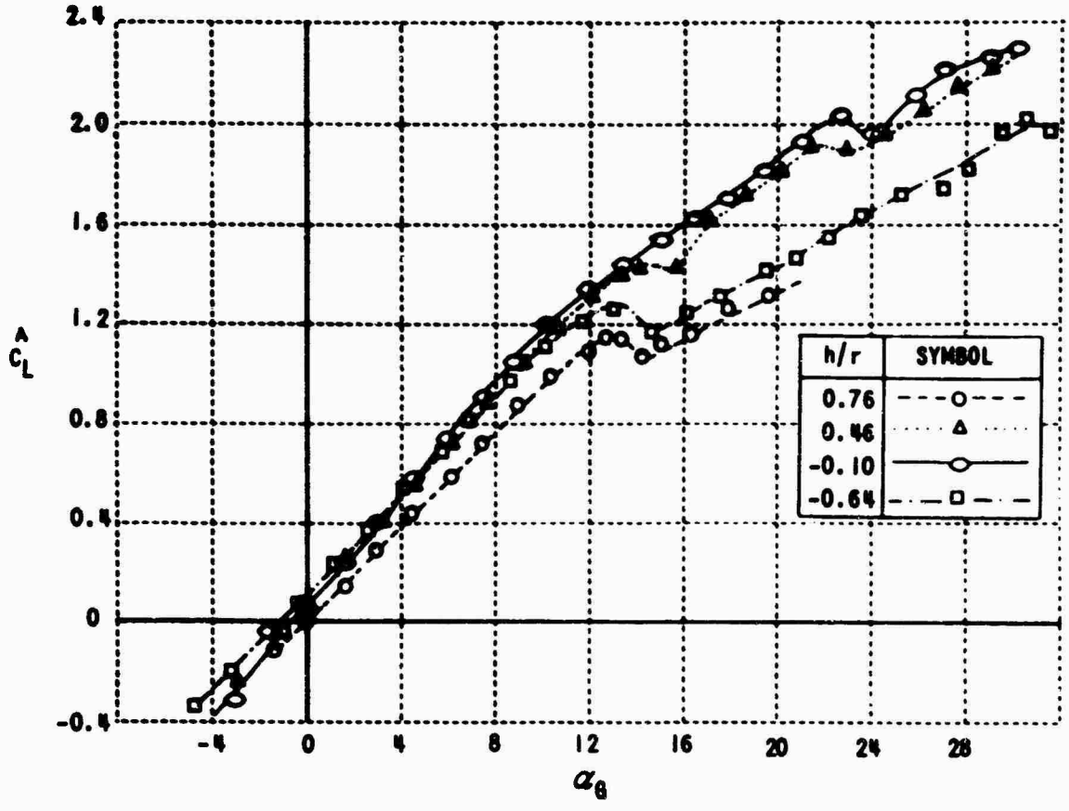

(c) NONDIMENSIONAL LATERAL DISTANCE FROM JET CENTERLINE IN JET RADII, z/r = 1.03

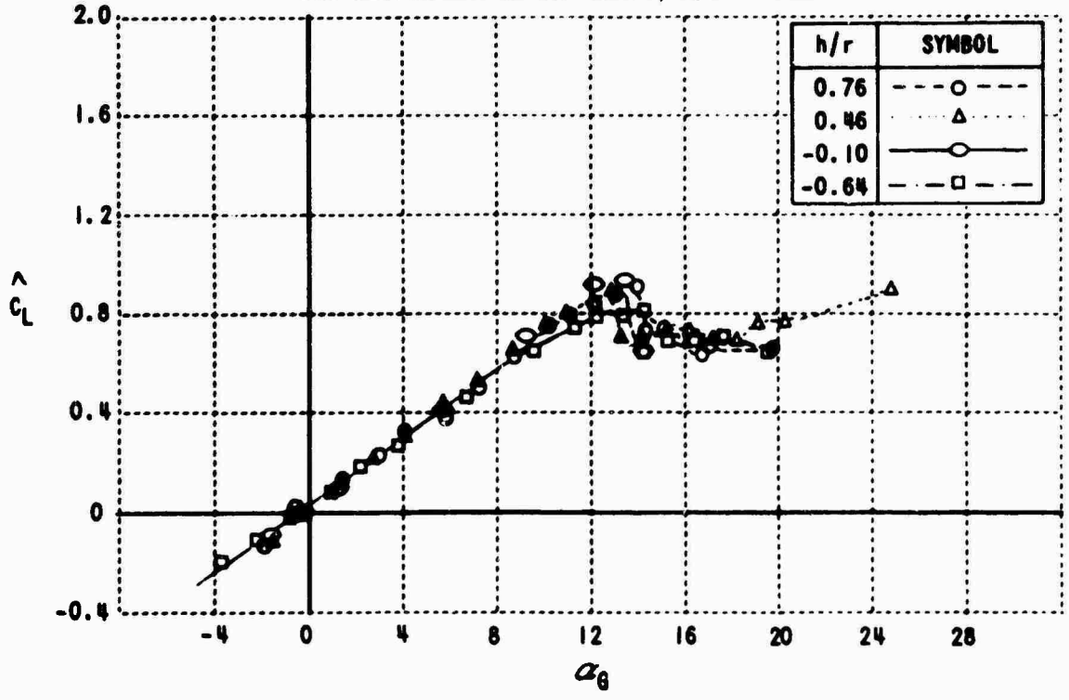

(d) NONDIMENSIONAL LATERAL DISTANCE FROM JET CENTERLINE IN JET RADII, z/r = 1.54

Figure 25. VARIATION OF $\hat{C}_L$ WITH GEOMETRIC ANGLE OF ATTACK AND h/r AT VARIOUS VALUES OF z/r

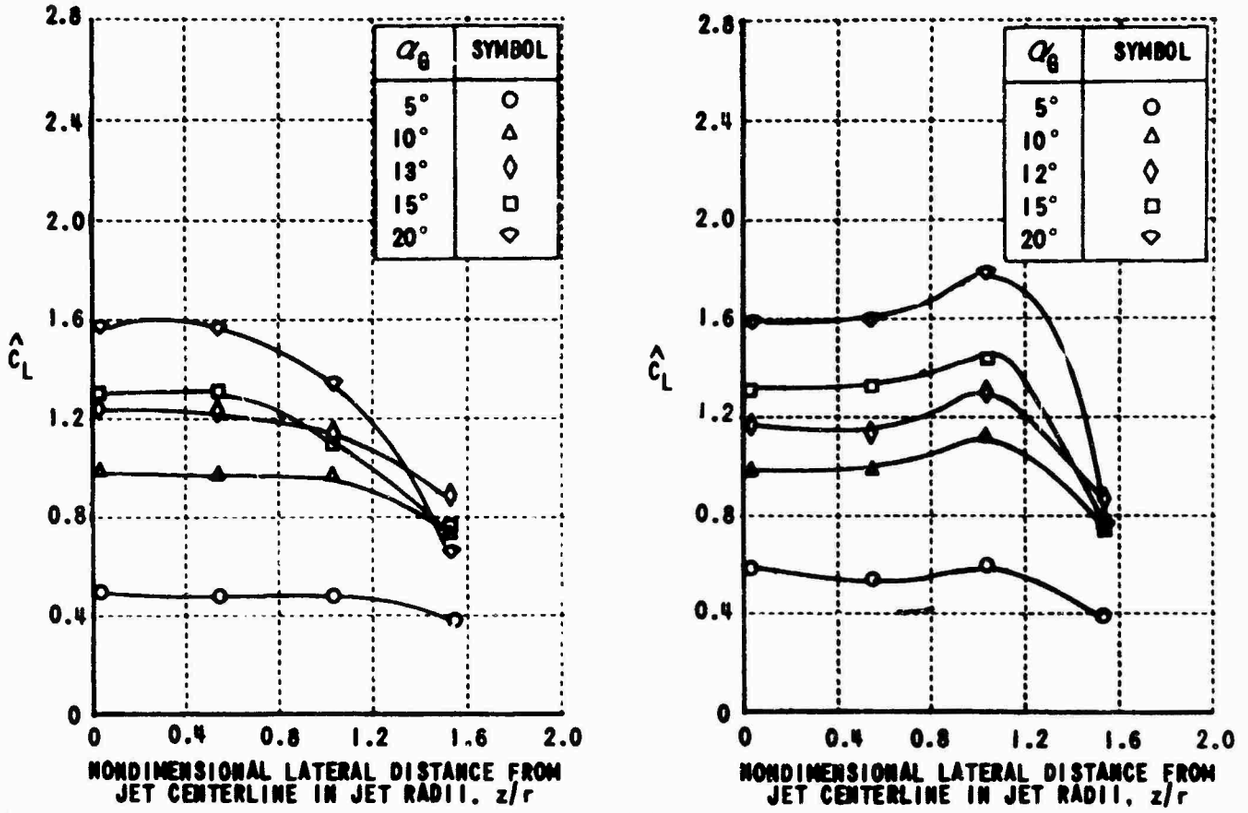

(a) NONDIMENSIONAL HEIGHT OF WING MIDCHORD ABOVE JET CENTERLINE IN JET RADII, h/r = 0.76

(b) NONDIMENSIONAL HEIGHT OF WING MIDCHORD ABOVE JET CENTERLINE IN JET RADII, h/r = 0.46

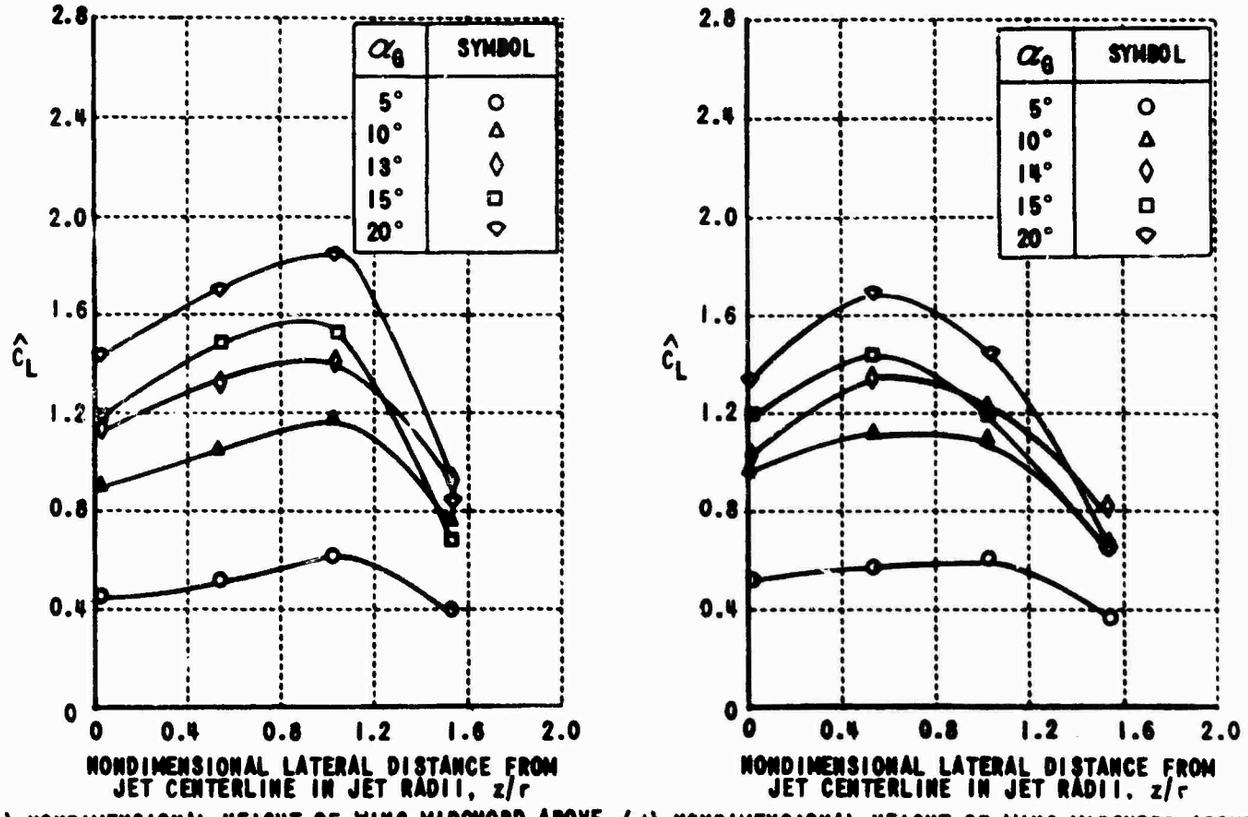

(c) NONDIMENSIONAL HEIGHT OF WING MIDCHORD ABOVE JET CENTERLINE IN JET RADII, h/r = -0.10

(d) NONDIMENSIONAL HEIGHT OF WING MIDCHORD ABOVE JET CENTERLINE IN JET RADII, h/r = -0.64

Figure 26. SPANWISE LIFT DISTRIBUTIONS

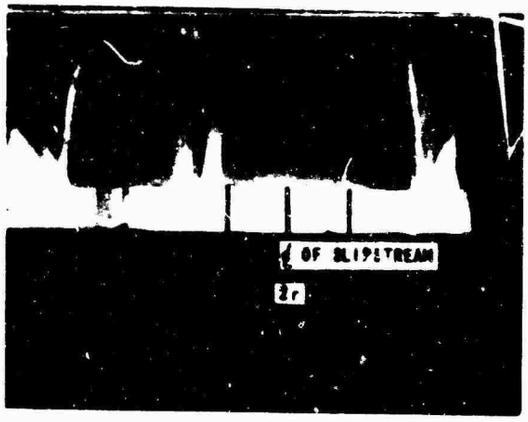

$\alpha = 8°$

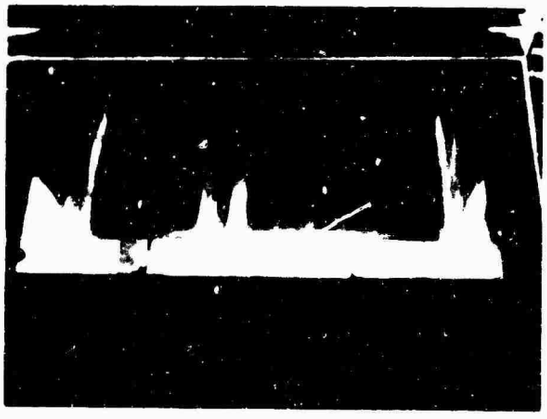

$\alpha = 11°$

$\alpha = 12°$

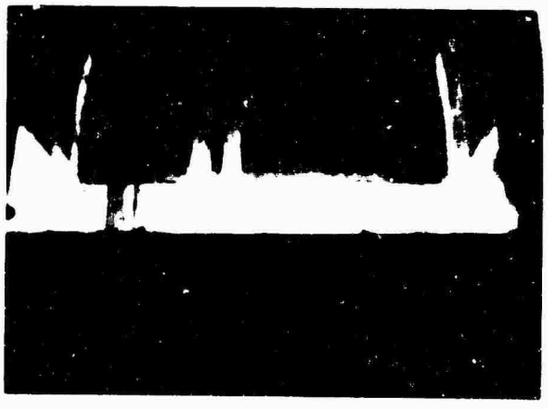

$\alpha = 12\frac{1}{2}°$

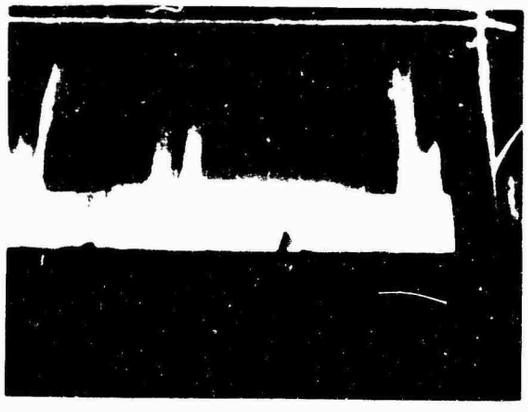

$\alpha = 16\frac{1}{2}°$

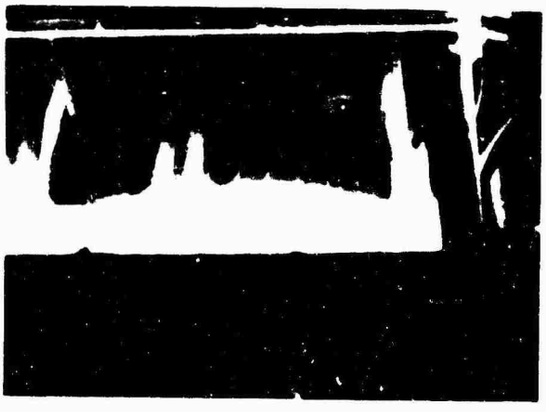

$\alpha = 17\frac{1}{2}°$

Figure 27. FLOW VISUALIZATION TEST RESULTS, h/r = -0.10

α = 20°

α = 24°

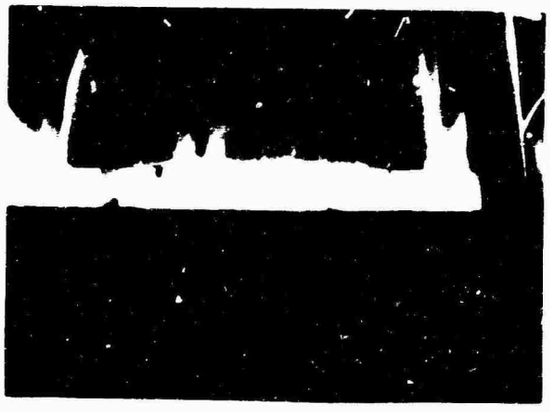

α = 26°

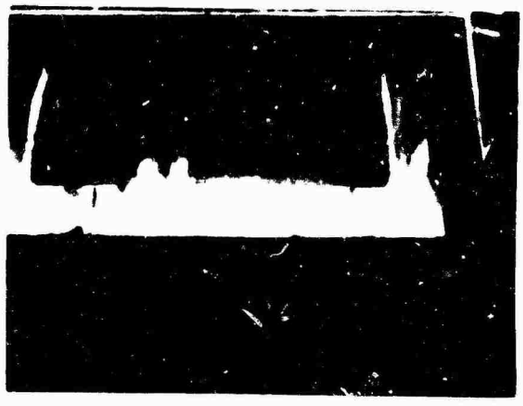

α = 28°

Figure 27. FLOW VISUALIZATION TEST RESULTS, h/r = -0.10

BIBLIOGRAPHY

1. Sowyrda, A., Theory of Cambered Joukowski Airfoils in Shear Flow, CAL Report No. AI-1190-A-2, Cornell Aeronautical Laboratory, Inc., Buffalo, New York, September 1959.

2. Two-Dimensional Effects of Slipstream Shear on Airfoil Characteristics, TREC Technical Report 60-56, U. S. Army Transportation Research Command, Fort Eustis, Virginia, September 1960.

3. The Influence of Two-Dimensional Stream Shear on Airfoil Maximum Lift, TCREC Technical Report 61-93, U. S. Army Transportation Research Command, Fort Eustis, Virginia, August 1961.

4. The Effects of Axisymmetric Slipstream Shear on Airfoil Characteristics, TCREC Technical Report 61-138, U. S. Army Transportation Research Command, Fort Eustis, Virginia, December 1961.

5. Tsien, H. S., "Symmetrical Joukowski Airfoils in Shear Flow", Quarterly of Applied Mathematics, Vol. I, No. 2, 1943, pp. 130-148.

6. Jones, E. E., "The Forces on a Thin Airfoil in Slightly Parabolic Shear Flow", ZAMM, Vol. 37, 1957, pp. 362-370.

7. Nagamatsu, H. T., "Circular Cylinder and Flat Plate Airfoil in a Flow Field With Parabolic Velocity Distribution", Journal of Mathematics and Physics, Vol. 30, 1951, p. 131.

8. Lighthill, M. J., "The Fundamental Solution for Small Steady Three-Dimensional Disturbances to a Two-Dimensional Parallel Shear Flow", Journal of Fluid Mechanics, Vol. 3, 1957, pp. 113-144.

9. Theoretical Studies of Impinging Uniform and Nonuniform Jets, TRECOM Technical Report 64-42, U. S. Army Transportation Research Command, Fort Eustis, Virginia, August 1964.

10. Hess, John L., "Calculation of Potential Flow About Bodies of Revolution Having Axes Perpendicular to the Free-Stream Direction", Journal of the Aerospace Sciences, Vol. 29, No. 6, June 1962, pp. 726-742.

11. Lovitt, William Vernon, Linear Integral Equations, First Edition, Dover Publications, Inc., New York, 1950, pp. 23-25.

12. Hall, I. M., "The Displacement Effect of a Sphere in a Two-Dimensional Shear Flow", Journal of Fluid Mechanics, Vol. I, Part 2, July 1956, pp. 129-141.

13. Pope, Alan, Wind-Tunnel Testing, Second Edition, John Wiley & Sons, Inc., New York, 1954, p. 291.

14. Brenckmann, M., Experimental Investigation of the Aerodynamics of a Wing in a Slipstream, UTIA Technical Note No. 11, Institute of Aerophysics, University of Toronto, April 1957.